THE UNIVERSITY OF CALGARY

Kinetics of Gas Hydrate Formation from Methane, Carbon Dioxide and Their Mixtures

by

Mahendra B. Malegaonkar

A THESIS

SUBMITTED TO THE FACULTY OF GRADUATE STUDIES

IN PARTIAL FULFILMENT OF THE REQUIREMENTS FOR THE

DEGREE OF MASTER OF SCIENCE IN CHEMICAL ENGINEERING

DEPARTMENT OF CHEMICAL AND PETROLEUM ENGINEERING

CALGARY, ALBERTA

SEPTEMBER, 1996

THE UNIVERSITY OF CALGARY

FACULTY OF GRADUATE STUDIES

The undersigned certify that they have read, and recommend to the Faculty of Graduate Studies for acceptance, a thesis entitled "Kinetics of Gas Hydrate Formation from Methane, Carbon Dioxide and Their Mixtures" submitted by Mahendra B. Malegaonkar in partial fulfilment of the requirements for the degree of Master of Science in Chemical Engineering.

P.R. Bishnoi

Dr. P.R. Bishnoi, Supervisor/Committee Chairperson

Department of Chemical and Petroleum Engineering

Anil Mehrotra

Dr. A.K. Mehrotra

Department of Chemical and Petroleum Engineering

J.A.C. Kentfield.

Dr. J.A.C. Kentfield

Department of Mechanical Engineering

Sept. 16, 96

Date

ABSTRACT

Kinetic data for gas hydrate formation from mixtures of methane and carbon dioxide were obtained in a semi-batch stirred tank reactor at three different isotherms. The Englezos et al. (1987a) model was used to predict the kinetic rate constant for gas hydrate formation from pure methane and pure carbon dioxide. The rate constant for carbon dioxide was higher than for methane.

A solubility model for the mixture of gases was developed to predict the solubility of gases in liquid water and the gas composition in the gas phase of the reactor. The two-film model was used for estimating the rates of multicomponent mass transfer from the exact solution of the Maxwell-Stefan equation. The model could not predict the observed reverse diffusion of methane gas during the absorption of the two gases. This can be attributed to the limitation of the solubility model which assumes that the liquid is an ideal solution.

The Englezos et al. (1987b) model for gas hydrate formation from gas mixtures was adapted to predict the growth of hydrates. The model predictions had large deviations from the experimental data. This can be attributed to the limitation of the kinetic model which also assumes that the liquid is an ideal solution.

ACKNOWLEDGEMENTS

I wish to acknowledge the valuable help and support provided by my supervisor Dr. P. R. Bishnoi and would like to express my sincere gratitude for his continuous guidance, encouragement and supervision of this thesis. Working with Dr. Bishnoi was a very pleasant and rewarding experience.

I am also indebted to Dr. Anil Mehrotra, for his encouragement, constructive criticism and for the guidance he offered.

I am thankful to my research colleagues in the "Gas Hydrate Research Group" for their helpful advice and special thanks to Mr. Pankaj Dholabhai, Dr. Kal Mahadev and Dr. Amitabha Majumdar for their help in conducting the experimental work.

The financial support provided by the Department of Chemical and Petroleum Engineering and the Natural Sciences and Engineering Research Council (NSERC) is greatly appreciated.

The thesis is dedicated to my Parents, **Brahmanand** and **Sitadevi**
for their blessings, inspiration and vision making this work possible

&

To my brothers **Rajesh** and **Shailendra**
and to my friend **Uttamchandani**

TABLE OF CONTENTS

LIST OF TABLES

LIST OF FIGURES

NOMENCLATURE

a,b,c,d	constants
a	interfacial area per unit of liquid volume, m^2/m^3
A	gas-liquid surface area, m^2
$A_{(g-l)}$	gas-liquid interfacial area, m^2
A_p	surface area of the particles, m^2
$[B]$	matrix function of inverted binary diffusion coefficients, s/m^2
c	concentration of gas in the liquid water, mol/m^3
c_t	mixture molar density, mol/m^3
c_{w0}	initial concentration of water molecules, mol/m^3
D	Fick diffusivity of the gas, m^2/s
$[D]$	matrix of Fick diffusion coefficients, m^2/s
$Đ_{ij}$	Maxwell-Stefan diffusivity for pair i-j, m^2/s
f	fugacity of gas, MPa
G	linear growth rate, m/s
H	Henry's constant, MPa
$[I]$	identity matrix
J	molar diffusion flux, $mol/m^2.s$
k	zero-flux mass transfer coefficients, m/s
k^*	finite-flux mass transfer coefficients, m/s
$[k]$	square matrix of zero-flux mass transfer coefficients, m/s
$[k^*]$	square matrix of finite-flux mass transfer coefficients, m/s
k_L	liquid side mass transfer coefficient, m/s
K	$\pi.\mu_2.K^*$
K^*	combined rate parameter, $mol/(m^2.s.MPa)$
l	film thickness, m
L	distance between (g-l) interface and the bottom of reactor, m
M	molar mass of the hydrate of the form $X.n_wH_2O$ and $\theta_1CH_4.\theta_2CO_2.n_wH_2O$

n	moles of gas consumed or number of components
n_{eq}	moles of gas dissolved at three phase equilibrium
n_i	moles of the gas consumed of component 'i'
n_t	total moles of the gas consumed
n_w	number of water molecules per gas molecule
n_{w0}	initial number of water molecules in the reactor
n_{tb}	moles of the gas dissolved at turbidity point
N_i	molar flux of component 'i', mol/m^2.s
N_t	total molar flux, mol/m^2.s
P	pressure, MPa
r	crystal radius, m
R	universal gas constant, MPa.m^3/mol.K
$R_y(t)$	global reaction rate, mol/m^3.s
R_z	the rate of transfer of dissolved gas per unit surface area, mol/m^2.s
s	particle size (diameter), m
t	time, s
T	temperature, K
v_m	molar volume of the hydrate, m^3/mol
v_w	molar volume of water, m^3/mol
V	volume, m^3
x	liquid mole fraction
y	distance from the (g-l) interface, m
y_i	gas mole fraction of component 'i'
y_L	film thickness, m
Y	methane gas composition, %
z	compressibility factor
z	distance from the (g-l) interface, m

Greek Letters

$\phi(s,t)$ crystal size distribution, m^{-4}

$\psi(s)ds$ fraction of the crystals born in the size range from s to s+ds

μ_n n^{th} moment of the crystal size distribution, m^n/m^3

μ_n^0 initial n^{th} moment of the crystal size distribution

γ Hatta number

α_2 nucleation constant, nuclei/m^2.s

ρ hydrate density, kg/m^3

σ surface energy for the system hydrate-water, J/m^2

Δg free energy change per unit volume of product, J/m^3

θ secondary nucleation rate per unit volume or mole fraction of the gas in the hydrate phase on a water free basis

Γ thermodynamic factor

$[\Gamma]$ square matrix of thermodynamic factors

η dimensionless distance

Φ mass transfer rate factor

$[\Phi]$ square matrix of mass transfer rate factors

φ mass transfer parameter

(φ) column matrix of mass transfer parameters

ϕ mass transfer rate factor for explicit method

$[\phi]$ $[\Gamma]^{-1}[\Phi]$

δ_{ij} Kronecker delta, 1 if i=k, 0 if i≠k

γ_i activity coefficient of component i in solution

Ξ correction factor for high fluxes

$[\Xi]$ square matrix of high flux correction factors

$[\beta]$ bootstrap matrix

Subscripts

0	time, 0 or gas-liquid interface
1	initial equilibrium state for the Ruska pump experiment or component 1
2	final equilibrium state for the Ruska pump experiment or component 2
av	average
b	bulk of the liquid phase
cr	critical
exp	experimental conditions
eq	three phase equilibrium condition
g	reactor gas phase
g-l	gas-liquid interface
i	component
j	component
L	reactor liquid phase
n	n^{th} component
p	particle
R	reactor
s	crystal surface
S	supply reservoir
t	time,t
tb	turbidity
w	water

Superscripts

0	initial condition
g	gas phase
i	interface
*******	plane of gas liquid surface

1. INTRODUCTION

1.1 Background

Gas hydrates are crystalline compounds that occur when water forms a cage-like structure around smaller guest molecules. The hydrate forming gas molecules are methane, ethane, propane, isobutane, nitrogen, carbon dioxide and hydrogen sulfide. Hydrate formation is possible in any place where water exits with such molecules in natural or artificial environments and at temperatures above and below 0 °C when the pressure is elevated.

Gas hydrates normally form in one of two small repeating crystal structures (I and II), shown in Figure 1.1. The smallest repeating unit of a crystal structure is a "unit cell". The unit cell of structure I hydrate consists of 46 water molecules and includes two small and six large cavities. The maximum linear dimension of the small and large cavities are 5.1 °A and 5.8 °A, respectively. For structure II gas hydrates, the unit cell consists of 136 water molecules and includes sixteen small and eight large cavities. The maximum linear dimension of the small and large cavities of structure II are 5.0 °A and 6.7 °A, respectively. In both the structures, the water molecules are tetrahedrally coordinated, as in ordinary ice, and the hydrate forming gases are linked to the water lattice by van der Waals forces. Structure I, a body-centered cubic structure, forms with molecules smaller than propane. The methane and carbon dioxide are known to form structure I. Structure II, a diamond lattice within a cubic framework forms when natural gases or oils contain molecules larger than ethane but smaller than pentane. The structural details of natural gas hydrates have been well investigated and are described in the literature (Claussen, 1951; von Stackelberg and Muller, 1954; Jeffery and McMullan, 1965; Makogon, 1981).

Hydrates are considered a nuisance because they block transmission lines, plug blowout preventers, jeopardize the foundation of deepwater platforms and pipelines, cause tubing and casing collapse and foul process heat exchangers, valves, and expanders. On the other

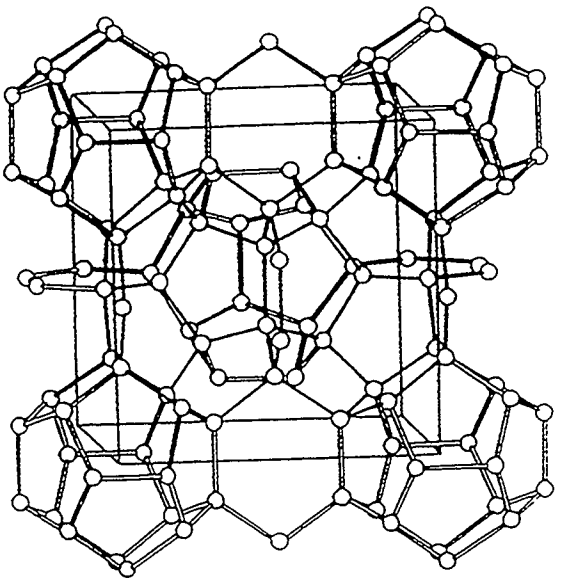

Structure I - Body Centered Cubic

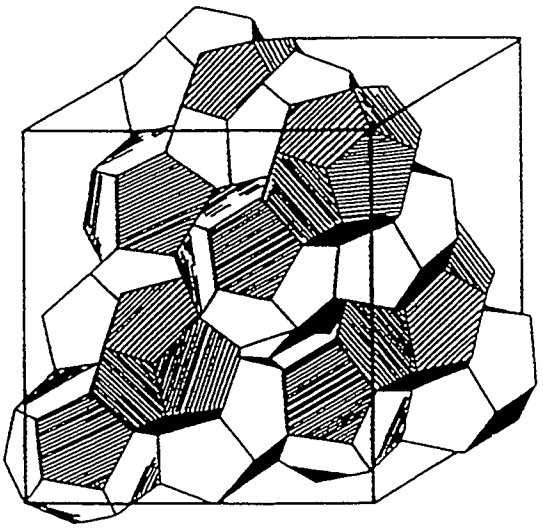

Structure II - Diamond Lattice

Figure 1.1 Structures of Gas Hydrates

(from Sloan, 1990)

hand, the hydrate deposits both in deep oceans and in the permafrost provide a large natural reserves of hydrocarbons yet to be commercially exploited. The primary importance of the hydrates is in the oil and gas industry for pipeline, platform and drilling applications. The importance of hydrates is also recognized as a means for separation, as a gas storage medium and in gas recovery from in-situ hydrates. Prevention of hydrate formation can be accomplished by thermodynamic inhibition or kinetic inhibition. A comprehensive understanding of the thermodynamics and formation / decomposition kinetics of hydrates is of primary importance in dealing with the problems and opportunities offered by natural gas hydrates.

1.2 Gas Hydrates : Thermodynamics and Kinetics

The thermodynamics of hydrate formation has been investigated experimentally by several researchers (Marshall et al., 1964; Holder et al., 1980; Sloan, 1990; Adisasmito et al., 1991; Dholabhai et al., 1991 and Englezos et al., 1991). The computational prediction of the hydrate forming conditions using thermodynamic models was studied in detail (van der Waals and Platteuw, 1959; Parrish and Prausnitz, 1972; Ng and Robinson, 1976; John et al., 1985 and Englezos et al., 1988, 1991).

The other area of hydrate research that is of vital importance is the kinetics of gas hydrate formation. Although not as extensive as thermodynamic studies, there are some published data on hydrate kinetics (Vysniauskas et al., 1983, 1985; Bishnoi et al., 1985, 1986; Englezos et al., 1987(a), 1987(b); Dholabhai et al., 1993). Vysniauskas et al. (1983, 1985) developed a semi-empirical model to correlate the experimental kinetic data of methane and ethane gas hydrates. Their study was the first attempt ever made to quantitatively describe and model the kinetics formation of gas hydrates. These studies indicated that the hydrate formation consists of the appearance of nuclei and their subsequent growth. The growth is dependent on the interfacial area, pressure, temperature

and the degree of supercooling. However, these models were found rather inadequate in fully describing the kinetics formation.

Based on the crystallization theory coupled with the two-film theory for the gas absorption in the liquid phase, Englezos et al. (1987a) proposed a mechanistic model with only one adjustable parameter which represents the rate constant for the growth of the hydrate particles. They have determined the kinetics of methane and ethane hydrates formation from aqueous solution. Their study revealed that the formation rate is proportional to the difference in the fugacity of the dissolved gas and the three-phase equilibrium fugacity at the experimental temperature and to the second moment of particle size distribution i.e. the particle surface area. The kinetic rate constants indicated a very weak temperature dependence. They also extended the model to the formation of hydrates from mixtures of methane and ethane (Englezos et al. 1987b). Dholabhai et al. (1993) applied the model developed by Englezos et al. (1987a) to predict the kinetics of methane hydrate formation in aqueous electrolyte solutions and found that the kinetic rate constant remains unaffected by the presence of electrolytes. The kinetics of gas hydrate decomposition have also been studied (Kim et al., 1987).

1.3 Scope of the Study

The main objective of this work was to obtain the experimental data on the kinetics of hydrate formation from methane and carbon dioxide mixtures and to model the amounts of gas consumed during the hydrate formation. In the present work, the model developed by Englezos et al. (1987a) was studied and corrected. This model was used to predict the kinetic rate constant for methane and carbon dioxide. The kinetic data for methane hydrate formation in pure water were obtained from work reported by Bishnoi et al. (1985, 1986) and data for carbon dioxide hydrate formation in pure water were available from previous work in this department. The data were available at four different temperatures of 274, 276, 279 and 282 K, at different pressures in the range of 3.29 to 8.90 MPa for methane

and at three different temperatures of 274, 276 and 278 K, at different pressures in the range of 1.59 to 2.79 MPa for carbon dioxide. The experiments were conducted, as a part of this work, to obtain data on the kinetics of hydrate formation from the binary mixture of methane (80.3 %) and carbon dioxide at three different temperatures of 274, 276 and 278 K and at pressures in the range of 2.69 to 4.58 MPa. The experimental pressures and temperatures were chosen so that no condensation of the gas occurred during the experiments. All the data were collected under isothermal - isobaric conditions by contacting the gas and water in a semi-batch stirred tank reactor. The stirring rate was set at 400 RPM. The experimental apparatus and procedure described by Englezos et al. (1987a) and Dholabhai et al. (1993) was modified by integrating the gas chromatograph and the gas sampling line to analyze the reactor gas phase for mixture of gases.

The experimental data obtained for the mixture of gases represent the absorption of gases before the turbidity point and growth of the hydrate particles after the turbidity point. A mass transfer model was developed for the simultaneous absorption of methane and carbon dioxide gases in water to predict the solubility of gases in water and the gas composition in the gas phase of the reactor. The model developed by Englezos et al. (1987b), which was an extension of the pure component kinetic model, was used to predict the hydrate formation for mixture of gases. It does not contain any adjustable parameters since the kinetic parameters for the crystal growth used in this model were obtained from the pure component hydrate formation experiments.

The solubility and kinetic model for the mixture of gases predicted large deviations from the experimental data which is likely due to the assumption of ideal liquid mixtures. Hence a new solubility and kinetic model is proposed for future consideration, taking into effects the non ideal liquid mixtures by incorporating the activity coefficients. These models need evaluation using the experimental data.

2. EXPERIMENTAL APPARATUS AND PROCEDURE

The experimental apparatus and procedure described by Englezos et al. (1987a) and Dholabhai et al. (1993) was modified by integrating the gas chromatograph and the gas sampling line to analyze the reactor gas phase for the mixture of gases. A brief description of the apparatus and the procedure is given below to facilitate an understanding of the nature of the data and the concepts involved in their modeling.

2.1 Experimental Apparatus

A schematic diagram of the experimental apparatus is shown in Figure 2.1. The equipment is the same as that described by Dholabhai et al. (1993) with a few modifications in order to analyze the gas phase of the reactor. The principal components of the experimental set-up are a semi-batch agitated reactor system, the pressure and temperature measuring systems, the DORIC data acquisition system, a gas chromatography system, and supply and reference gas reservoirs.

The semi-batch agitated reactor system comprises of a stainless steel reactor with a design working pressure of about 140 bars and with an internal volume of 500 cm^3. The reactor is fitted with two marine type Lucite windows to observe the presence of gas hydrates in the reactor. In order to avoid the formation of vortices baffles are placed in the reactor. A magnetic stirrer bar coupled to a ceramic magnetic stirrer mounted on a driver outside the reactor was used to agitate the liquid solution. The stirring rate could be controlled by a RPM controlled DC motor. A sampling line connects the reactor to the gas chromatograph to analyze the reactor gas phase using thermal conductivity detectors.

The supply reservoir R1 was used to supply the necessary gas, as the hydrate formation ensued, in order to maintain constant reactor pressure. The initial supply reservoir R3 was used to supply additional gas in case the gas is insufficient in the reservoir R1. The

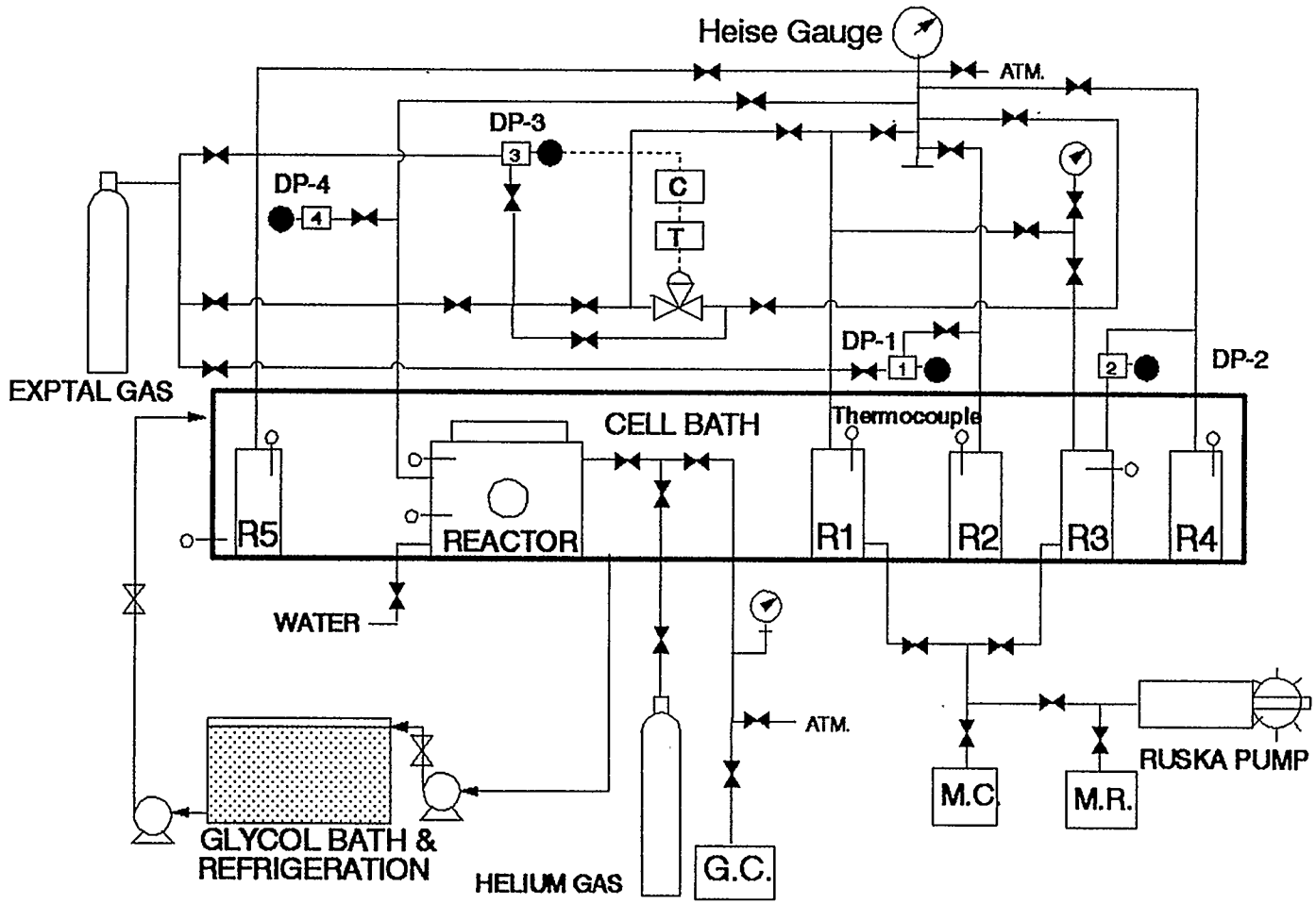

Figure 2.1 Schematic Diagram of the Experimental Apparatus.

reference reservoirs R2, R4 and R5 were used to provide reference pressures for several Differential Pressure or DP transmitters.

The differential pressure transmitters DP1, DP2, DP3 and DP4 were used to measure the pressures in the reservoirs R1, R3 and reactor respectively. The bias sides of DP1, DP2 and DP3 were connected to the reference reservoirs R2, R4 and R5 respectively while the bias side of DP4 was open to the atmosphere. A Heise Gauge was used to set the pressures in R2, R4 and R5. The signal from DP1 is fed to a PID controller (C) via pressure transmitter (T) which actuates the pneumatic control valve between the reactor and R1 to regulate the reactor pressure. As the pressure in the reactor decreases due to gas consumption in the reactor owing to the dissolution or hydrate formation, the control valve opens to admit the gas from R1 until the pressure in the reactor is restored to the desired set pressure.

Temperatures inside the reactor and reservoirs were measured using copper-constantan thermocouples. The reservoirs and reactor were kept immersed in a glycol bath whose temperature was controlled using an auxiliary glycol refrigeration. A Digitrend 235 DORIC data acquisition system and a PC 286 were used to record the temperature and pressure of the system after every 15 s. The Trebble-Bishnoi EOS (Trebble 1987, 1988) was incorporated in the program to perform on-line computations of the cumulative moles of the gas consumed throughout the experiment. The binary interaction parameters were obtained from Trebble (1990).

The resolution of pressure measurement on DORIC was 0.01% of the span of the transmitters and that of temperature 0.1 K. DP1 and DP3 were calibrated to 0.5 MPa while DP2 was calibrated to 2.0 MPa. The differential pressure transmitters have accuracy of 0.2% of their span. The error in the Heise gauge is $\pm$ 25 kPa. The errors in pressure and temperature measurements are thus $\pm$ 25 kPa and $\pm$ 0.1 K, respectively.

2.2 Gas Chromatography System

The SRI 8610 gas chromatograph having a thermal conductivity detector (TCD) and flame ionization detector (FID) was installed for the gas sample analysis. In this work the TCD detector was used to analyze the methane and carbon dioxide gas. The TCD measures the variation in resistance in a filament that has current applied to it as the carrier gas flows over it. The SRI TCD employs the Wheatstone bridge design, utilizing four heated tungsten-rhenium wire filaments for optimum response. Four heated wire filaments are configured so that sample-laden carrier gas passes over two diagonally-opposed filaments while clean carrier gas is passed over the other two filaments, which provide a stable reference signal to the amplifier. As sample components elute from the column and into the detector block which contains all four filaments, the effluent is directed only over the two filaments in the sample stream. This upsets the balance of the bridge current with respect to the reference signal due to the change in filament resistance, and this deflection is translated into an analog signal that is sent to the data system for analysis. The detector block is located within a temperature-controlled oven for high stability.

Helium gas was used as the carrier at the steady flow of 28.8 mL/min. The Porapaq-N column of 10 ft. length and 1/8 in. outer diameter SS was used for the separation of the gas mixture. The temperature of TCD oven, load-injector valve and column was maintained at 150, 70 and 70 °C respectively. The TCD current was set to high. The above operating condition was optimized to obtain the highest sensitivity and resolution of the binary mixture of methane and carbon dioxide gas and to minimize the gas analysis time. The gas chromatograph was then calibrated using pure methane and carbon dioxide gas. The thermal response factor of 1.37 was obtained for carbon dioxide to methane ratio, while 1.35 ± 3% is reported by Dietz (1967). The error in gas composition measurement is ± 0.5 mole %.

Ultra high purity methane gas supplied by Matheson Gas Inc. and Coleman Instrument grade CO_2 (Linde's) were used. The water was de-ionized and double-distilled.

The gas sampling line was taken from the side of the reactor, just above the gas-liquid interface (see Figure 2.1). This line was connected to the flushing gas (helium) and to the gas chromatograph sampling loop via needle valves. A pressure gauge was installed to monitor the pressure in the gas sampling line. A bleed was provided for flushing of the sampling line to ensure that the line was free of residue from the previous sample.

2.3 Experimental Procedure

For each gas under study, a partial three phase equilibrium diagram for the gas water system was computed. For the CH_4 and CO_2 gas mixtures, the dew point pressure was calculated using the MEGHA Simulator (a software package) and the hydrate equilibrium pressure was obtained from the correlation given by Adisasmito et al. (1991). Figure 2.2 shows the hydrate equilibrium conditions for the binary gas mixture of CH_4 and CO_2 mixtures. The dotted line indicates the dew points of the binary gas mixture and the solid line the three phase equilibrium conditions. All formation experiments were conducted in the region above the equilibrium line and below the dew pressure curve. Each experiment corresponded to a particular point on the P-T diagram within the above region.

At the start of the experiment, the reactor was rinsed twice with de-ionized and distilled water. 300 cm^3 of the water were then introduced into the reactor. Subsequently, the reactor was purged with the experimental gas to drive away any air that may have entered during the charging of the solution. The solution was then allowed to cool. In the meantime, the bias reservoirs R2 and R5 (see Figure 2.1) were pressurized to a value roughly 0.1 MPa less than the experimental pressure and the supply reservoir R1 to about 0.4 MPa above the experimental pressure. When the solution attained thermal equilibrium, the reactor was pressurized to the experimental pressure by supplying gas from the

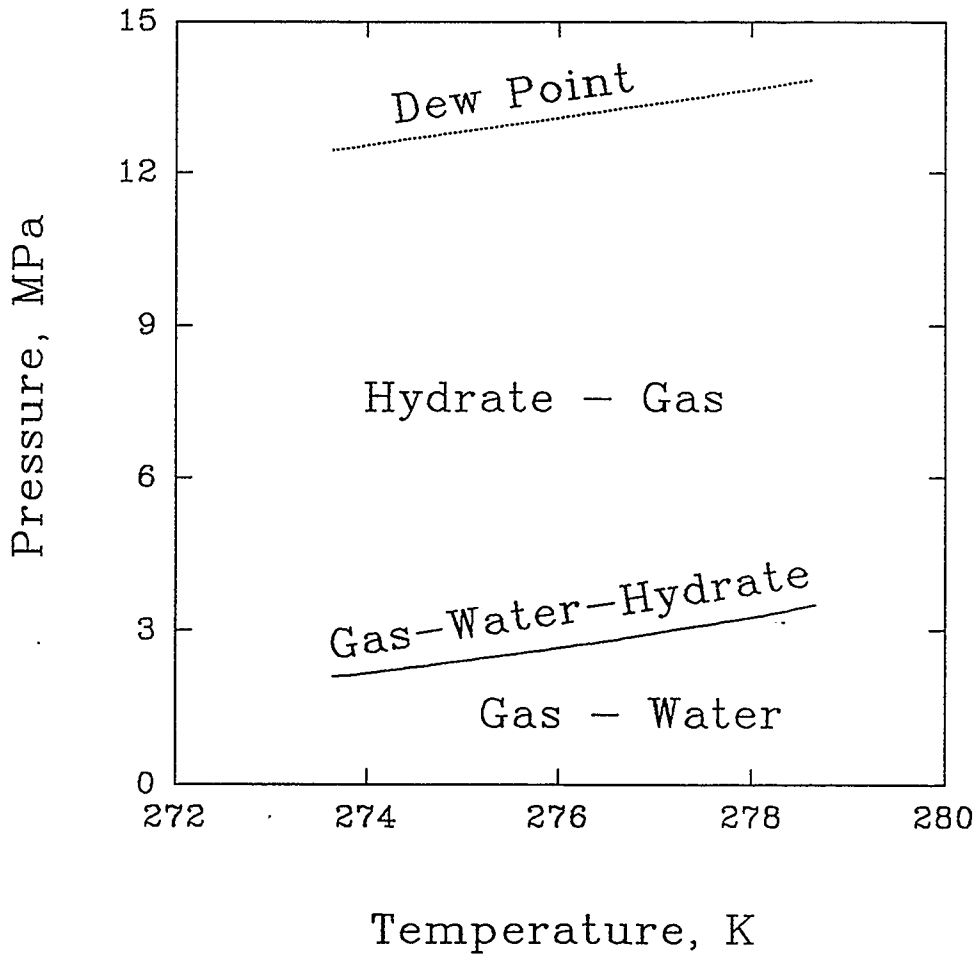

Figure 2.2 Hydrate Equilibrium Conditions for the Binary Gas Mixture of CH_4 (80.3%) & CO_2

cylinder. A sample was withdrawn from the reactor gas phase and injected in the gas chromatograph for its analysis at the start of the experiment. As the temperature and pressure of the reactor gas phase stabilizes, the pressure controller was put on auto, the data acquisition was commenced and the stirrer was started at the rate of 400 RPM. Since the time taken for the gas analysis of every sample was 5 minutes, the gas phase of the reactor was analyzed after every 6 minutes by withdrawing the sample and injecting into the gas chromatograph. After each gas analysis, the sampling line was flushed with the flushing gas (same as carrier gas - helium) to drive away the residue of the previous sample. The reactor contents were watched constantly for turbidity in the liquid phase. The solution is considered turbid when it becomes translucent due to sudden emergence of hydrate particles (nuclei). When the turbidity occurs, the "turbidity time" was noted. Hydrate growth was continued for 100 minutes after the turbidity time.

2.4 Ruska Pump Experiment

The Ruska Pump Experiment is performed to determine the volume of the supply reservoir needed for the calculations of the amount of gas consumed in moles, during the hydrate forming experiment. In the Ruska Pump experiment a known volume of mercury was pumped into the reservoir and the pressure was measured before and after the mercury was pumped in. Since the number of gas molecules within the reservoir remained constant, the pressure and volume of the reservoir have the following relation

$$\frac{P_1 V_{S,1}}{P_2 V_{S,2}} = \frac{z_1 T_1}{z_2 T_2} \qquad 2.1$$

Hence the volume of gas in the reservoir, V_S is given by the relation

$$V_S = V_{S,2} = \frac{(V_{S,1} - V_{S,2})}{\left(\frac{P_2 z_1 T_1}{P_1 z_2 T_2} - 1\right)} \qquad \textbf{2.2}$$

where subscript **1** and **2** denote the initial and final equilibrium state before and after the mercury injection into the reservoir respectively. The compressibility factor z was obtained from the Trebble-Bishnoi equation of state and the volume difference ($V_{S,1}$ - $V_{S,2}$), which was equal to the volume of mercury pumped, was measured from the Ruska Pump reading. The experimental error involved in the measurement of volume difference was less than 0.01 cm^3.

3. EXPERIMENTAL DATA

The experiments were conducted, as part of this work, to obtain data on the kinetics of hydrate formation from a binary mixture of methane (80.3 %) and carbon dioxide at three different temperatures of 274, 276 and 278 K and at pressures in the range of 2.69 to 4.58 MPa. All the data were collected under isothermal - isobaric conditions by contacting the gas and water in a semi-batch stirred tank reactor. The stirring rate was set at 400 RPM. The experimental apparatus and procedure was modified, as described earlier, by integrating the gas chromatograph and the gas sampling line to analyze the reactor gas phase for mixture of gases. The method to calculate the number of the moles of the gas consumed due to dissolution and hydrate formation during the experiment is given here. Finally the experimental gas consumption curves and results are presented.

3.1 Analysis of Reactor Gas Phase

From the experimental data of pure methane and carbon dioxide, it was observed that the carbon dioxide has higher solubility in water than methane. Hence for the experiments to be conducted with the binary mixture of methane and carbon dioxide, it becomes essential to analyze the gas phase of the reactor. The analysis of the reactor gas phase for the CH_4 - CO_2 mixtures was done every 6 minutes during an experiment. The following sigma function was used to represent the methane gas composition (Y, %) in the reactor gas phase with time (t, min.). The constants a, b, c and d were estimated from the experimental results by minimizing the sum of the squares of the deviations.

$$Y = a + \frac{b}{\left(1+\exp\left(-\frac{(t-c)}{d}\right)\right)} \qquad 3.1$$

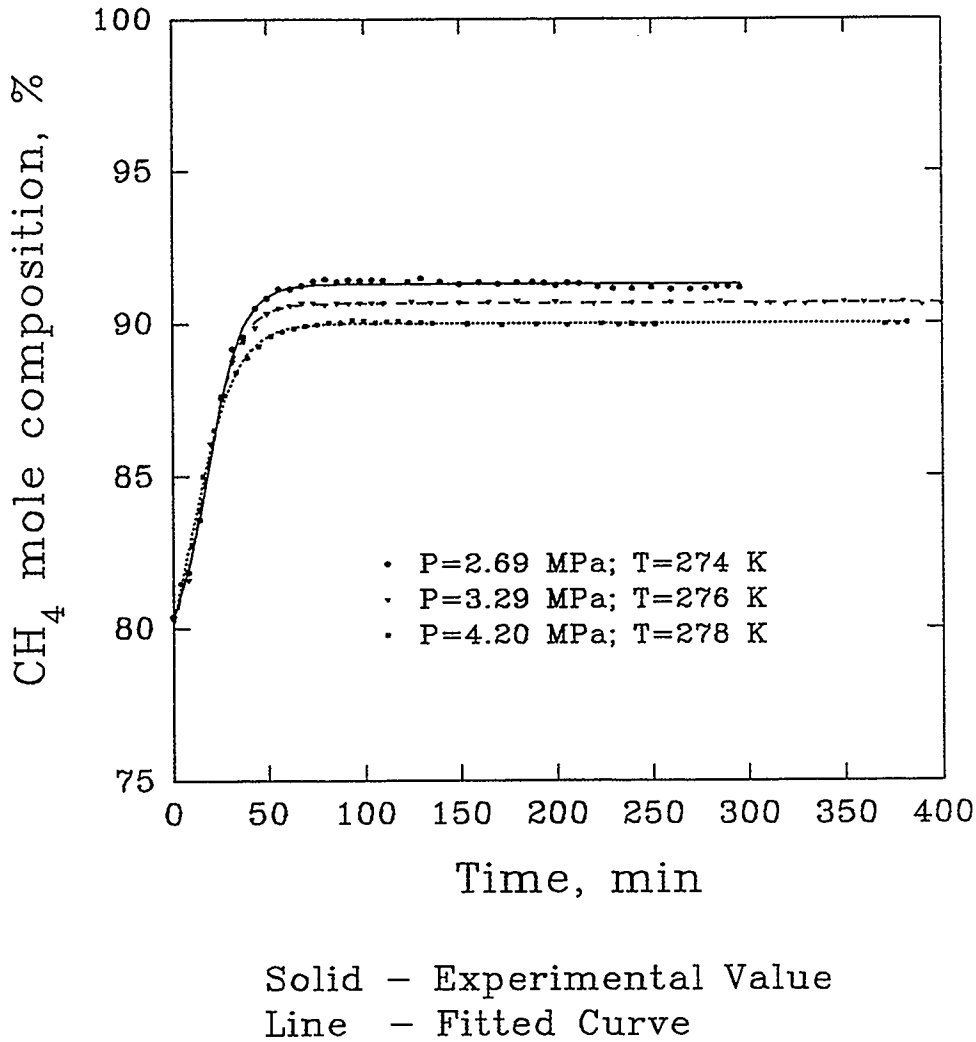

Figure 3.1 Reactor Gas Phase Analysis for the Binary Gas Mixture of CH_4 (80.3%) and CO_2.

Figure 3.1 shows the reactor gas phase analysis at various time intervals during an experiment for three different isotherms. It indicates that Equation 3.1 fits the experimental data very well. Also it was found that the methane gas composition in the reactor gas phase first increases and then remains constant. From the experimental data, it was observed that during hydrate formation the change in the mole fraction of a component in the gas phase of the reactor from the turbidity point till the end of a run was less than 0.005. Table 3.1 list the experimental gas composition at the turbidity point for all the experiments for a binary mixture of methane and carbon dioxide hydrate formation.

3.2 Calculation of the Amounts of Gas Consumed

During an experiment the data acquisition scans the pressures and temperatures of the reactor and the reservoirs every 15 seconds. The number of the moles of the individual gas that have been transported into the liquid is the difference between the number of the moles of the gas present in the reactor and supply reservoir at time t=0 (start of the stirring) and the number of moles of the gas at time t. Namely,

$$n_i = \left[V_R \left(\frac{y_i P}{zRT} \right)_R + V_S \left(\frac{y_i P}{zRT} \right)_S \right]_{t=0} - \left[V_R \left(\frac{y_i P}{zRT} \right)_R + V_S \left(\frac{y_i P}{zRT} \right)_S \right]_{t=t} \qquad 3.2$$

where subscripts ***i, R, S*** stand for component, reactor and supply reservoir respectively. The V_R is the volume of reactor gas phase including tubing and V_S is the volume of the supply reservoir, determined from the Ruska Pump experiment. The gas composition in the reactor gas phase was obtained from Equation 3.1 and z was calculated using the Trebble-Bishnoi EOS.

The moles calculated from Equation 3.2 were corrected to account for the moles of gas consumed during initial dissolution due to the time given for stabilizing the temperature

Table 3.1 Experimental Methane Gas Composition at Turbidity Point for Binary Mixture of CH_4 (80.3%) and CO_2 Hydrate Formation.

No.	Nominal Temperature (K)	Experimental Temperature (K)	Experimental Pressure (MPa)	Turbidity Point (min.)	Gas Composition at turbidity point (CH_4 mol %)
1	274	274.0	2.69	177.0	91.4
2	274	273.9	2.79	108.5	91.2
3	274	274.0	2.88	74.5	91.3
4	274	274.0	2.99	87.5	91.2
5	276	276.1	3.29	303.0	90.6
6	276	276.0	3.39	119.0	90.6
7	276	276.1	3.48	94.0	90.5
8	276	276.0	3.68	69.0	90.1
9	278	278.1	4.20	232.5	89.9
10	278	278.0	4.29	96.0	89.8
11	278	278.1	4.38	95.0	89.9
12	278	278.1	4.58	92.0	89.7

and pressure of the reactor, i.e the time between the charging of the reactor and commencing of the data acquisition (prior to the start of the stirrer). Assuming that there was no interaction effect during the simultaneous absorption of gases into quiescent liquid water, the moles of the gas absorbed in water during initial dissolution are given by (refer to Appendix A for the derivation)

$$n_{i0} = \frac{2 A f_i c_{w0}}{H_i} \sqrt{\frac{D_i t}{\pi}} \qquad 3.3$$

where A is the gas liquid surface area, f_i is the fugacity of gas 'i' at initial composition of the gas in the reactor, H is the Henry's constant, c_{w0} is the initial concentration of water molecules, D is the diffusivity and t is the time between the charging of the reactor and commencing of the data acquisition.

The total amount of the gas consumed in the liquid is the summation of all individual gases consumed in the liquid.

$$n_t = \sum_{i=1}^{N} n_i + n_{i0} \qquad 3.4$$

3.3 Experimental Gas Consumption Curve

Equations 3.1 - 3.4 were used to calculate the number of moles of the gas consumed due to dissolution and hydrate formation during the experiment. Figures 3.2 - 3.7 represent the experimental gas consumption curve for the gas mixture of CH_4 (80.3%) and CO_2 (19.7%), which is a plot of the number of moles of gas consumed versus time. The t_{tb} is the turbidity time, indicated by the arrow line, at which the nuclei appear. From the beginning of the experiment until the turbidity point, the process is simply a physical

absorption of the gas. From the turbidity time onwards, the process is a gas hydrate formation. Both parts of the experimental data have been modeled in this work.

3.4 Experimental Results and Discussion

As seen from Figure 3.1, the methane gas composition in the reactor gas phase increases linearly and then approaches an asymptotic value. This is due to the higher solubility of carbon dioxide in water than methane (see Figures 3.2 - 3.7). As the water gets saturated with carbon dioxide, the gas phase composition also attains a constant value.

Figures 3.2 and 3.3 represent the gas consumption curves at a temperature of 274 K with small and large driving forces. The driving force is the difference between the gas fugacity and the three phase equilibrium fugacity. For the higher driving force, the time taken for the solution to get saturated is small and thus the turbidity time for the hydrate nuclei to appear is small. Before the turbidity time, the consumption of the carbon dioxide gas in water is larger than the methane gas due to a higher solubility. It was also observed that there was a reverse diffusion of methane gas during the absorption of the two gases, which implies that there is a strong interaction between the two gases during dissolution. The formation of gas hydrates is a phase transformation which requires a supersaturated environment to occur. It is seen that at the turbidity point the moles consumed for carbon dioxide reaches a plateau while that for methane still increases. After the turbidity time, the rate of methane gas consumption is higher than that of carbon dioxide gas. During hydrate formation, both small and large cavities of structure I are occupied by methane and carbon dioxide. This is because the molecular diameter of both the gases are less than the diameter of the cavity. The hydrate equilibrium composition on water free basis is given in Table 3.2. It is seen that methane composition in the hydrate phase on water free basis is higher than that of carbon dioxide. This probably explains for the higher rate of methane gas consumption during hydrate formation. A similar effect was also observed for

the experiments at different isotherms (see Figures 3.4 - 3.7). Also with the increase in temperature and pressure, the consumption of both the gases increased.

Figure 3.8 represents the methane and carbon dioxide gas consumption for all the experiments till the turbidity point. It is interesting to note that for methane gas consumption the maxima occur at nearly the same time and the moles consumed are almost same for all the experiments. Similar was the case for the minima too.

Table 3.2 Equilibrium Hydrate Composition on Water Free Basis

No.	Nominal Temperature (K)	Experimental Temperature (K)	Experimental Pressure (MPa)	Equilibrium Pressure (MPa)!	Equilibrium Hydrate Comp. on H_2O Free Basis (mol %)!	
					CH_4	CO_2
1	274	274.0	2.69	2.46	81.48	18.52
2	274	273.9	2.79	2.43	81.18	18.82
3	274	274.0	2.88	2.46	81.33	18.67
4	274	274.0	2.99	2.46	81.18	18.82
5	276	276.1	3.29	3.01	80.64	19.36
6	276	276.0	3.39	2.98	80.63	19.37
7	276	276.1	3.48	3.00	80.44	19.56
8	276	276.0	3.68	2.96	79.95	20.05
9	278	278.1	4.20	3.65	80.02	19.98
10	278	278.0	4.29	3.61	79.75	20.25
11	278	278.1	4.38	3.65	79.95	20.05
12	278	278.1	4.58	3.65	79.68	20.32

! Computed using MEGHA Simulator (a software package) for the experimental temperature and pressure and the gas composition at the turbidity point.

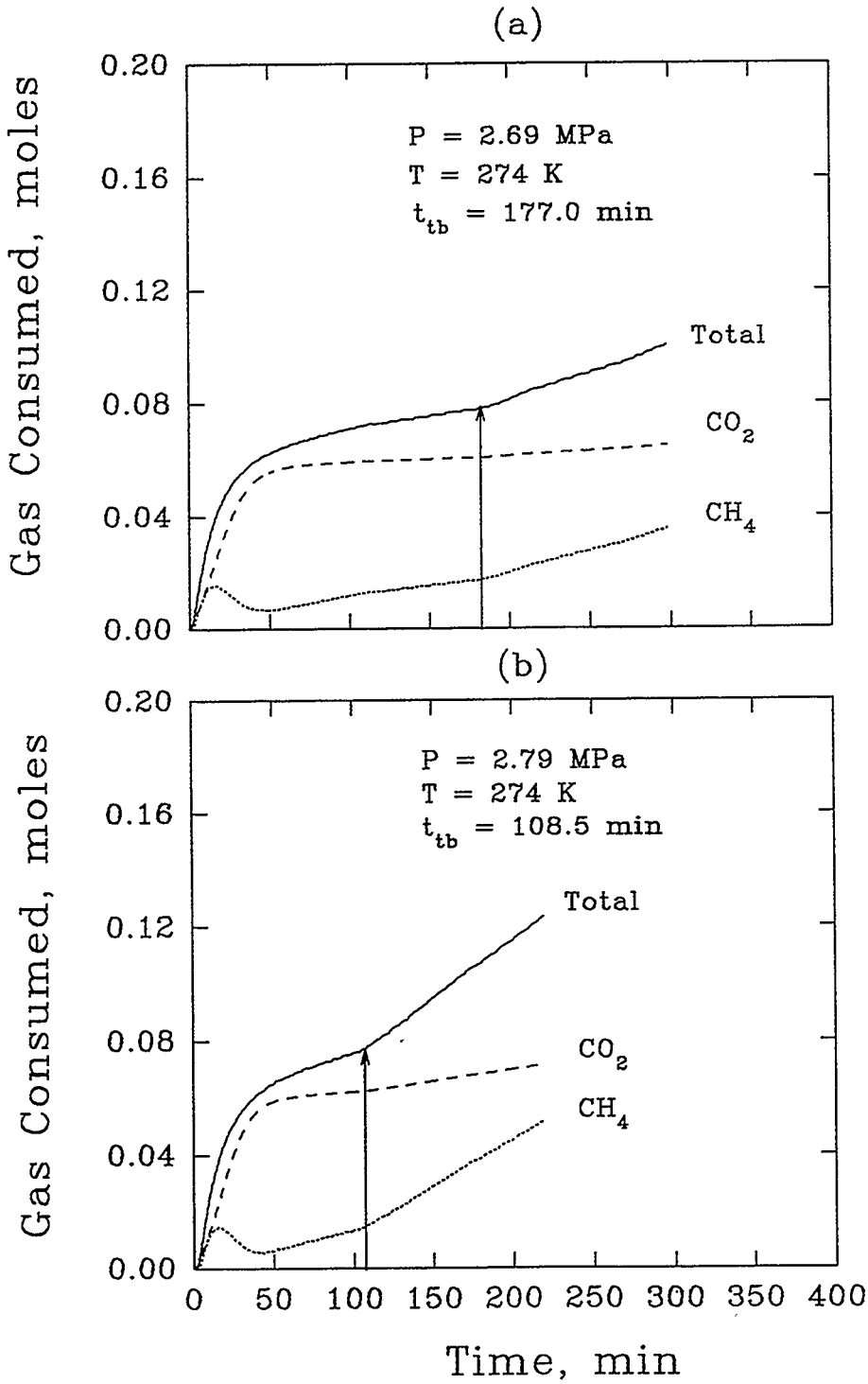

Figure 3.2 Experimental Gas Consumption Curve for the CH_4 (80.3%) and CO_2 (19.7%) Gas Mixture at T=274 K and P=2.69 MPa (a); P=2.79 MPa (b).

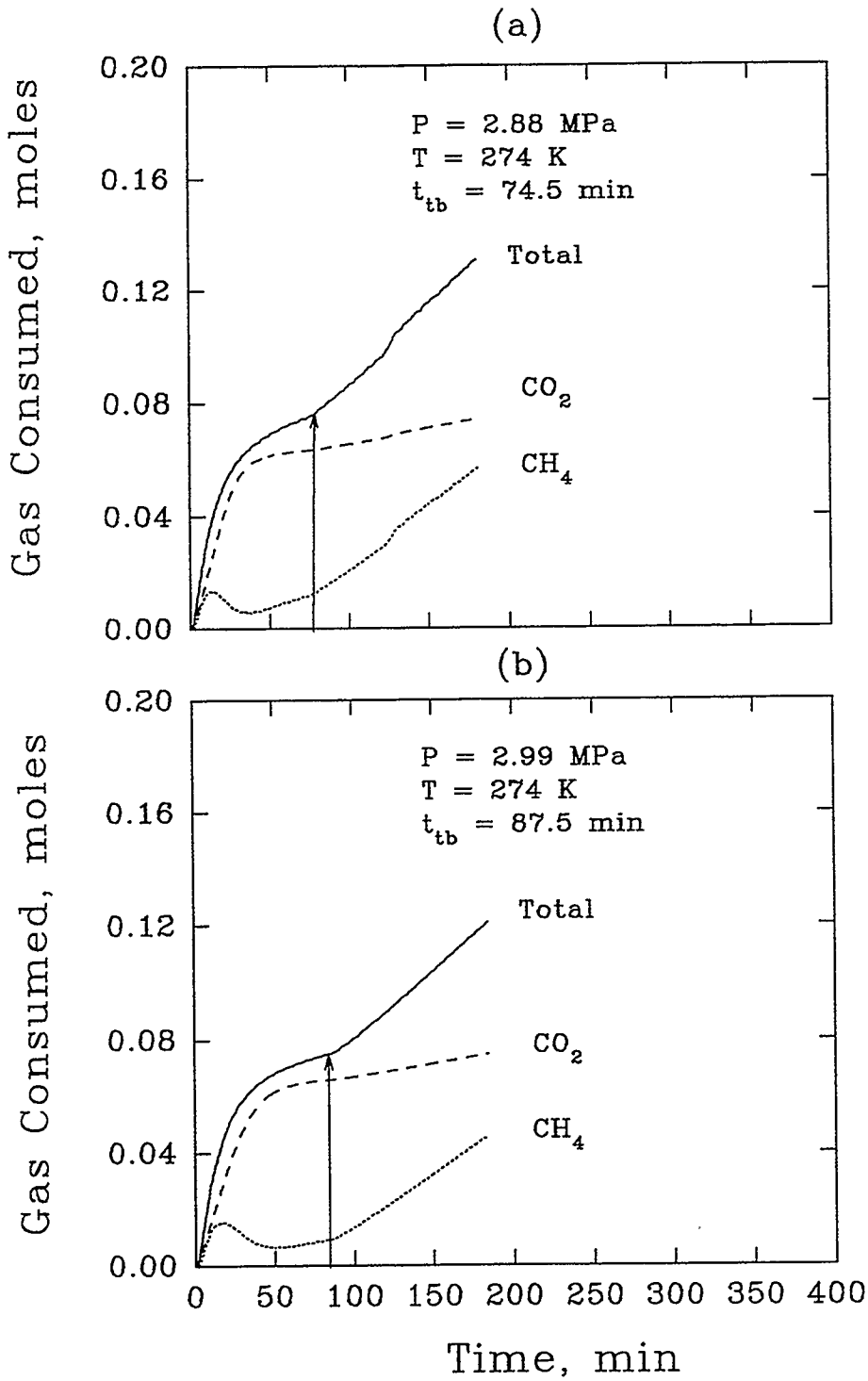

Figure 3.3 Experimental Gas Consumption Curve for the CH_4 (80.3%) and CO_2 (19.7%) Gas Mixture at T=274 K and P=2.88 MPa (a); P=2.99 MPa (b).

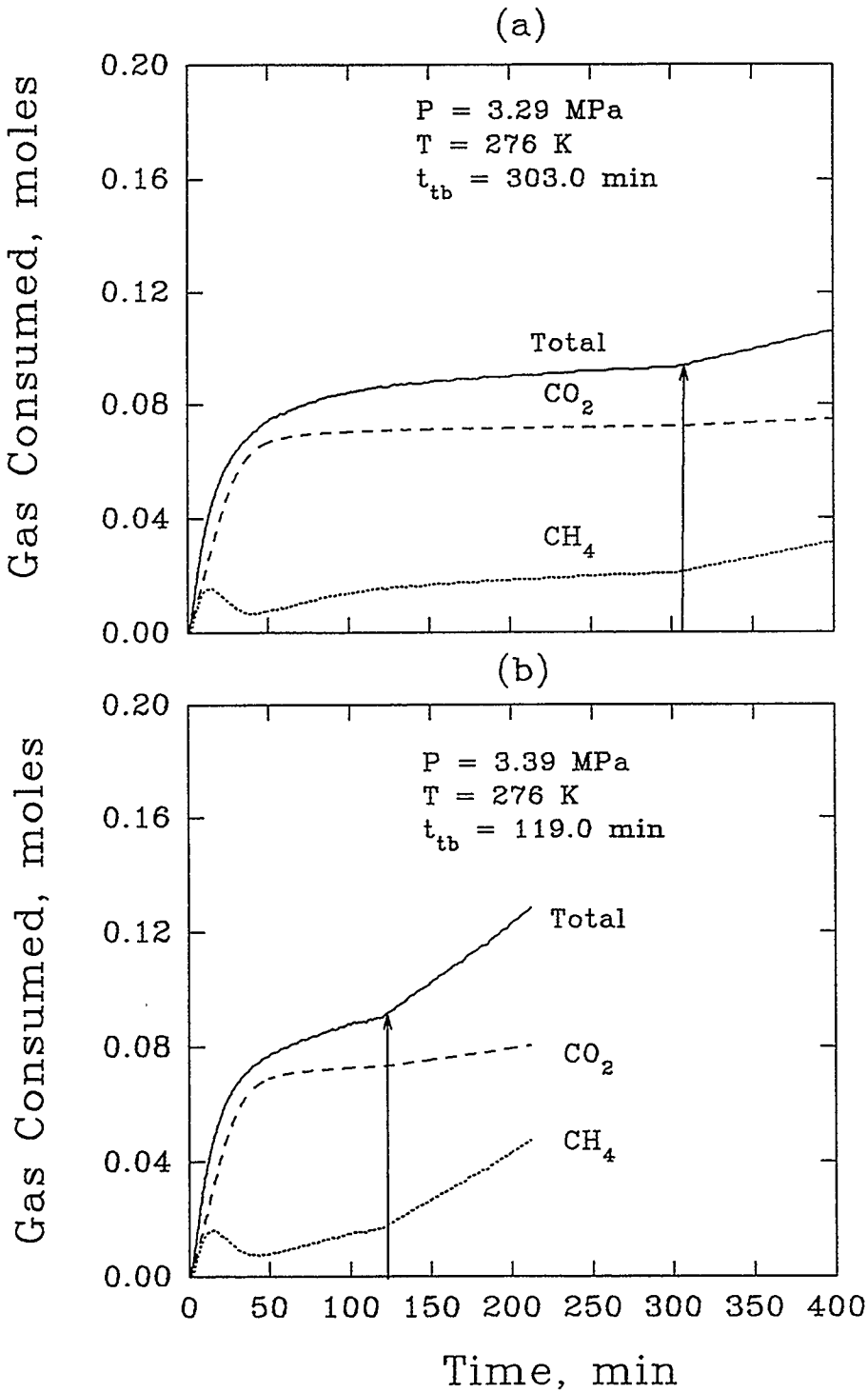

Figure 3.4 Experimental Gas Consumption Curve for the CH_4 (80.3%) and CO_2 (19.7%) Gas Mixture at T=276 K and P=3.29 MPa (a); P=3.39 MPa (b).

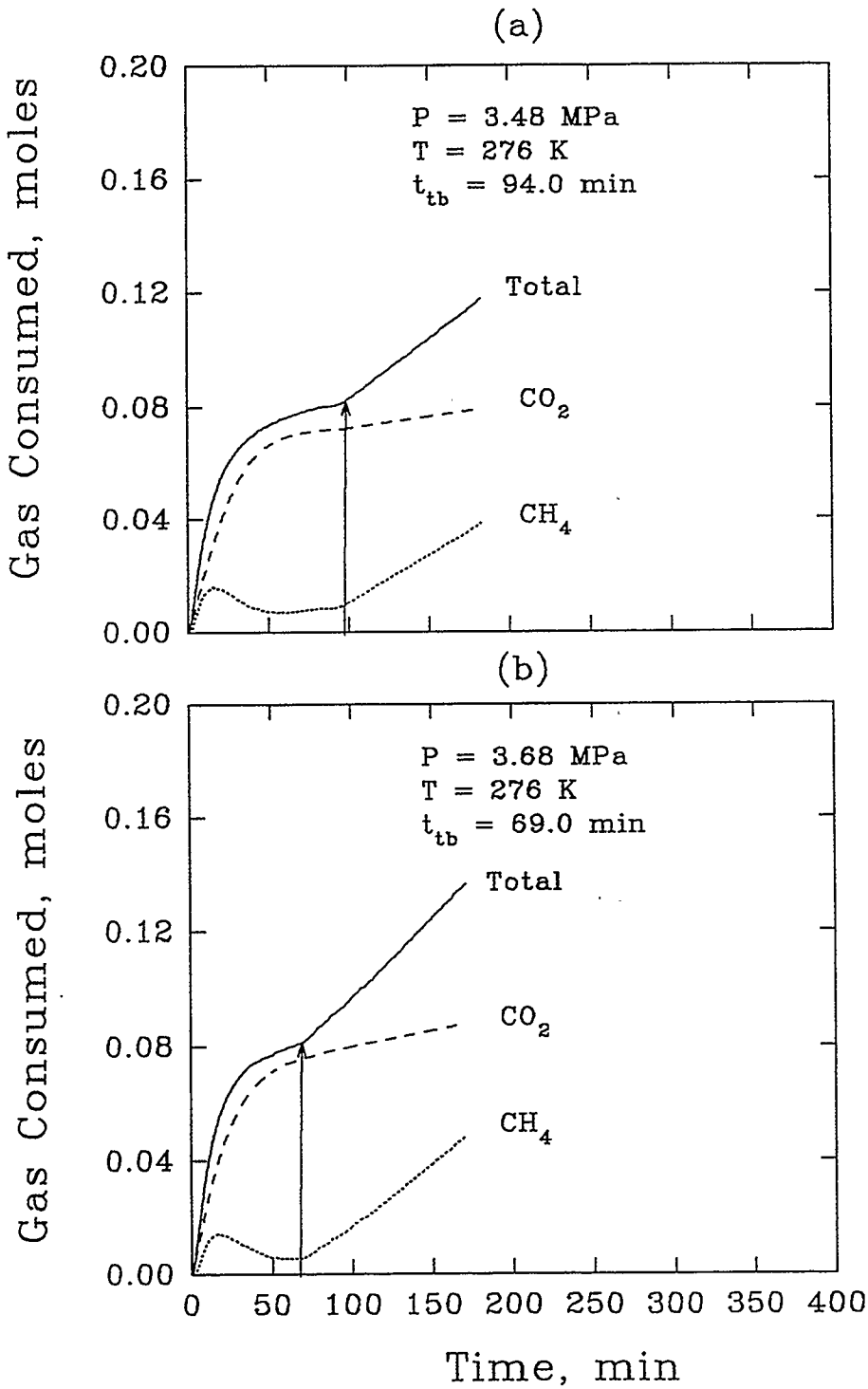

Figure 3.5 Experimental Gas Consumption Curve for the CH_4 (80.3%) and CO_2 (19.7%) Gas Mixture at T=276 K and P=3.48 MPa (a); P=3.68 MPa (b).

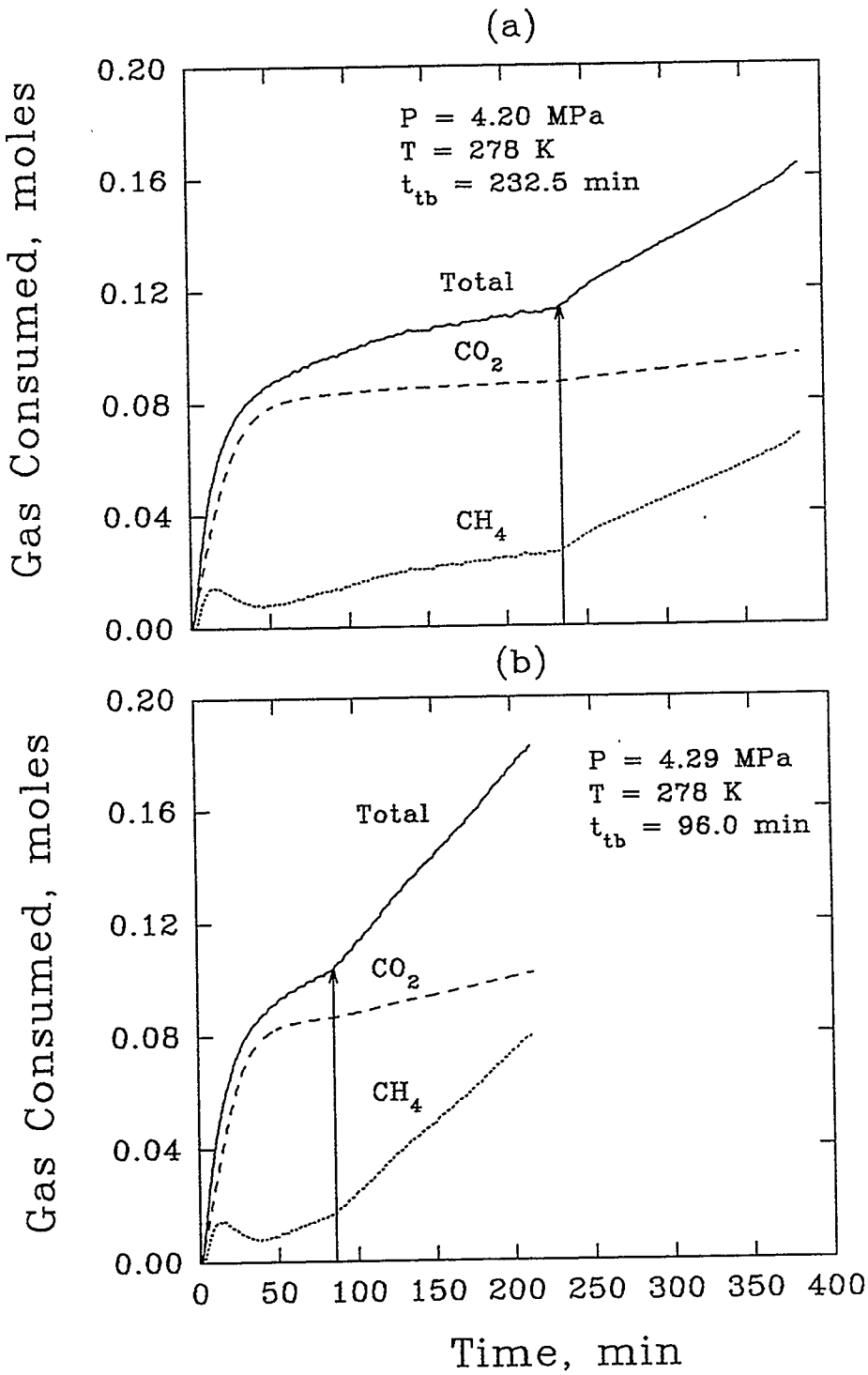

Figure 3.6 Experimental Gas Consumption Curve for the CH_4 (80.3%) and CO_2 (19.7%) Gas Mixture at T=278 K and P=4.20 MPa (a); P=4.29 MPa (b).

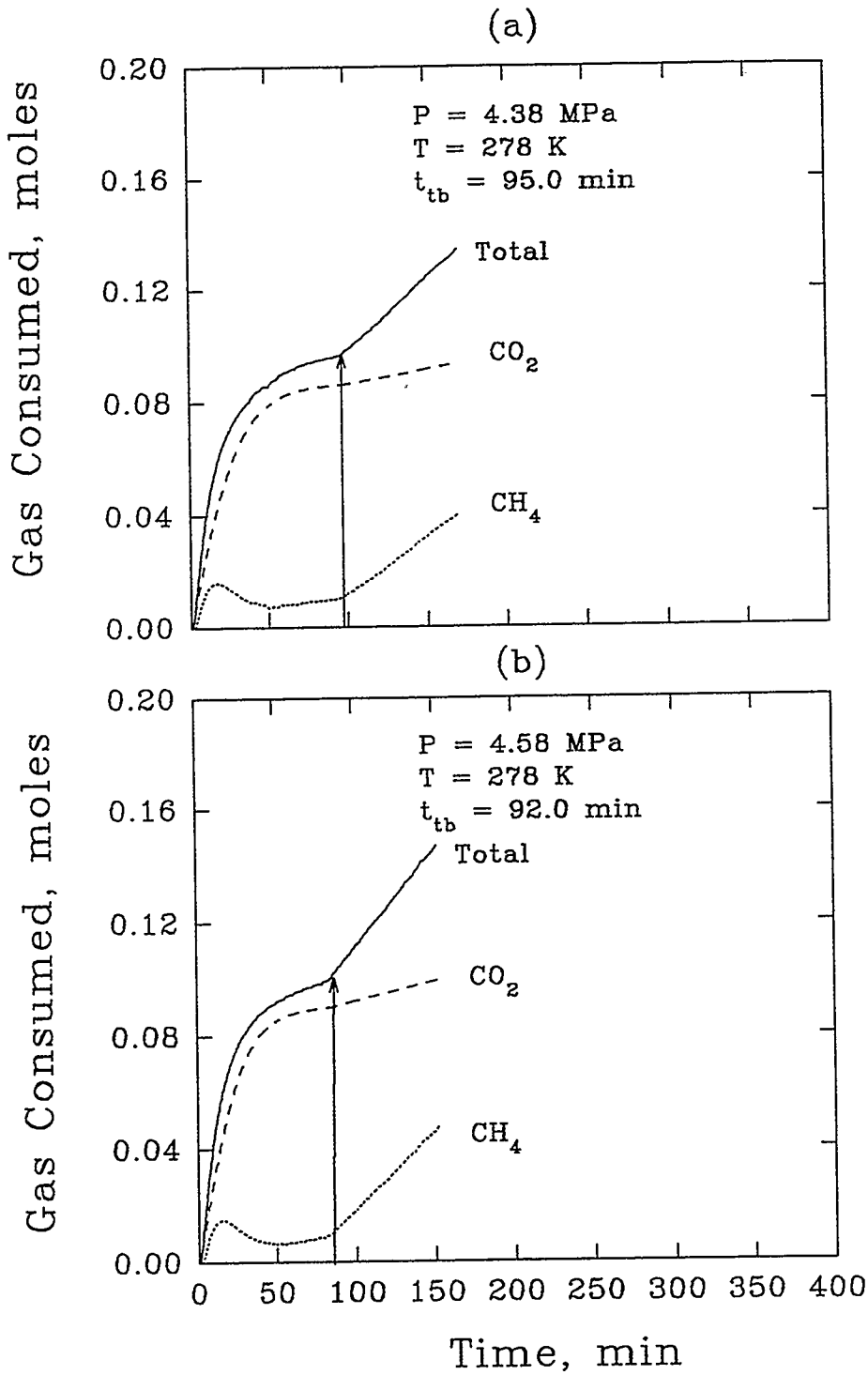

Figure 3.7 Experimental Gas Consumption Curve for the CH_4 (80.3%) and CO_2 (19.7%) Gas Mixture at T=278 K and P=4.38 MPa (a); P=4.58 MPa (b).

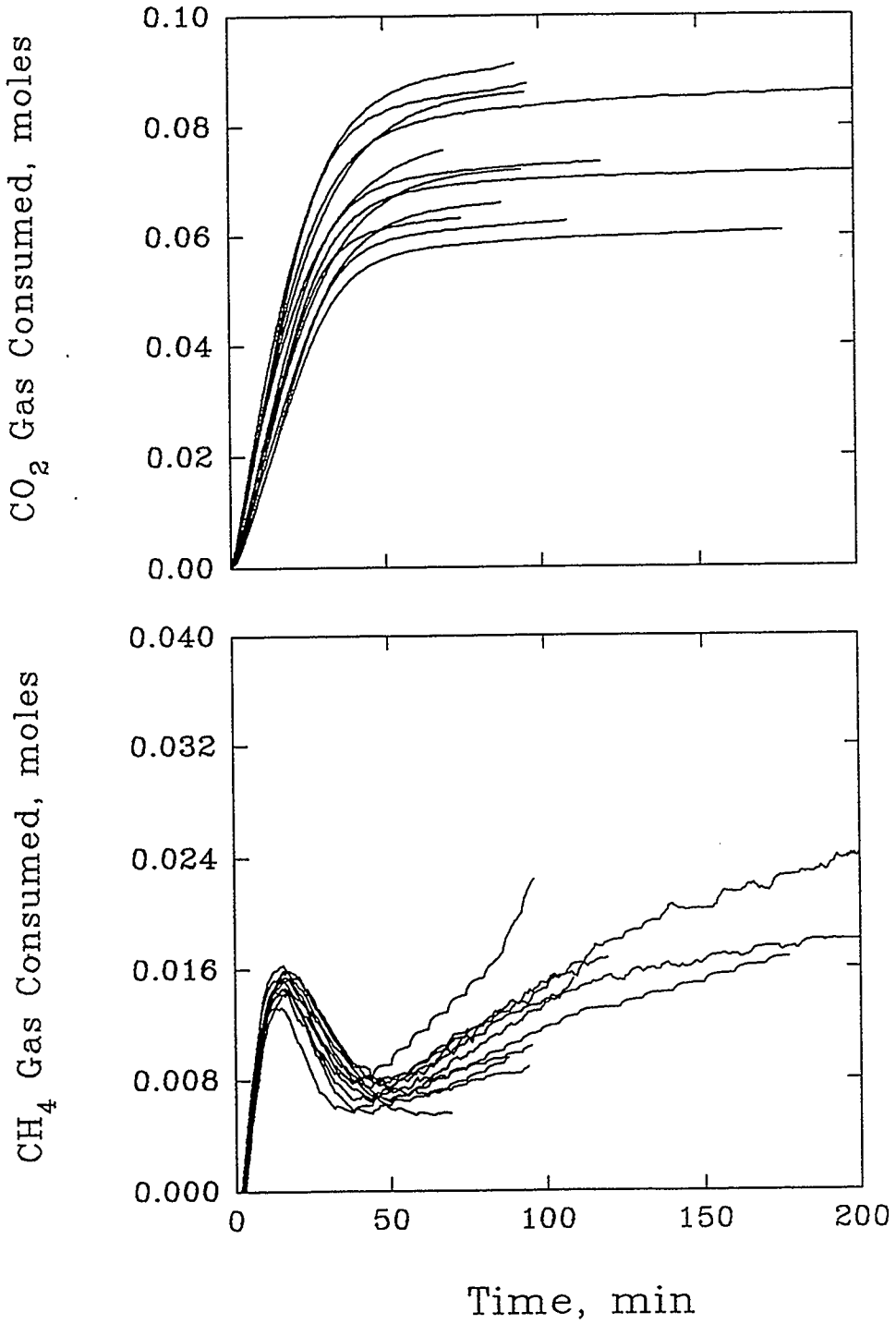

Figure 3.8 Methane and Carbon Dioxide Gas Consumption Curve for All the Experiments Till the Turbidity Point

4. KINETICS OF PURE GAS HYDRATE FORMATION

A brief overview of the kinetic model developed by Englezos et al. (1987a) for pure gas hydrate formation is given here. This kinetic model was adapted to determine the kinetic rate constants of CH_4 and CO_2 gas hydrates from the kinetic data, obtained from the work of Bishnoi et al. (1985, 1986) and additional previous work in this department. The model parameters and their computational method or source is also described. Finally the experimental results and the predictions are presented.

4.1 Kinetic Modeling

Englezos et al. (1987a) considered the growth of hydrate crystals as a two-step process and used the two-film theory to describe the absorption of gas at the gas-liquid interface. As shown in Figure 4.1, each particle, which was assumed to be spherical, is surrounded by an adsorption "reaction" layer followed by a stagnant diffusion layer. Particles could be located either in the liquid film at the gas-liquid interface or in the bulk of the solution. The dissolved gas diffuses from the solution surrounding the stagnant layer to the hydrate particle-water interface and then, by an adsorption process, the gas molecules are incorporated into the structured water framework. The driving forces for the diffusion around the particles is $(f - f_s)$ and that for the "reaction" step is $(f_s - f_{eq})$. At steady state, the rates of the two steps are equal, f_s can be eliminated from the individual rate expressions to yield the rate of growth per particle:

$$\left(\frac{dn}{dt}\right)_p = K^* A_p \left(f - f_{eq}\right) \qquad 4.1$$

The quantity $(f - f_{eq})$, which is the difference in the fugacity of the dissolved gas and its fugacity at the three phase equilibrium, defines the overall driving force. K^* is the

combined rate constant for the diffusion and adsorption processes and A_p is the surface area of each particle. A global reaction rate for all the particles is given by

$$R_y(t) = \int_0^\infty \left(\frac{dn}{dt}\right)_p \phi(s,t)\,ds \qquad 4.2$$

$$= \int_0^\infty K^* A_p \left(f - f_{eq}\right) \phi(s,t)\,ds \qquad 4.3$$

$$= \pi K^* \mu_2 \left(f - f_{eq}\right) \qquad 4.4$$

$$= K\left(f - f_{eq}\right) \qquad 4.5$$

where $\phi(s,t)$ is the particle size distribution and μ_2 is the second moment of the particle given by

$$\mu_2 = \int_0^\infty s^2 \phi(s,t)\,ds \qquad 4.6$$

The two film theory has been used to describe the absorption of the gas at the gas-liquid interface. Assuming quasi-steady-state conditions, the diffusion and reaction in the liquid film are given by

$$D\frac{d^2c}{dy^2} = K\left(f - f_{eq}\right) \qquad 4.7$$

Assuming the number of moles of the water remains practically constant, the concentration of gas in the aqueous phase at three phase equilibrium can be estimated by

$$c_{eq} = \frac{c_{wo} f_{eq}}{\left(H - f_{eq}\right)} \qquad 4.8$$

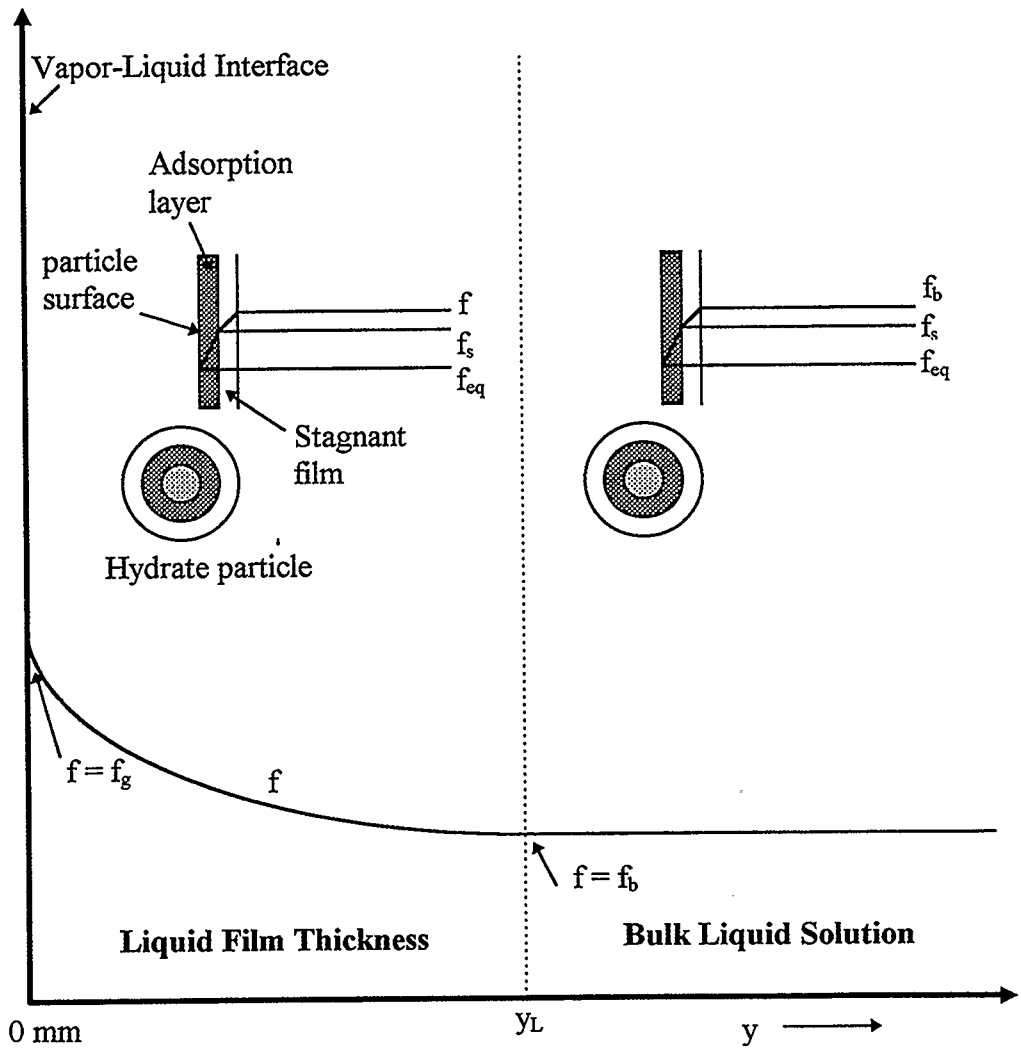

Figure 4.1 Schematic Representation of the Fugacity of Gas in the Liquid and Around a particle (Dholabhai et al. 1993)

The change in the concentration of the gas in the aqueous phase can be computed as, (refer to Appendix B for the derivation)

$$\delta c = \left(\frac{c_{eq}+c_{wo}}{H-f_{eq}}\right)\delta f \qquad 4.9$$

where $\delta c = c - c_{eq}$ and $\delta f = f - f_{eq}$. Thus equation 4.7 can be written as

$$D^{*}\frac{d^2Y}{dy^2} = KY \qquad 4.10$$

where,

$$Y = f - f_{eq}, \qquad D^{*} = D\left(\frac{c_{eq}+c_{wo}}{H-f_{eq}}\right) \qquad 4.11$$

Equation 4.10 satisfies the following boundary conditions:

$$\begin{aligned} &at \quad y=0, \qquad Y = f_g - f_{eq} \\ &at \quad y=y_L, \qquad Y = f_b - f_{eq} \end{aligned} \qquad 4.12$$

Analytical solution of Equation 4.10 with the above boundary conditions yields the fugacity profile for the gas in the liquid film:

$$f = f_{eq} + \left(\frac{1}{\sinh\gamma}\right)\left\{\left(f_g - f_{eq}\right)\sinh\left(\gamma\left(1-\frac{y}{y_L}\right)\right) + \left(f_b - f_{eq}\right)\sinh\left(\gamma\frac{y}{y_L}\right)\right\} \qquad 4.13$$

where γ is the Hatta number given by :

$$\gamma = y_L\sqrt{\frac{\pi K^{*}\mu_2}{D^{*}}} \qquad 4.14$$

The flux at the interface can then be obtained from

$$(J)_{y=0} = -D\left(\frac{dc}{dy}\right)_{y=0} = -D^{*}\left(\frac{df}{dy}\right)_{y=0} \qquad 4.15$$

The rate of transportation of the gas to the liquid phase, where it either goes into solution or is converted to hydrates, is related to the flux at the gas-liquid interface by the following equation:

$$\frac{dn}{dt} = (J)_{y=0} A_{(g-l)} \qquad 4.16$$

Substitution of Equation 4.13 into Equation 4.15 and subsequent expression into 4.16 yields

$$\frac{dn}{dt} = \left(\frac{D^{*}\gamma A_{(g-l)}}{y_L}\right)\frac{\left((f_g - f_{eq})\cosh\gamma - (f_b - f_{eq})\right)}{\sinh\gamma} \qquad 4.17$$

The initial condition for this equation is the number of moles of the gas that have been transported into the aqueous phase up to the "turbidity point". This is available from the experimental data. The variation in the fugacity of gas in the bulk aqueous phase with respect to time is obtained by a mass balance in the bulk:

$$\frac{df_b}{dt} = \left(\frac{D^{*}\gamma a (H - f_{eq})^2}{H c_{wo} y_L \sinh\gamma}\right)\left\{(f_g - f_{eq}) - (f_b - f_{eq})\cosh\gamma\right\} - \frac{\pi K^{*}\mu_2 (H - f_{eq})^2 (f_b - f_{eq})}{H c_{wo}} \qquad 4.18$$

It is assumed in the model that at the turbidity point the fugacity of gas in the bulk aqueous phase drops to the three-phase equilibrium value instantaneously.

In addition to the mass balances, a population balance is needed in order to estimate μ_2 vs. time. According to Kane et al. (1974), the population balance is given by

$$\frac{\partial \phi}{\partial t} + \frac{\partial (G\phi)}{\partial s} = \theta \psi(s) \qquad 4.19$$

The first term on the left-hand side represents the change in the number of crystals in the size range 's' to 's + ds' as a function of time. The second term is the number of crystals growing out of the size range. The term on the right-hand side expresses the number of new crystals nucleated into this size range due to secondary nucleation. It is assumed that:

(a) the linear growth rate is independent of the crystal size;

(b) new crystals are nucleated at near zero time; and

(c) the secondary nucleation rate is proportional to the second moment of the particle size distribution, namely

$$\theta = \alpha_2 \int_0^\infty s^2 \phi(s) ds = \alpha_2 \mu_2 \qquad 4.20$$

This equation implies that the nucleation rate is proportional to the total surface of the particles. Under the above assumptions, it is not necessary to solve equation 4.19 to obtain $\mu_2(t)$. Instead, only the following three ordinary differential equations need to be solved (Englezos et al., 1987a):

$$\frac{d\mu_0}{dt} = \alpha_2 \mu_2; \qquad \mu_0(0) = \mu_0^0 \qquad 4.21$$

$$\frac{d\mu_1}{dt} = G\mu_0; \qquad \mu_1(0) = \mu_1^0 \tag{4.22}$$

$$\frac{d\mu_2}{dt} = 2G\mu_1; \qquad \mu_2(0) = \mu_2^0 \tag{4.23}$$

An average growth rate required for the computation of the first and second moments can be defined as

$$G_{av} = \left(\frac{1}{L}\right)\left[\int_0^{y_L}\left(\frac{ds}{dt}\right)dy + \left(\frac{ds}{dt}\right)_b (L-y_L)\right] \tag{4.24}$$

Since the mass of a particle is $(\rho\ \pi\ s^3)\ /\ 6$, the linear growth rate, ds/dt, is related to $(dn/dt)_p$ through

$$\left(\frac{dn}{dt}\right)_p = \frac{\rho\pi s^2}{2M}\frac{ds}{dt} \tag{4.25}$$

Therefore using Equation 4.1, the linear growth rate is given by

$$\frac{ds}{dt} = \frac{2K^*M(f-f_{eq})}{\rho} \tag{4.26}$$

Upon substitution into Equation 4.24 we obtain

$$G_{av} = \left(\frac{2K^*M}{\rho L}\right)\left(y_L\frac{(f_g+f_b-2f_{eq})(\cosh\gamma-1)}{\gamma\sinh\gamma}+(L-y_L)(f_b-f_{eq})\right) \tag{4.27}$$

The number of particles per unit volume of the aqueous phase at turbidity, μ_0^0, is computed from the moles of the gas that have dissolved just prior to the appearance of the hydrates and the critical radius of the nucleus:

$$\mu_0^0 = \frac{3M\left(n_{tb}-n_{eq}\right)}{4\pi V_L \rho r_{cr}^3} \qquad 4.28$$

If n_{tb} moles of gas have dissolved into the aqueous phase at the turbidity point then the moles of the gas used up for the formation of the nuclei are equal to n_{tb} - n_{eq}. The value of n_{eq} is obtained from f_{eq} and the Henry's constant. The critical radius of the nucleus (Englezos et al., 1987a) is given by $r_{cr} = -(2\sigma/\Delta g)$ and the free energy per unit volume of the product formed, Δg, is obtained from:

$$-\Delta g = \left(\frac{RT_{\exp}}{v_m}\right)\left(\ln\frac{f_{tb}}{f_{eq}} + \frac{n_w v_w\left(P_{\exp}-P_{eq}\right)}{RT_{\exp}}\right) \qquad 4.29$$

where f_{tb}/f_{eq} is the supersaturation ratio evaluated just before the turbidity time and f_{tb} is the bulk fugacity of the gas in the liquid given by

$$f_{tb} = H\left(\frac{n_{tb}}{n_{tb}+n_{w0}}\right) \qquad 4.30$$

The initial conditions for the other two moments of the particle size distribution are

$$\mu_1^0 = 2r_{cr}\mu_0^0 \quad \& \quad \mu_2^0 = 4r_{cr}^2\mu_0^0 \qquad 4.31$$

In the model developed by Englezos et al. (1987a), the particle size was represented as the particle radius. This term was overlooked as particle diameter while deriving the equation

for the initial conditions for the first and second moments of the particle size distribution. Thus in Equations (37) and (38) of Englezos et al. (1987a) the factors of 2 and 4 respectively appeared which, in case of a particle radius do not exist. Hence in this work, the inaccuracy of the above equation was corrected and the equations of the model were re-derived considering the particle size as the particle diameter (Nyvlt et al., 1985).

4.2 Determination of Model Parameters

All the model parameters, except the rate constant K^*, could be determined *a priori.* Diffusivity of methane and carbon dioxide in pure water was obtained using the Wilke and Chang correlation with improved parameters given by Hayduk and Laudie (1974). Henry's constant and liquid mass transfer coefficient, $k_L a$, were calculated from solubility data obtained in our laboratory. Solubility experiments were carried out at each nominal temperature. Gas phase fugacities were computed using the TB equation of state (Trebble and Bishnoi, 1987 & 1988). Three phase equilibrium pressures for methane and carbon dioxide were predicted using the method of Englezos and Bishnoi (1991). The gas-liquid interfacial area $A_{(g-l)}$ was determined experimentally for the same apparatus under identical hydrodynamic conditions by Englezos et al. (1987a) to be 127.7 cm^2. Due to a lack of data for hydrates the surface tension , σ, was taken to be equal to that of ice in water. The film thickness was obtained from

$$y_L = \frac{Da}{k_L a} \qquad 4.32$$

Table 4.1 lists the model constant parameters and their values or sources used for the computation of methane and carbon dioxide gas.

Table 4.1 Model Constant Parameters and Their Value/Source.

Parameter	Value/Source	
	Methane Hydrate	*Carbon Dioxide Hydrate*
n_w	5.75 (assumed full occupancy)	5.75 (assumed full occupancy)
Formula	$CH_4.5.75.H_2O$	$CO_2.5.75.H_2O$
M, kg/kmol	119.5	147.5
ρ, kg/m^3	900 (Makogon, 1981)	1100 (Makogon, 1981)
v_m, m^3/mol	0.1328e-3	0.1341e-3
σ, J/m^2	0.026 (Adamson, 1976)	0.026 (Adamson, 1976)
v_w, m^3/mol	1.80e-5	1.76e-5
V_L, m^3	3.0e-4	3.0e-4
$A_{(g-l)}$, m^2	0.01277 (Englezos, 1987a)	0.01277 (Englezos, 1987a)
a, m^2/m^3	42.57	42.57

In solubility experiments the temperature of the aqueous phase increased initially (typically by 0.2 K) due to gas dissolution and then gradually decreased back to its initial value. The average of the recorded temperatures was taken as T_{sol}, which was generally within 0.3 K of the nominal temperature. Henry's constant was computed at T_{sol}. These values were compared with the values available in the literature reported by Lekvam and Bishnoi (1995) and Munjal and Stewart (1971) for CH_4 and CO_2 gas, respectively. During the hydrate formation experiments, the solution temperature increased at the time of turbidity, typically by about 0.2 K for CH_4 and 1.0 K for CO_2. The highest temperature recorded was taken as T_{eq} for the computation of P_{eq}. The values of f_{eq}, n_{eq} and r_{cr} were calculated using these values of P_{eq} and T_{eq}. Subsequent to this surge in temperature, the solution cooled off and in longer experiments, attained the temperature about 0.1 K for CH_4 and 0.6 K for CO_2 higher than that recorded prior to the turbidity point. The average of the recorded temperatures was taken as T_{exp} for all computations of CH_4 gas, which was generally within 0.3 K of the nominal temperature. Due to the substantial rise of the solution temperature during CO_2 hydrate formation, the solution temperature at the time intervals were used for the computations.

4.3 Estimation of K^*.

The five differential equations 4.17, 4.18, 4.21, 4.22 and 4.23 with their initial conditions constitute the governing equations which describe the dynamic behavior of the physical system. The experimental data for each isotherm were then used to determine the only unknown parameter in the model , rate constant K^*, by minimizing the difference between the model predictions and the experimental measurements of moles of gas consumed during hydrate formation. The resulting nonlinear least-squares problem was solved iteratively using Gauss-Newton method with an optimal step-size policy and Marquardt's modification to ensure rapid convergence (Kalogerakis and Luus, 1983). The model and sensitivity equations were integrated using IMSL's DGEAR differential equation solver.

4.4 Experimental Results and Model Predictions.

In Figures 4.2 - 4.5 the experimental data for methane together with the estimated consumption curves are shown. Similarly, the results for carbon dioxide are shown in Figures 4.6 - 4.8. In the above figures, the data are shown only after the turbidity point has occurred which is defined as the zero time in the plots. The nature of the experimental and the fitted curves is similar for all the isotherms. Observing the data at any particular isotherm, it is seen that there is a strong dependence of the rate of formation on the driving force which indicates that greater deviations from the three-phase equilibrium line cause higher consumption rates. Overall, the model predictions match the experimental data very well with the largest prediction error being less than 10.9 % for methane and 1.6 % for carbon dioxide.

The estimated parameter values at each isotherms are shown in Tables 4.2 and 4.3 for methane and carbon dioxide respectively. In these tables, the 95 % confidence intervals of fit for each parameter are also shown. The change of kinetic rate constant with respect to the temperature does not seem to be significant. It is also observed that the kinetic rate constants for carbon dioxide was greater than for methane.

Table 4.4 shows the comparison of the kinetic rate constant for methane hydrate formation obtained from this work and Englezos et al. (1987a). The difference has resulted due to the inaccuracy of Equations (37) and (38) in the model developed by Englezos et al. (1987a) as discussed earlier.

Table 4.2 Kinetic Parameter (K^*) for Methane Hydrate Formation

Temperature (K)	$K^* * 10^4$ (mol/m^2.s.MPa)	95 % Confidence Interval of fit (% of K^*)
274	0.31	0.87
276	0.21	1.04
279	0.28	0.44
282	0.29	1.06

Table 4.3 Kinetic Parameter (K^*) for Carbon Dioxide Hydrate Formation

Temperature (K)	$K^* * 10^3$ (mol/m^2.s.MPa)	95 % Confidence Interval of fit (% of K^*)
274	0.49	1.62
276	0.19	2.00
278	0.35	1.23

Table 4.4 Comparison of K^* for Methane Hydrate Formation from this work & Englezos et al. (1987a).

Temperature (K)	This Work : $K^* * 10^4$ (mol/m^2.s.MPa)	Englezos : $K^* * 10^5$ (mol/m^2.s.MPa)
274	0.31	0.65
276	0.21	0.55
279	0.28	0.57
282	0.29	0.58

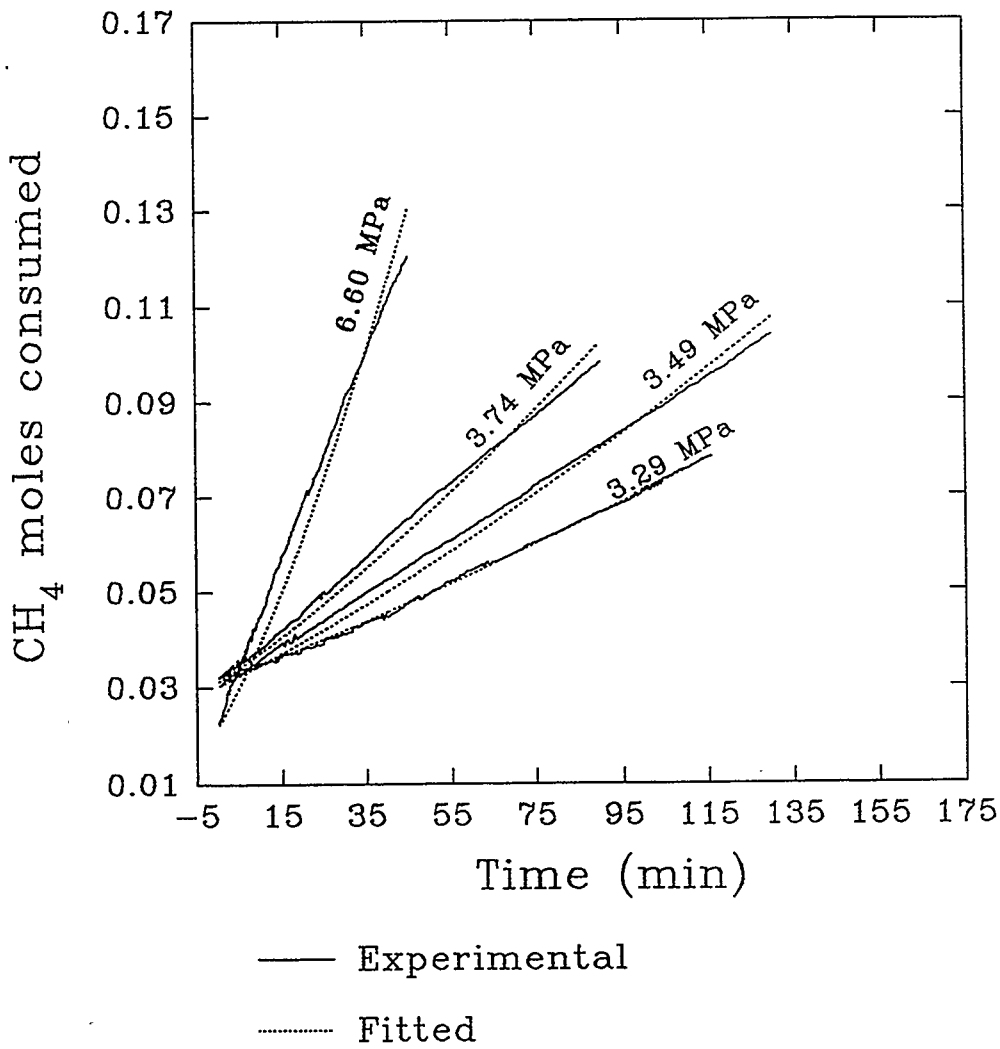

Figure 4.2 Methane Hydrate Formation at a Nominal Temperature of 274 K

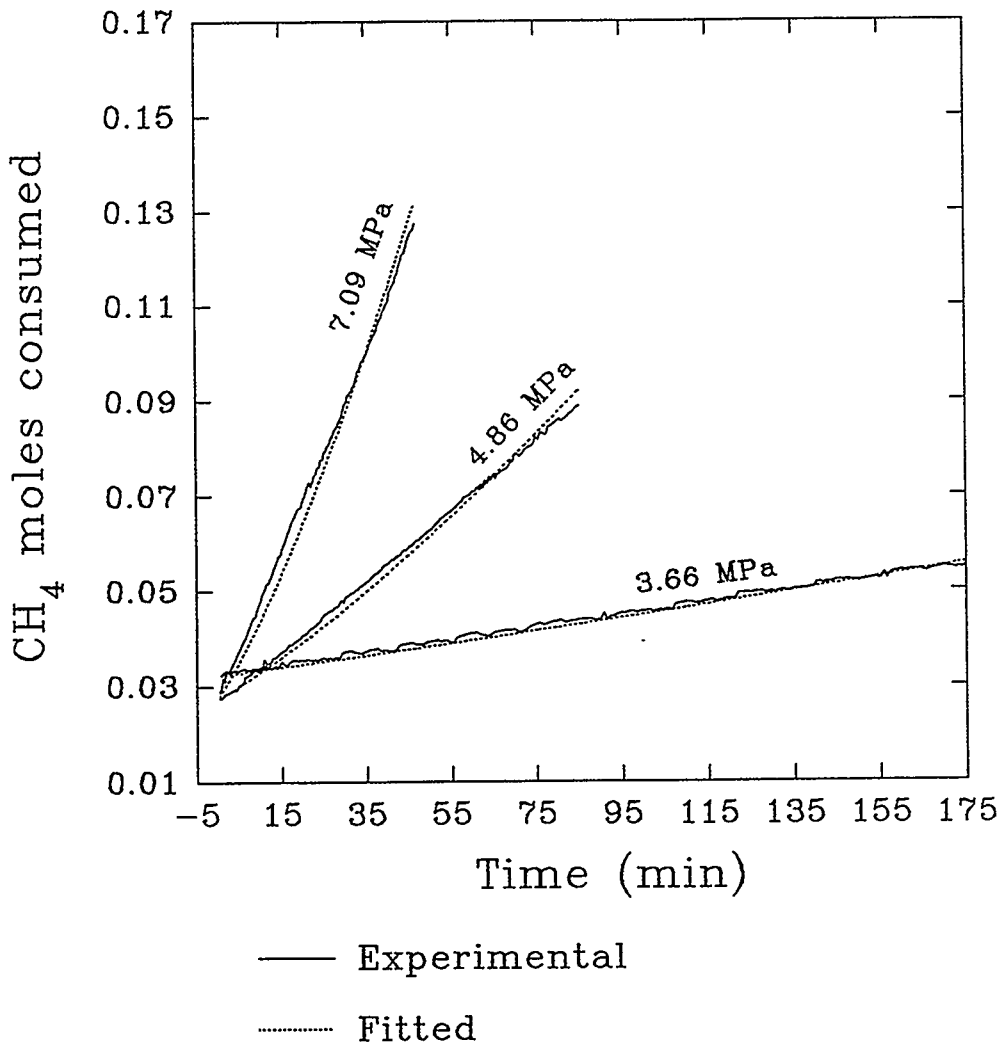

Figure 4.3 Methane Hydrate Formation at a Nominal Temperature of 276 K

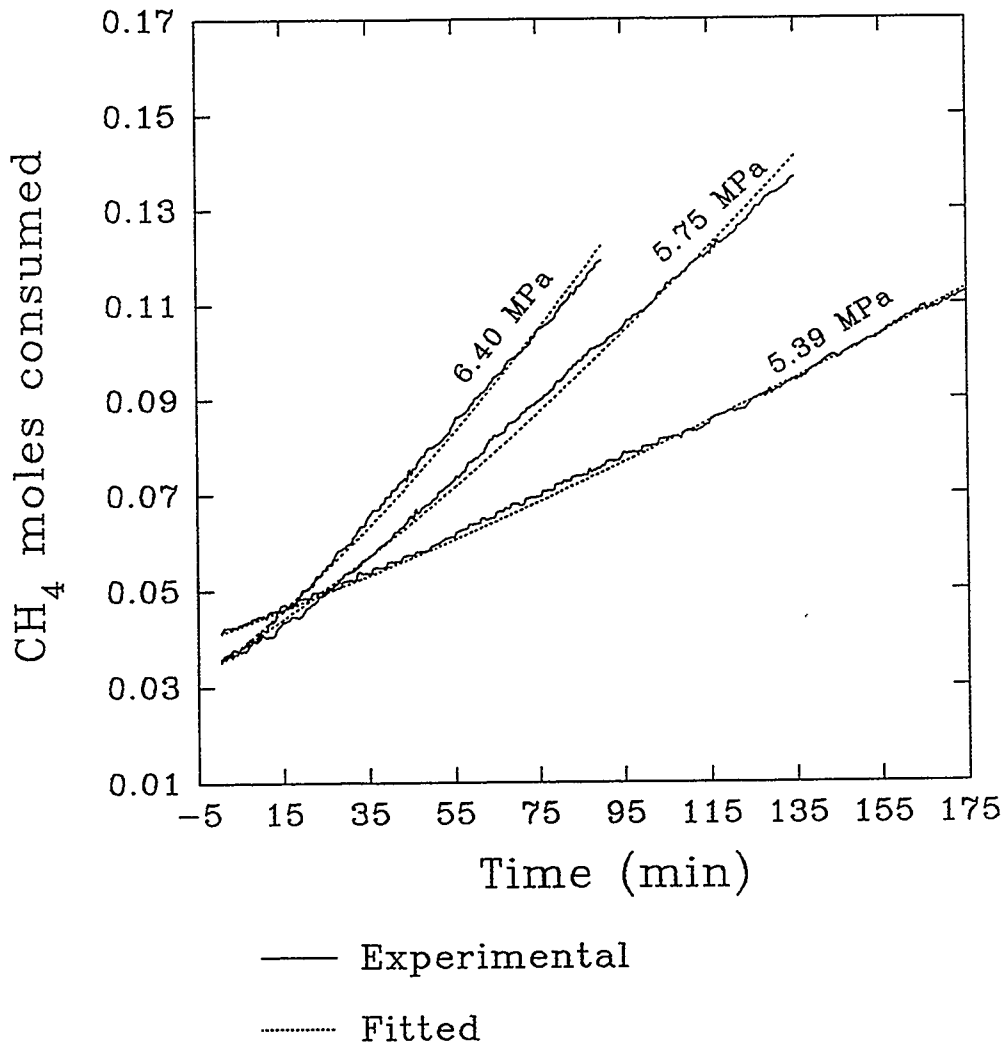

Figure 4.4 Methane Hydrate Formation at a Nominal Temperature of 279 K

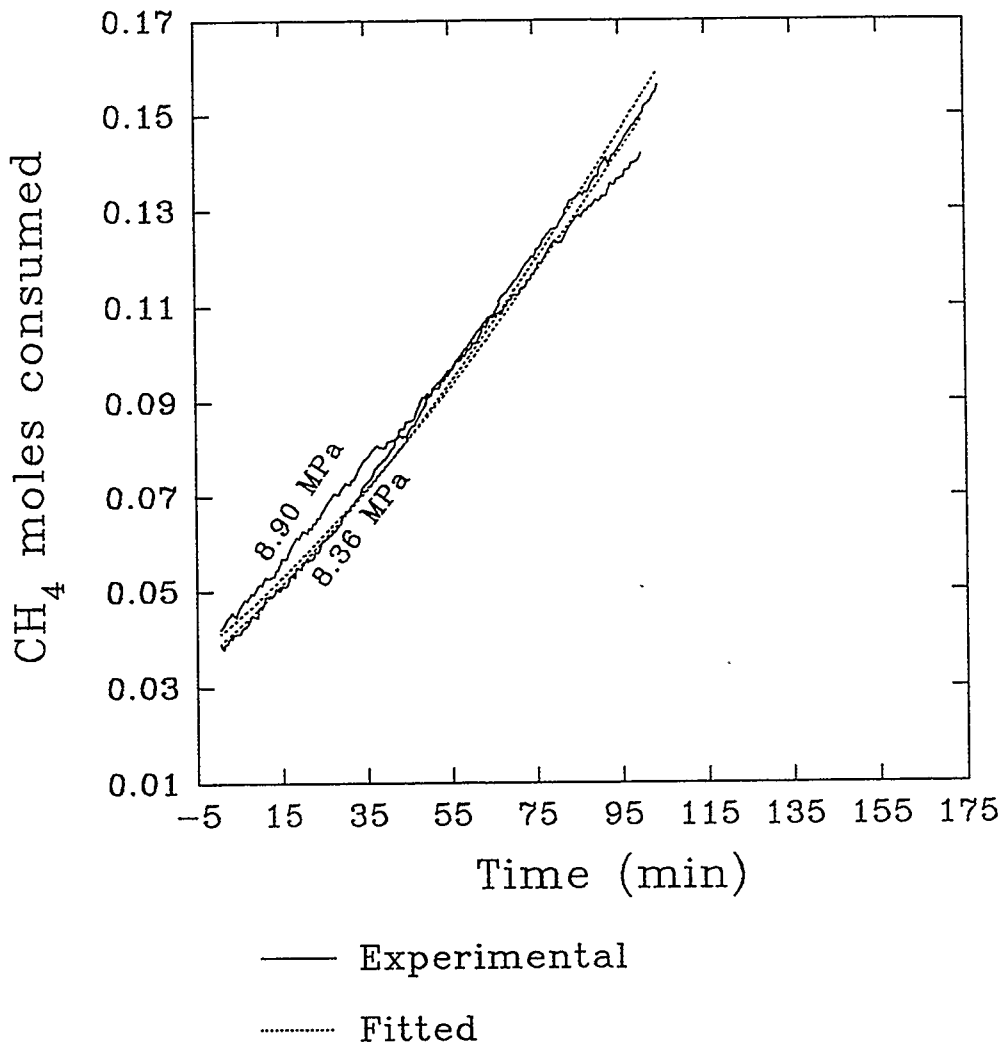

Figure 4.5 Methane Hydrate Formation at a Nominal Temperature of 282 K

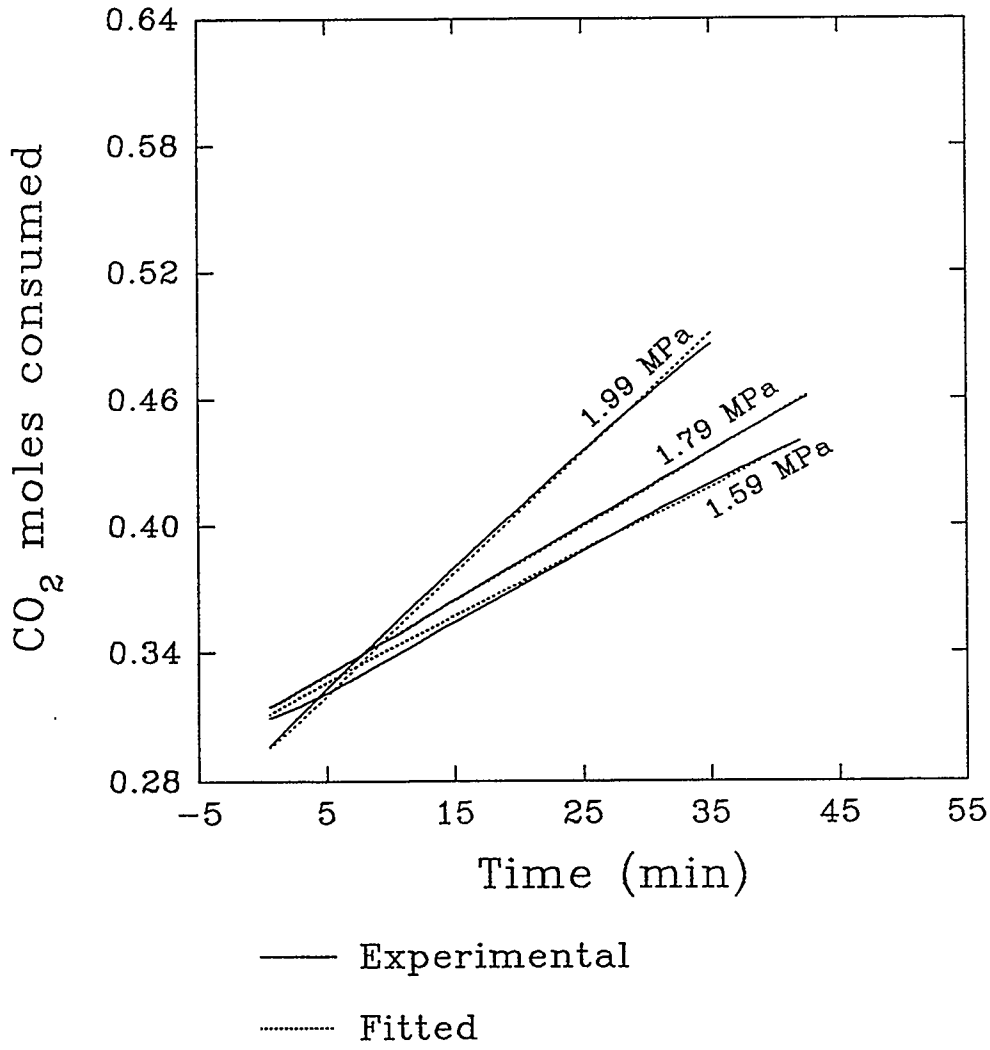

Figure 4.6 Carbon Dioxide Hydrate Formation at a Nominal Temperature of 274 K

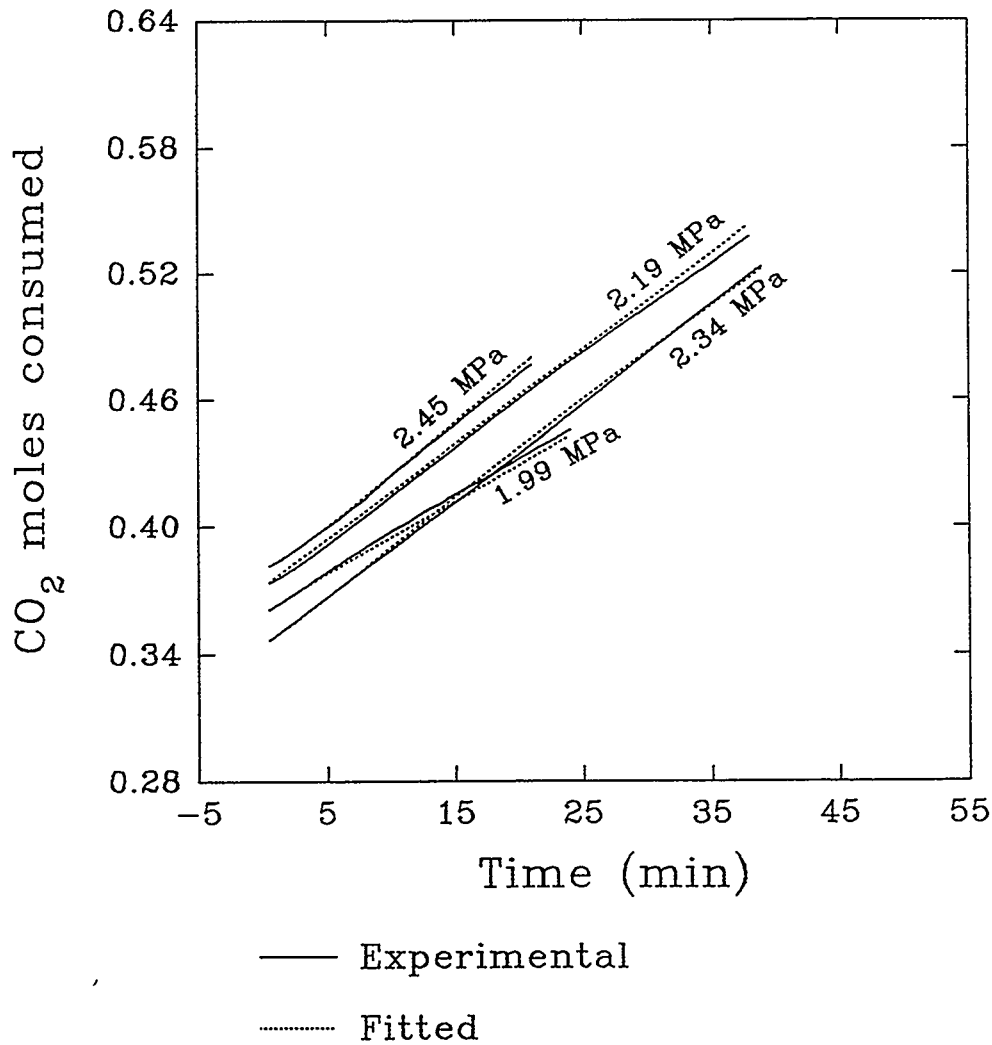

Figure 4.7 Carbon Dioxide Hydrate Formation at a Nominal Temperature of 276 K

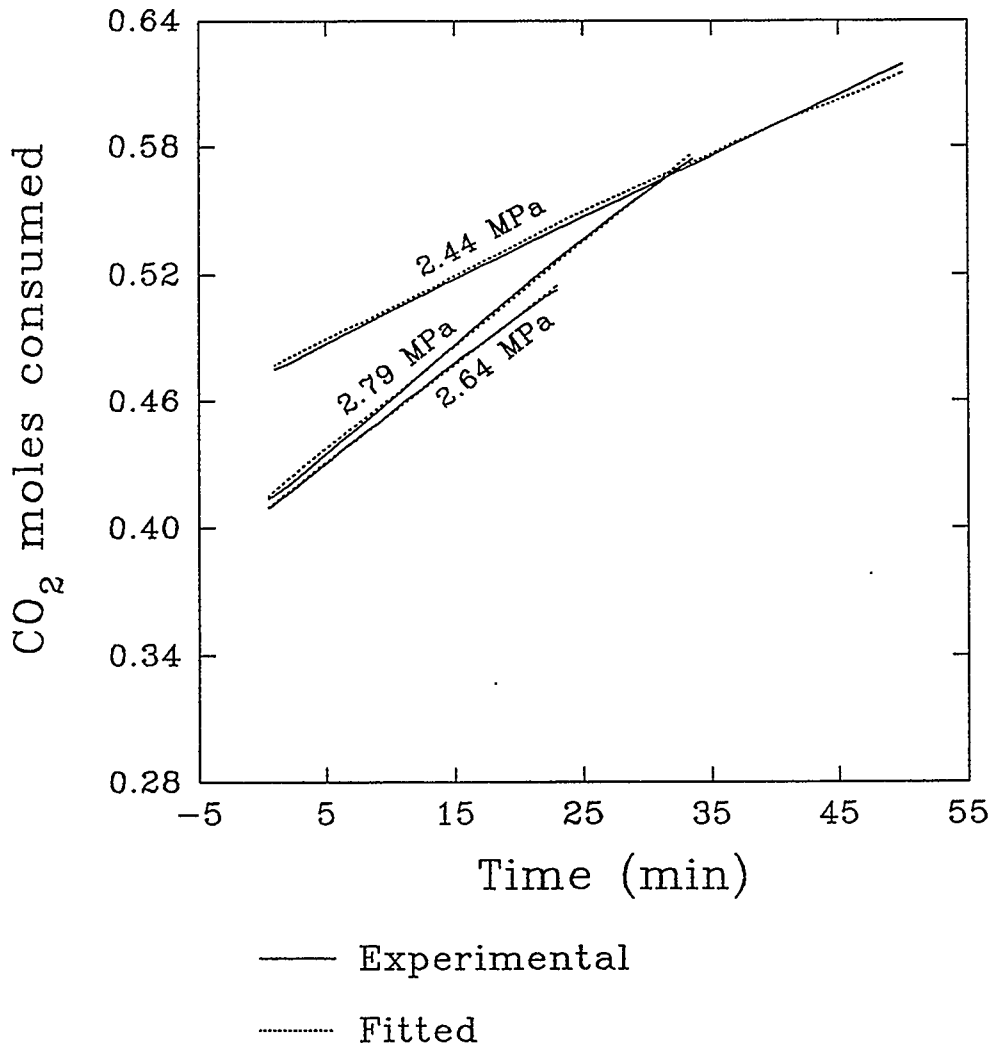

Figure 4.8 Carbon Dioxide Hydrate Formation at a Nominal Temperature of 278 K

5. SOLUBILITY MODEL FOR GAS MIXTURES

This chapter describes the development of a solubility model to predict the CH_4 and CO_2 gas composition in the reactor gas phase and the solubility of the gases in the reactor liquid phase (water). The two-film model was used for estimating the rates of multicomponent mass transfer from the exact solution of the Maxwell-Stefan equation. It has been shown by Toor (1957), Krishna and Standart (1979) and Reinhardt and Dialer (1981) that in multicomponent mass transfer the reverse diffusion, diffusion barrier or osmotic diffusion may occur. The methodology for predicting the rates of multicomponent mass transfer given by Smith and Taylor (1983) and Krishna et al. (1993) was adopted. The model equations were solved and the results were compared with the experimental data obtained from the kinetic experiments of CH_4 and CO_2 gas mixtures under isothermal and isobaric condition before the turbidity point.

5.1 Model Development

A schematic diagram of the equipment for the solubility of gases into liquid is shown in Figure 5.1. The equipment system comprises of a reactor and a reservoir, placed in a constant temperature bath. During the experiment, the CH_4 and CO_2 gases get dissolved into water in the reactor. To maintain the constant pressure in the reactor, additional gas is supplied from the reservoir. The liquid phase of the reactor is well agitated by a magnet driven stirrer (not shown).

5.1.1 Reactor Gas Phase

The mole balance was done on the reactor gas phase based on the following assumptions:

1. The reactor gas phase is well mixed and hence gas side film resistance is neglected.
2. The water content in the gas phase is negligible (due to low vapor pressure).

Figure 5.1 A Schematic Diagram of the Equipment for the Solubility of Gases into Liquid.

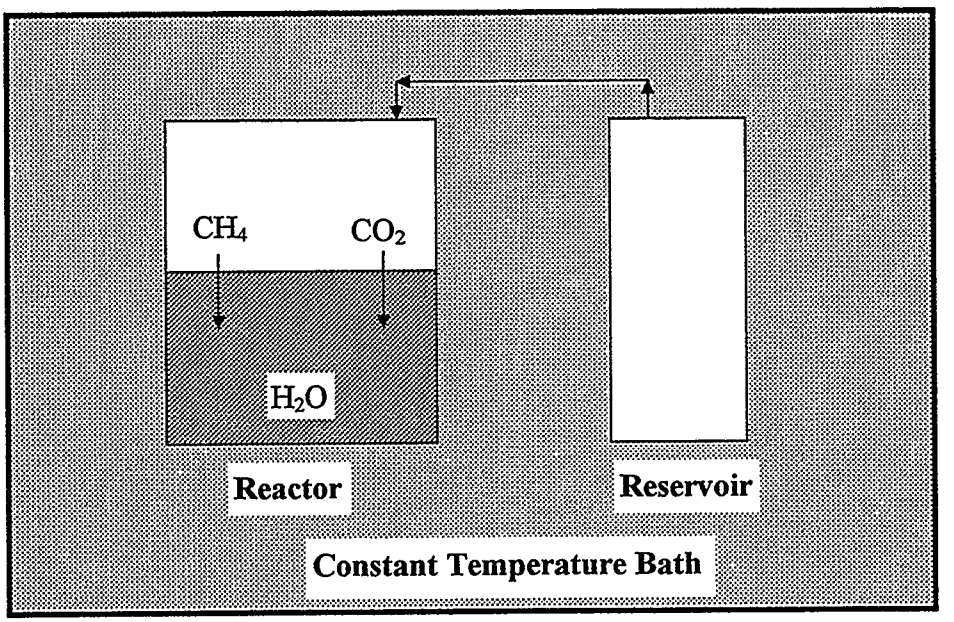

3. The change in compressibility factor due to change in gas composition in time interval Δt is negligible.

Since the gas phase consists of only two components, $CH_4(1)$ and $CO_2(2)$, the mole fraction summation equation is given by

$$y_1 + y_2 = 1.0 \qquad 5.1$$

The gas supplied by the reservoir is either consumed into the liquid or accumulated in the reactor gas phase. Thus the component mole balance yields

$$\left(\frac{V_S y_{1S}}{z_S RT_S}\right)\frac{dP_S}{dt} = \left(\frac{dn_1}{dt}\right)_L + \left(\frac{PV_g}{z_g RT}\right)\frac{dy_1}{dt} \qquad 5.2$$

$$\left(\frac{V_S(1-y_{1S})}{z_S RT_S}\right)\frac{dP_S}{dt} = \left(\frac{dn_2}{dt}\right)_L + \left(\frac{PV_g}{z_g RT}\right)\frac{dy_2}{dt} \qquad 5.3$$

Since the pressure, temperature and volume of reactor gas phase are constant, the overall mole balance is given by

$$\frac{V_S}{z_S RT_S}\frac{dP_S}{dt} = \left(\frac{dn_1}{dt}\right)_L + \left(\frac{dn_2}{dt}\right)_L \qquad 5.4$$

Combining Equations 5.1 - 5.4 yields

$$\frac{dy_1}{dt} = \left(\frac{z_g RT}{PV_g}\right)\left[(y_{1S}-1)\left(\frac{dn_1}{dt}\right)_L + y_{1S}\left(\frac{dn_2}{dt}\right)_L\right] \qquad 5.5$$

The initial condition for the solution of above equation is $y_1 = y_{10}$.

5.1.2 Reactor Liquid Phase

The following assumptions were made to develop the model.

1. The vapor-liquid interface is at equilibrium.
2. The volume of the solution is constant and is equal to the initial volume of water.
3. The molar flux of water is negligible.

The liquid phase mole fraction summation equation is given as

$$x_1 + x_2 + x_3 = 1.0 \qquad 5.6$$

where component 1, 2 and 3 represent CH_4, CO_2 and H_2O respectively.

Using Henry's law and assuming equilibrium, the compositions at the gas-liquid interface are given by

$$\begin{aligned} x_1^i &= \frac{f_1^g}{H_1} \\ x_2^i &= \frac{f_2^g}{H_2} \end{aligned} \qquad 5.7$$

where H is henry's constant and f_1^g is the fugacity of the methane in the gas mixture.
The rate with which the gas has been transferred into the liquid due to dissolution is given by

$$\left(\frac{dn_1}{dt}\right)_L = A_{(g-l)} N_1 \qquad 5.8$$

$$\left(\frac{dn_2}{dt}\right)_L = A_{(g-l)} N_2 \qquad 5.9$$

where N is the molar flux of component. The flux is computed using the two film model for the multicomponent mass transfer, and $A_{(g-l)}$ is the gas-liquid interfacial area. The initial condition for the above equations are

$$t = 0; \qquad n_1 = 0 \;\; \& \;\; n_2 = 0 \qquad 5.10$$

5.1.3 Film Model for Multicomponent Mass Transfer

The multicomponent mass transfer model discussed below is adapted from Chapters 2, 7 and 8 of a book by Krishna and Taylor (1993).

The two-film theory was used for describing the multicomponent mass transfer of gases into liquid. The assumptions made were:

1. The gas film resistance is negligible.
2. The molecular diffusion in the liquid film is at a steady state.
3. The liquid mixture is considered as an ideal solution.
4. Mass transfer occurs through the liquid film in the direction normal to the interface.

The one-dimensional steady state equations of continuity in moles of species i is given by

$$\frac{dN_i}{dz} = 0 \qquad \frac{dN_t}{dz} = 0 \qquad 5.11$$

which shows that the molar fluxes, N_i, for steady state diffusion through a plane film are position invariant. These fluxes are made of diffusive and convective terms as

$$N_i = J_i + x_i N_t; \qquad i = 1,2,\ldots,n.$$
$$N_t = \sum_{i=1}^{n} N_i \qquad 5.12$$

where N_t is the total flux and J_i is the molar diffusive flux.

For steady state unidirectional diffusion under isobaric, isothermal conditions the Maxwell-Stefan equations can be written as

$$\sum_{j=1}^{n-1} \Gamma_{ij} \frac{dx_j}{dz} = \sum_{j=1}^{n} \frac{\left(x_i N_j - x_j N_i\right)}{c_t Đ_{ij}}; \qquad i = 1,2,\ldots,n. \qquad 5.13$$

where $Đ_{ij}$ is the Fick's binary diffusion coefficient of the i-j pairs. The $Đ_{ij}$ and c_t are assumed to be constant in the film. Γ_{ij}, the thermodynamic factor, is defined by

$$\Gamma_{ij} = \delta_{ij} + x_i \left.\frac{\partial \ln \gamma_i}{\partial x_j}\right|_{T,P,x_k,k\neq j=1\ldots n-1} \qquad 5.14$$

The Γ_{ij} for the liquid mixtures can be evaluated from the activity coefficient models, however in this work the liquid mixture is assumed to be ideal and thus Γ_{ii} are 1; Γ_{ij} are 0. δ_{ij} is the Kronecker delta.

Only n-1 of Equation 5.13 are independent because the mole fractions add to unity, and the mole fraction gradient ($dx_i/d\eta$) and the molar diffusion fluxes (J_i) sum over n species to zero. Thus eliminating x_n from Equation 5.13 yields (see Appendix C)

$$\sum_{j=1}^{n-1} \Gamma_{ij} \frac{dx_j}{d\eta} = \Phi_{ii} x_i + \sum_{\substack{j=1 \\ j\neq i}}^{n-1} \Phi_{ij} x_j + \varphi_i; \qquad i = 1,2,\ldots,n-1 \qquad 5.15$$

where η is a dimensionless distance defined by

$$\eta = \frac{z}{l} \qquad 5.16$$

in which l is the film thickness.

The coefficients Φ_{ii}, Φ_{ij} and φ_i are defined by

$$\Phi_{ii} = \frac{N_i}{c_t \mathcal{D}_{in} / l} + \sum_{\substack{k=1 \\ i \neq k}}^{n} \frac{N_k}{c_t \mathcal{D}_{ik} / l} \qquad 5.17$$

$$\Phi_{ij} = -N_i \left(\frac{1}{c_t \mathcal{D}_{ij} / l} - \frac{1}{c_t \mathcal{D}_{in} / l} \right) \qquad 5.18$$

$$\varphi_i = -\frac{N_i}{c_t \mathcal{D}_{in} / l} \qquad 5.19$$

Equation 5.15 is more conveniently written in n-1 dimensional matrix form as

$$[\Gamma] \frac{d(x)}{d\eta} = [\Phi](x) + (\varphi) \qquad 5.20$$

where $[\Gamma]$ is a square matrix of thermodynamic factors (Γ_{ij}) of order n-1, $[\Phi]$ is a square matrix of mass transfer rate factors of order n-1, (φ) is column matrix of order n-1 x 1 and (x) is the column matrix of liquid compositions of order n-1 x 1.

The boundary conditions of the film model are

$$\begin{array}{lll} z=0 & \eta=0 & x_i = x_{i0} \\ z=l & \eta=1 & x_i = x_{ib} \end{array} \qquad 5.21$$

Since c_t, N_i, Γ_{ij} and $Đ_{ij}$ are constant along the diffusion path, Equation 5.20 represents a set of linear differential equation with constant coefficients. The general solution, in n-1 dimensional matrix form, developed by Krishna et al. (1976) is

$$(x-x_0) \;=\; \{exp[\phi]\eta - [I]\}\left((x_0) + [\phi]^{-1}(\varphi)\right) \qquad 5.22$$

where $[\phi] = [\Gamma]^{-1}[\Phi]$ and $[I]$ is a unit matrix.

By applying the boundary condition $\eta=1$ into Equation 5.22 gives

$$\left((x_0) + [\phi]^{-1}(\varphi)\right) \;=\; \{\exp[\phi] - [I]\}^{-1}(x_b - x_0) \qquad 5.23$$

Combining Equations 5.22 and 5.23, the composition profiles through the film is given by

$$(x-x_0) \;=\; \{\exp[\phi]\eta - [I]\}\{\exp[\phi] - [I]\}^{-1}(x_b - x_0) \qquad 5.24$$

From the Maxwell-Stefan relations, the expression for diffusion fluxes can be obtained as

$$(J) \;=\; -\frac{c_t}{l}[B]^{-1}[\Gamma]\frac{d(x)}{d\eta} \;=\; -\frac{c_t}{l}[D]\frac{d(x)}{d\eta} \qquad 5.25$$

where $[D]$ is a square matrix of multicomponent diffusion coefficients of order n-1. The multicomponent diffusion coefficients are related to binary diffusion coefficients by

$$[D] = [B]^{-1}[\Gamma] \qquad 5.26$$

where matrix $[B]$ is given by

$$B_{ii} = \frac{x_i}{Đ_{in}} + \sum_{\substack{k=1 \\ i \neq k}}^{n} \frac{x_k}{Đ_{ik}} \qquad 5.27$$

$$B_{ij} = -x_i \left(\frac{1}{Đ_{ij}} - \frac{1}{Đ_{in}} \right) \qquad 5.28$$

The gradients in the mole fractions are obtained from Equation 5.24 as follows:

$$\frac{d(x)}{d\eta} = [\phi]\{\exp[\phi]\eta\}\{\exp[\phi] - [I]\}^{-1}(x_b - x_0) \qquad 5.29$$

The diffusion fluxes at $\eta=0$, J_{i0}, can be evaluated using Equations 5.25 and 5.29 as :

$$\begin{aligned} (J_0) &= -\frac{c_t[D_0]}{l}\frac{d(x)}{d\eta}\bigg|_{\eta=0} \\ &= \frac{c_t[D_0]}{l}[\phi]\{exp[\phi]-[I]\}^{-1}(x_0 - x_b) \end{aligned} \qquad 5.30$$

where the elements of matrix $[D_0]$ are obtained from $[B_0]^{-1}$, with the elements B_{ik} evaluated from Equations 5.27 & 5.28 using the mole fractions x_{i0}.

From Equation 5.30, the finite flux mass transfer coefficient is obtained as:

$$[k_0^*] = [k_0][\Xi_0] = \left\{\frac{[D_0]}{l}\right\}\left\{[\phi]\{exp[\phi]-[I]\}^{-1}\right\} \qquad 5.31$$

where $[k_0]$ is the zero flux mass transfer coefficient and $[\Xi_0]$ is the correction factor at the interface given by

$$[k_0] = \frac{[D_0]}{l} \qquad 5.32$$

$$[\Xi_0] = [\phi]\{\exp[\phi]-[I]\}^{-1} \qquad 5.33$$

Alternatively, the diffusion fluxes at $\eta=1$, J_{ib}, can be evaluated using Equations 5.25 and 5.29 as :

$$\begin{aligned}(J_b) &= -\frac{c_t[D_b]}{l}\frac{d(x)}{d\eta}\bigg|_{\eta=1} \\ &= \frac{c_t[D_b]}{l}[\phi][exp[\phi]]\{exp[\phi]-[I]\}^{-1}(x_0-x_b)\end{aligned} \qquad 5.34$$

giving the zero-flux mass transfer coefficients in the bulk

$$[k_b] = \frac{[D_b]}{l} \qquad 5.35$$

and the matrix of correction factors in the bulk

$$[\Xi_b] = [\phi][exp[\phi]]\{exp[\phi]-[I]\}^{-1} = [\Xi_0]exp[\phi] \qquad 5.36$$

The molar flux is related to diffusion flux by bootstrap matrix $[\beta]$ as :

$$(N) = [\beta](J) \qquad 5.37$$

where the bootstrap matrix elements for the Stefan Diffusion, a case of mass transfer in a mixture where one component has a zero flux, are given by (Krishna et al. 1979)

$$\beta_{ik} = \delta_{ik} + \frac{x_i}{x_n} \qquad (N_n = 0) \tag{5.38}$$

By invoking the bootstrap solution, the fluxes N_i can be evaluated from one of the two equivalent expressions

$$(N) = c_t [\beta_0][k_0][\Xi_0](x_0 - x_b) \tag{5.39}$$

$$(N) = c_t [\beta_b][k_b][\Xi_b](x_0 - x_b) \tag{5.40}$$

5.2 Determination of Model Parameters

All the model parameters could be determined *a priori*. The binary diffusion coefficients, $Đ_{ij}$, in dilute liquid mixtures were estimated using the Wilke and Chang correlation with improved parameters given by Hayduk and Laudie (1974). Henry's constant and liquid mass transfer coefficient, $k_{Lij}a$, for pure CH_4 and CO_2 gases in water were obtained from solubility data. Gas phase fugacities and compressibility factors were computed with the TB equation of state (Trebble and Bishnoi, 1987 & 1988). The gas-liquid interfacial area $A_{(g\text{-}l)}$ was determined experimentally by Englezos et al. (1987a) to be 127.7 cm^2. The volume of the reactor gas phase was obtained by performing the Ruska Pump Experiment. The film thickness was estimated from

$$l = \frac{Đ_{ij}\, a}{k_{Lij}\, a} \tag{5.41}$$

The above equation for CH_4 gas in water and CO_2 gas in water resulted in two different size of film thickness. But as per film model theory for multicomponent mass transfer, all of the resistance to mass transfer is concentrated in a thin film of same thickness, l. Thus the average of the two was taken as the film thickness.

5.3 Computational Technique

The differential equations 5.5, 5.8 and 5.9 with their initial conditions constitute the governing equations which describe the dynamic behavior of the physical system. ODE45 of the MATLAB software was used for the numerical solution of above three ordinary differential equations. They employ an automatically set step size for the Runge-Kutta-Fehlberg integration methods and use a 4th and 5th order pair for higher accuracy. The estimation of molar fluxes is required at every step-size from either equation 5.39 or 5.40. It involves an iterative procedure because the molar fluxes themselves are needed for the evaluation of the matrix of correction factors. Taylor and Webb (1980) have shown that equation 5.39 may not converge if the eigenvalues of $[\phi]$ are large and negative, whereas equation 5.40 may not converge if the eigenvalues of $[\phi]$ are large and positive. Hence for calculating the molar fluxes, equation 5.39 is first used. In the event it fails to converge, equation 5.40 is used for the calculations. Using the above technique, Krishnamurthy et al. (1982) developed a stable and efficient algorithm for computing the fluxes from an exact solution of the Maxwell-Stefan equations. This algorithm was used for the present work.

For the success of an iterative scheme, a good initial guess of the molar fluxes was required. Thus an explicit method of Taylor and Smith (1982) was used for the estimation of flux as described below:

The molar flux can be calculated using the average composition as

$$(N) = -\frac{c_t}{l}[\beta_{av}][D_{av}]\Xi(x_0 - x_b) \qquad 5.42$$

where Ξ is given by

$$\Xi = \frac{1}{2}\phi\frac{(\exp\phi+1)}{(\exp\phi-1)} \qquad 5.43$$

and ϕ by

$$\phi = \ln\left(\frac{x_{nb}}{x_{n0}}\right) \qquad 5.44$$

Successive substitution method may lead to slow convergence. Thus Newton's method was applied for solving the mass transfer rate equation. The Equation 5.12 represents n-1 independent mass transfer rate equations. Thus, one more equation was needed, which is $N_n=0$, due to Stefan diffusion. The calculation procedure consisted of estimating the molar fluxes using Equations 5.11 to 5.44. To reestimate the molar fluxes the Jacobian matrix was evaluated, the elements of which were obtained by differentiating Equation 5.12 with respect to independent variables, N_1 .... N_{n-1}. Finally the linear system was solved to estimate the new molar fluxes. The entire procedure was repeated until convergence was obtained.

5.4 Experimental Results and Model Predictions.

In Figures 5.2-5.7 the experimental and predicted data for the solubility's of methane and carbon dioxide in water together with the gas phase composition are shown for different isotherms. The experimental data were obtained from the kinetic experiments of methane and carbon dioxide gas mixtures before the turbidity point. The nature of experimental

data are similar for all the isotherms. Observing the data for any particular isotherm, the carbon dioxide gas consumption in water was higher than the methane gas consumption because of a higher solubility.

During dissolution period, initially both methane and carbon dioxide get absorbed in water. Later methane gas, though being almost saturated, became desorbed while carbon dioxide was still being absorbed. This desorption phenomenon is called reverse diffusion (Toor, 1957). The desorption of methane gas continued till the saturation of carbon dioxide gas and then again the process reverts back to its absorption. This implies that during simultaneous mass transfer of the two gases there is a strong diffusional interaction of carbon dioxide gas on methane gas. From the methane gas composition curve, it is seen that methane composition increases in the reactor gas phase till the saturation of carbon dioxide gas in the liquid phase occurs and then it attains a constant value.

The model predictions, indicated by dotted lines, show the trends for carbon dioxide gas consumption and the composition in the gas phase similar to those of the experimental data. The trends shown for the methane gas consumption's are however different. The prediction of methane gas consumption shows that there is no reverse diffusion of methane gas occurring during the absorption of the two gases. The model parameters were analyzed to see their influence on the predictions, as explained below:

The diffusional flux for the ternary system (CH_4-1; CO_2-2; H_2O-3) using equation 5.30 and 5.31 can be written as:

$$(J) = c_t \left[k^{\bullet}\right](\Delta x) = c_t \begin{bmatrix} k_{11}^{\bullet} & k_{12}^{\bullet} \\ k_{21}^{\bullet} & k_{22}^{\bullet} \end{bmatrix} \begin{bmatrix} \Delta x_1 \\ \Delta x_2 \end{bmatrix} \qquad 5.45$$

which simplifies to

$$J_1 = c_t k_{11}^{\bullet} \Delta x_1 + c_t k_{12}^{\bullet} \Delta x_2 \qquad 5.46$$

$$J_2 = c_t k_{21}^{\bullet} \Delta x_1 + c_t k_{22}^{\bullet} \Delta x_2 \qquad 5.47$$

where the finite flux mass coefficients, $k^{\bullet}$, is given by

$$[k^{\bullet}] = [k][\Xi] = \begin{bmatrix} k_{11} & k_{12} \\ k_{21} & k_{22} \end{bmatrix} \begin{bmatrix} \Xi_{11} & \Xi_{12} \\ \Xi_{21} & \Xi_{22} \end{bmatrix} \qquad 5.48$$

$$\begin{bmatrix} k_{11}^{\bullet} & k_{12}^{\bullet} \\ k_{21}^{\bullet} & k_{22}^{\bullet} \end{bmatrix} = \begin{bmatrix} k_{11}\Xi_{11} + k_{12}\Xi_{21} & k_{11}\Xi_{12} + k_{12}\Xi_{22} \\ k_{21}\Xi_{11} + k_{22}\Xi_{21} & k_{21}\Xi_{12} + k_{22}\Xi_{22} \end{bmatrix} \qquad 5.49$$

The zero-flux mass transfer coefficients for ternary system can be obtained from equation 5.26-5.28 and 5.32 as:

$$k_{11} = \frac{\left\{ Đ_{13}\left(x_1 Đ_{23} + (1-x_1) Đ_{12}\right)\Gamma_{11} + x_1 Đ_{23}\left(Đ_{13} - Đ_{12}\right)\Gamma_{21} \right\}}{\left\{ \left(x_1 Đ_{23} + x_2 Đ_{13} + x_3 Đ_{12}\right) l \right\}} \qquad 5.50$$

$$k_{12} = \frac{\left\{ Đ_{13}\left(x_2 Đ_{23} + (1-x_1) Đ_{12}\right)\Gamma_{12} + x_1 Đ_{23}\left(Đ_{13} - Đ_{12}\right)\Gamma_{22} \right\}}{\left\{ \left(x_1 Đ_{23} + x_2 Đ_{13} + x_3 Đ_{12}\right) l \right\}} \qquad 5.51$$

$$k_{21} = \frac{\left\{ Đ_{23}\left(x_2 Đ_{13} + (1-x_2) Đ_{12}\right)\Gamma_{21} + x_2 Đ_{13}\left(Đ_{23} - Đ_{12}\right)\Gamma_{11} \right\}}{\left\{ \left(x_1 Đ_{23} + x_2 Đ_{13} + x_3 Đ_{12}\right) l \right\}} \qquad 5.52$$

$$k_{22} = \frac{\left\{ Đ_{23}\left(x_2 Đ_{13} + (1-x_2) Đ_{12}\right)\Gamma_{22} + x_2 Đ_{13}\left(Đ_{23} - Đ_{12}\right)\Gamma_{12} \right\}}{\left\{ \left(x_1 Đ_{23} + x_2 Đ_{13} + x_3 Đ_{12}\right) l \right\}} \qquad 5.53$$

The parameters k_{ij}, $k_{ij}^{\bullet}$, Γ_{ij} and Ξ_{ij} with i=j pairs are called main coefficients and those with i≠j pairs are called cross coefficients. It is important to note that the cross coefficients play an important role in enhancing the diffusional interaction effects in multicomponent mass transfer. In the absence of interaction effects, all these terms tend to zero. In general all

the cross coefficients, $k_{12}^{\bullet}$, $k_{21}^{\bullet}$, Δx_1 and Δx_2 can take on any sign, depending on the physical constraints imposed on the system.

The desorption of methane gas implies that the diffusion flux, J_1, is negative though the Δx_1 is positive which is only possible when $k_{12}^{\bullet}\Delta x_2$ overshadows $k_{11}^{\bullet}\Delta x_1$ in magnitude and is of opposite sign (see Equation 5.46). Since the concentration of methane and carbon dioxide gas in water is very small, the $k_{12}^{\bullet}$ has to be large for large interaction effects. This is contributed by zero-flux mass transfer coefficient and correction factors which are influenced by binary diffusion coefficients and thermodynamic factors.

Due to the very low concentration of methane and carbon dioxide gas in water and the assumption that such liquid mixture is an ideal solution, Equations 5.50-5.53 can be approximated to

$$k_{11} \approx \frac{Đ_{13}}{l} \qquad 5.54$$

$$k_{12} \approx -\frac{x_1 Đ_{23}}{l} \qquad 5.55$$

$$k_{21} \approx -\frac{x_2 Đ_{13}}{l} \qquad 5.56$$

$$k_{22} \approx \frac{Đ_{23}}{l} \qquad 5.57$$

Since the liquid solution was assumed to be ideal, the only factor which can influence the interaction effect were the binary diffusion coefficients. Thus a study was done to see its influence on the simultaneous absorption of two gases.

5.5 Sensitivity Analysis

Figure 5.8 shows the effect of $Đ_{12}$ on the solubility of methane and carbon dioxide gas in water. The solid line indicates the experimental value and the dotted and dashed line indicates the predicted values for two different diffusivities in the range of $22.5e^{-3}$ to $22.5e^{+1}$ cm^2/min. It is seen that the increase in diffusion coefficients has no effect on the gas consumption and gas composition curve, which holds true due to the absence of $Đ_{12}$ in Equations 5.54-5.57.

Figure 5.9 shows the effect of $Đ_{13}$ on the solubility of methane and carbon dioxide gas in water. The solid line indicates the experimental value and the dotted and dashed lines indicate the predicted values for the two different diffusivities in the range of $0.52e^{-3}$ to $0.52e^{-2}$ cm^2/min. It is seen that increase in diffusivity has decreased the mass transfer resistance to the absorption of methane gas but had no interaction effect on carbon dioxide gas consumption (see Equation 5.56).

Figure 5.10 shows the effect of $Đ_{23}$ on the solubility of methane and carbon dioxide gas in water. The solid line indicates the experimental value and the dotted and dashed line indicates the predicted values for the two different diffusivities in the range of $0.63e^{-4}$ to $0.53e^{-3}$ cm^2/min. It is seen that increase in diffusivity has decreased the mass transfer resistance to the absorption of carbon dioxide gas but had no substantial interaction effect on methane gas consumption (see Equation 5.55). Also due to fast dissolution of carbon dioxide gas, the methane gas composition increases rapidly.

Figure 5.11 shows the effect of film thickness on the solubility of methane and carbon dioxide gas in water. The solid line indicates the experimental value and the dotted and dashed line indicates the predicted values for two different thickness in the range of $0.4e^{-2}$ to $0.7e^{-2}$ cm. It is seen that increase in film thickness has increased the mass transfer

resistance to both methane and carbon dioxide gas. However it had no influence on diffusional interaction effects.

Figure 5.12 shows the effect of Henry's constant for methane on the solubility of methane and carbon dioxide gas in water. The solid line indicates the experimental value and the dotted and dashed line indicates the predicted values for two different constants in the range of 22196 to 23000 bar. It is seen that an increase in Henry's constant has decreased the saturation value of methane but had no influence on diffusional interaction effects.

Figure 5.13 shows the effect of Henry's constant for carbon dioxide on the solubility of methane and carbon dioxide gas in water. The solid line indicates the experimental value and the dotted and dashed line indicates the predicted values for two different constants in the range of 750 to 814 bar. It is seen that an increase in Henry's constant has decreased the saturation value of carbon dioxide but had no influence on diffusional interaction effects.

From Equations 5.50-5.53, it seems that the thermodynamic factors may have a large influence on diffusional interaction effect as it contributes to both mass transfer coefficients and correction factors. Thus, an adequate liquid model must be used to predict the thermodynamic factors and the activity coefficients. If the above model is to be solved by considering the non-idealities of the liquid solution the only equation that needs to be modified is Equation 5.7, as follows:

$$x_1^i = \frac{f_1^g}{H_1 \gamma_1}$$
$$x_2^i = \frac{f_2^g}{H_2 \gamma_2} \qquad \textbf{5.58}$$

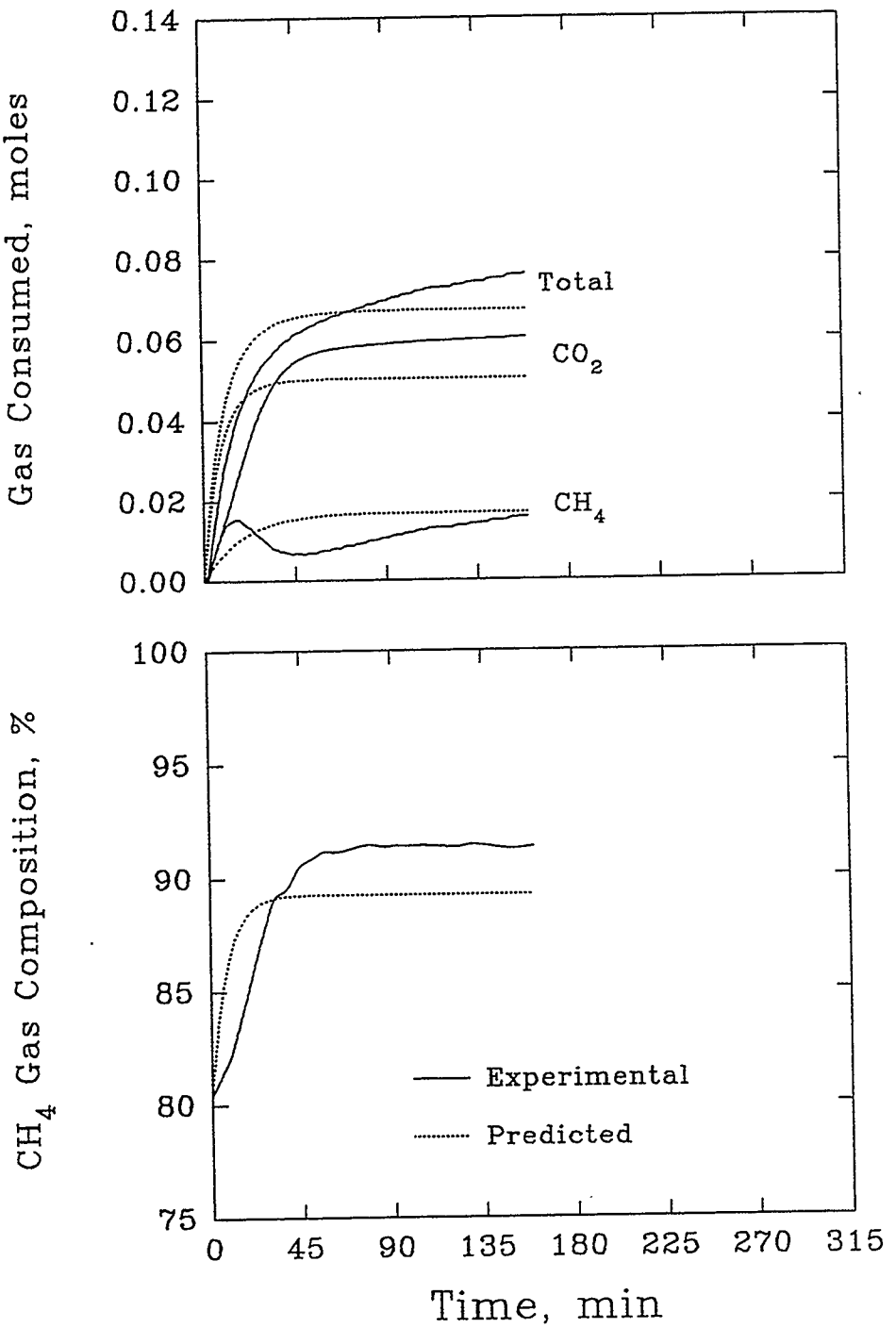

Figure 5.2 Solubility of CH_4 (80.3%) and CO_2 (19.7%) Gas in Water at P = 2.69 MPa & T = 274 K.

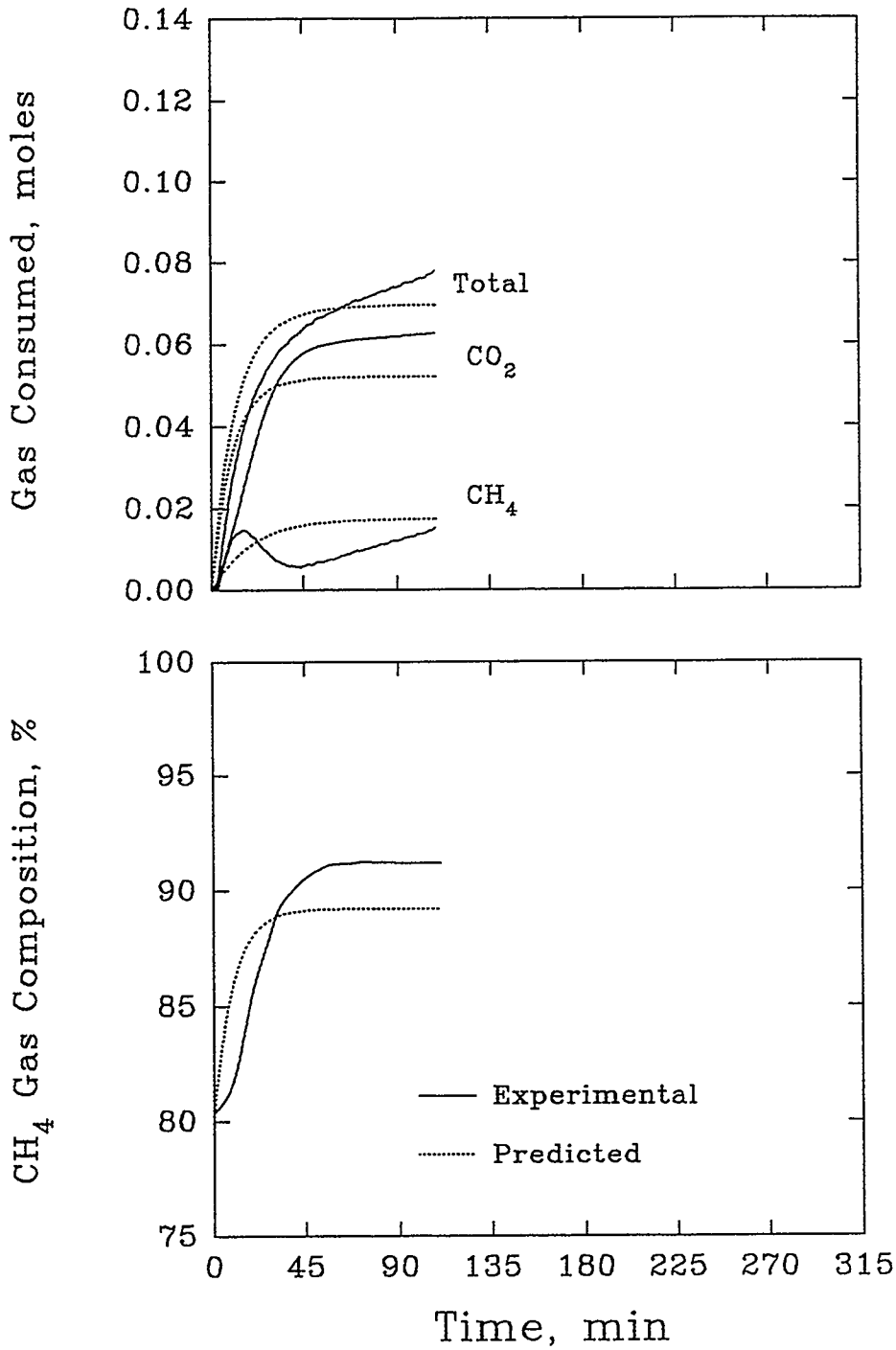

Figure 5.3 Solubility of CH_4 (80.3%) and CO_2 (19.7%) Gas in Water at P = 2.79 MPa & T = 274 K.

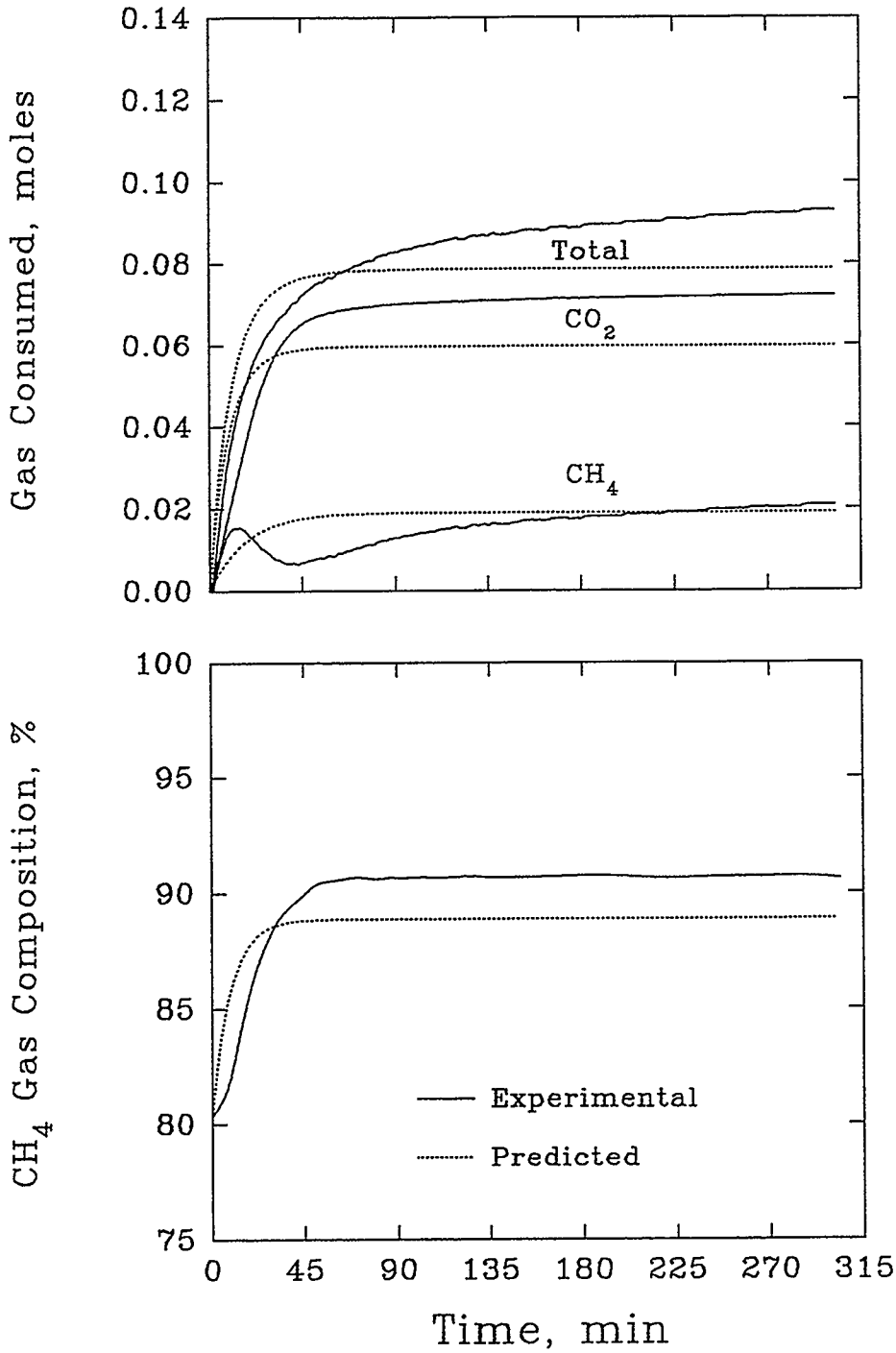

Figure 5.4 Solubility of CH_4 (80.3%) and CO_2 (19.7%) Gas in Water at P = 3.29 MPa & T = 276 K.

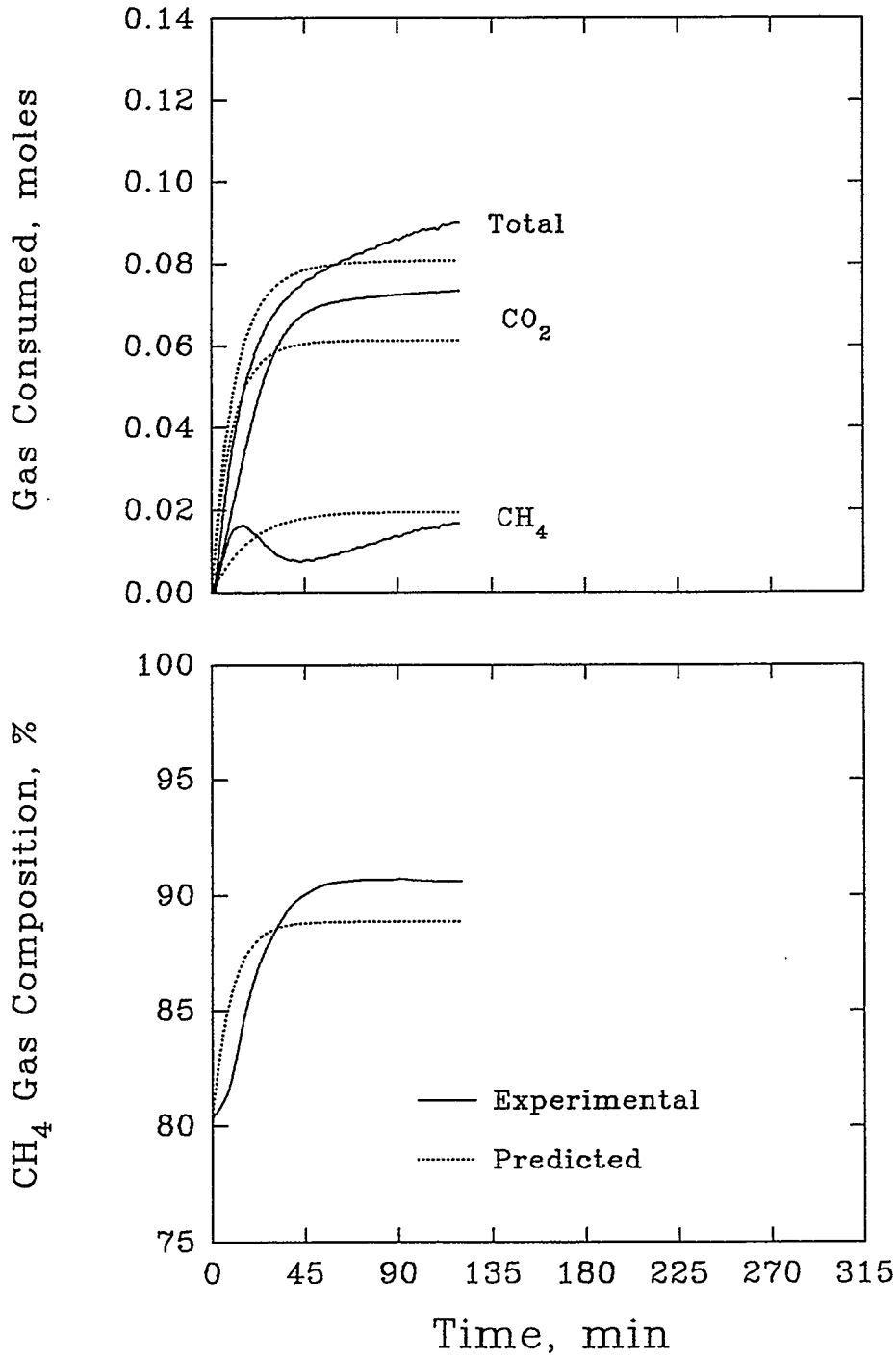

Figure 5.5 Solubility of CH_4 (80.3%) and CO_2 (19.7%) Gas in Water at P = 3.39 MPa & T = 276 K.

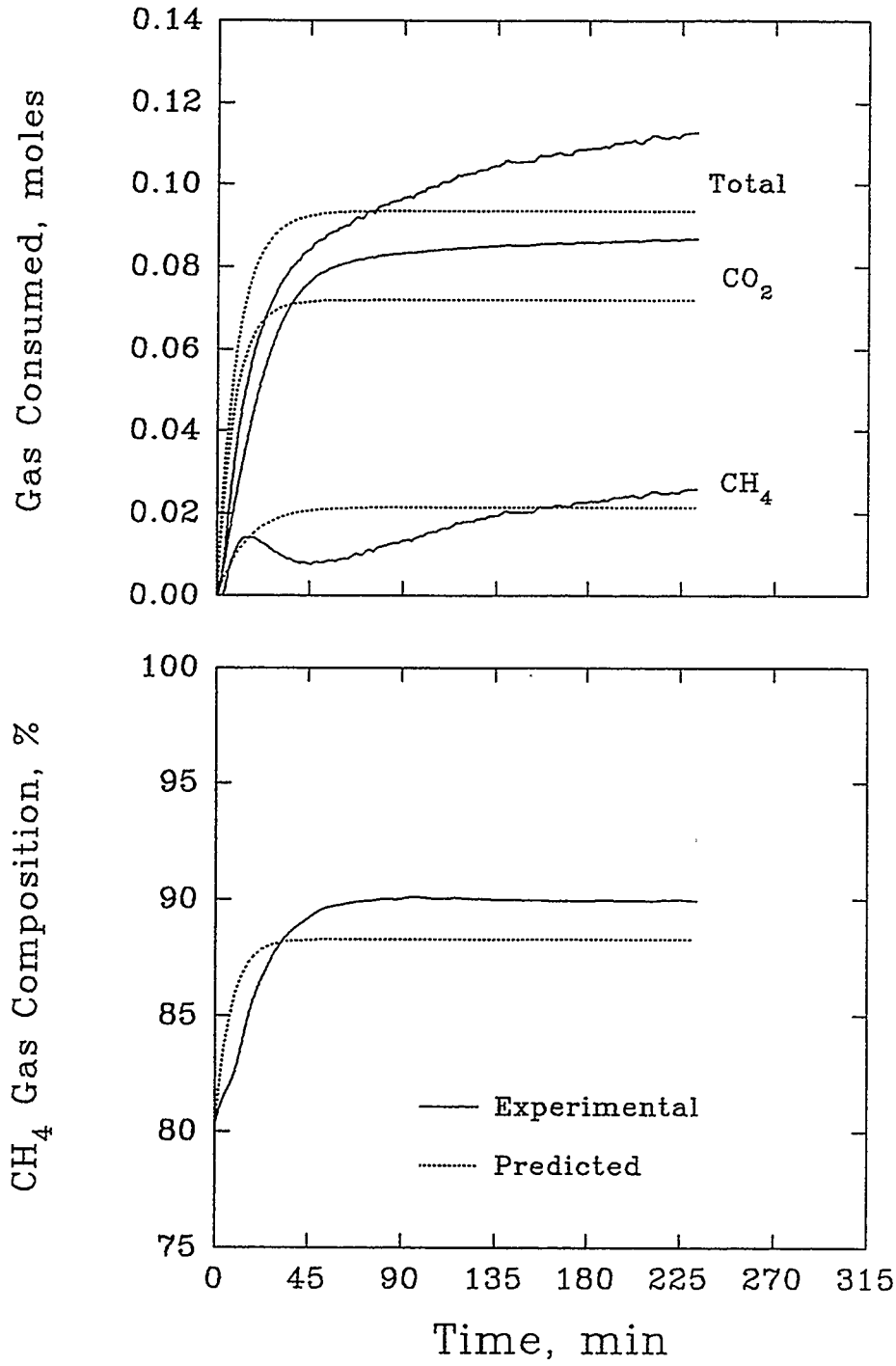

Figure 5.6 Solubility of CH_4 (80.3%) and CO_2 (19.7%) Gas in Water at P = 4.20 MPa & T = 278 K.

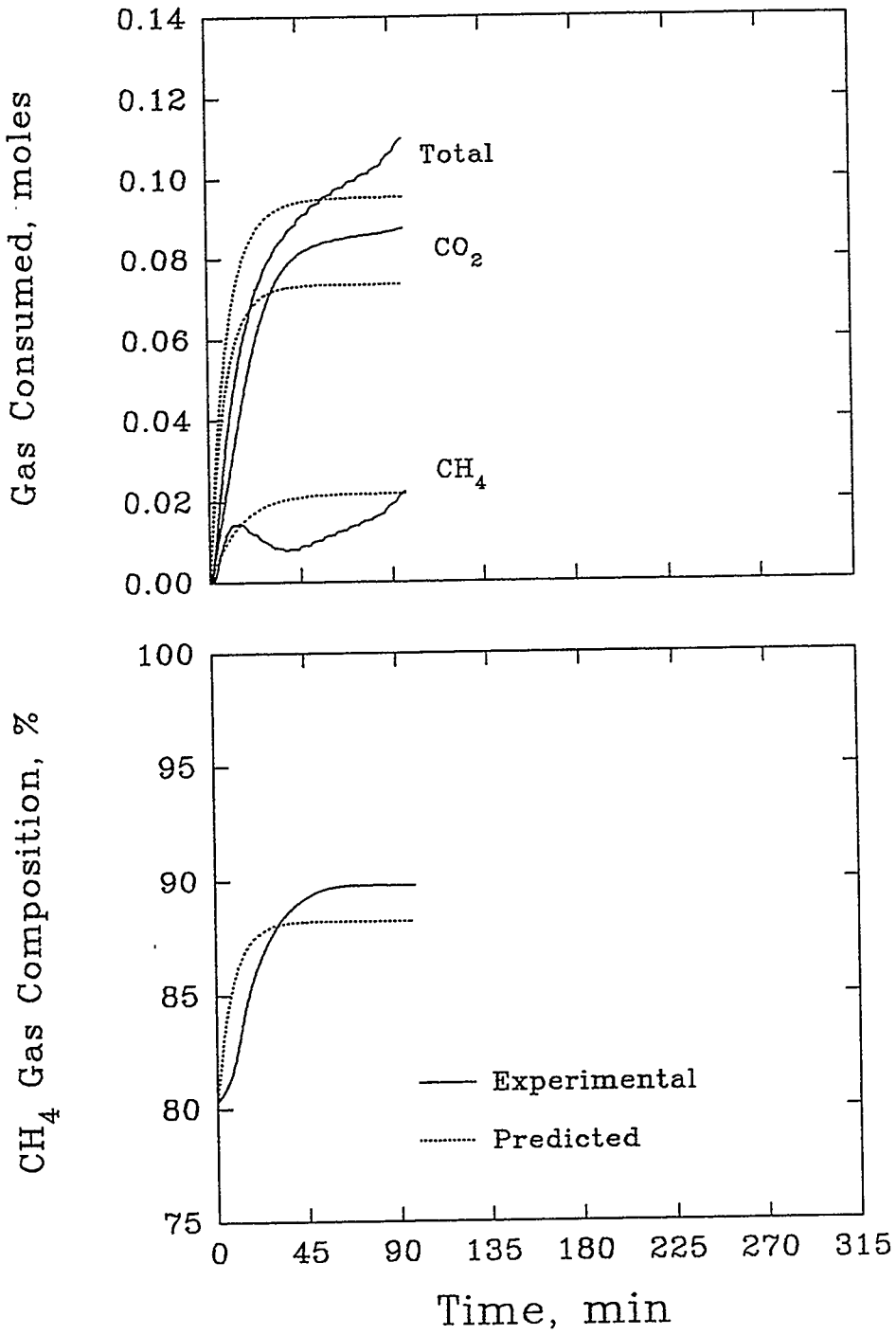

Figure 5.7 Solubility of CH_4 (80.3%) and CO_2 (19.7%) Gas in Water at P = 4.29 MPa & T = 278 K.

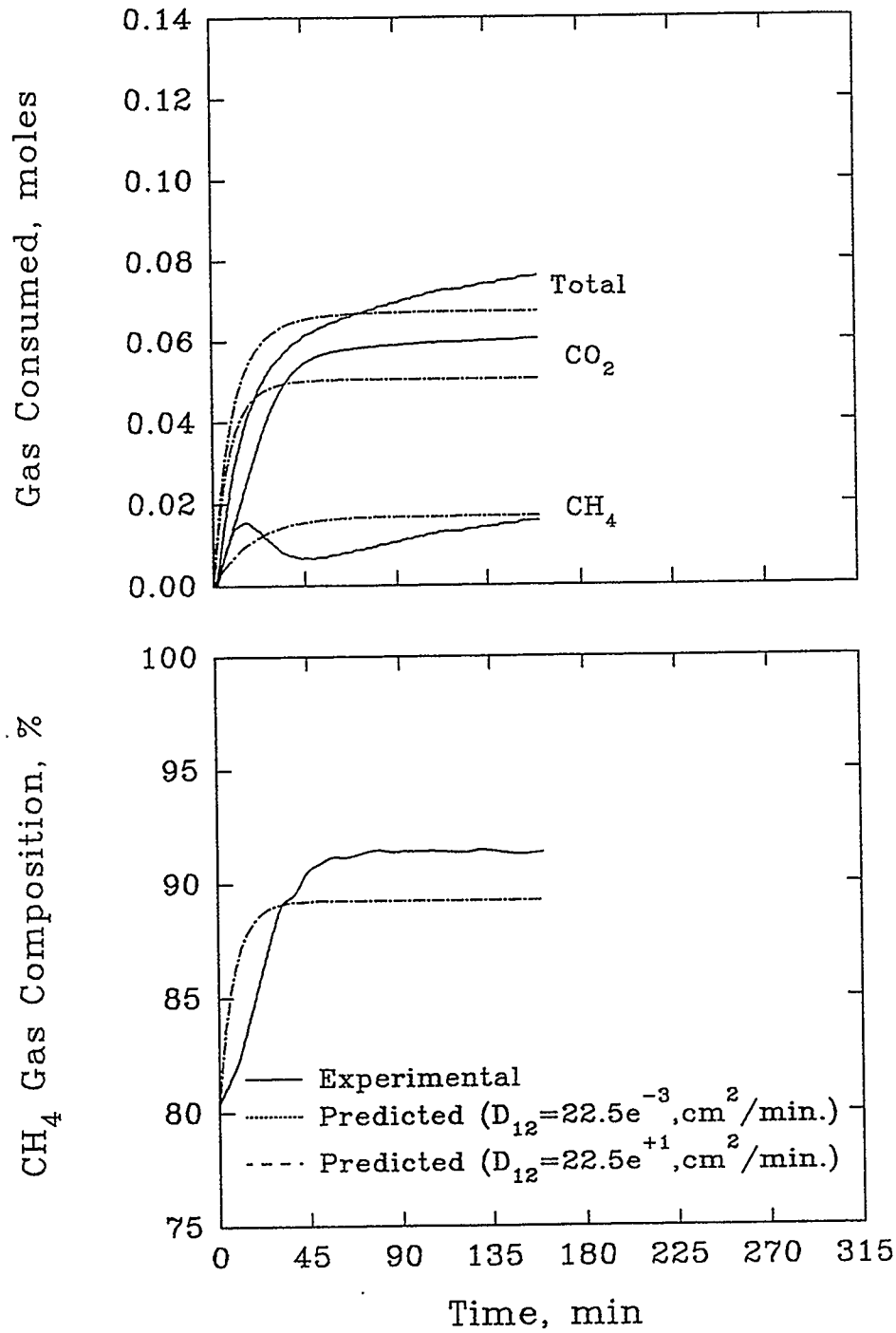

Figure 5.8 Effect of $Đ_{CH4-CO2}$ on Solubility of CH_4 (80.3%) and CO_2 (19.7%) Gas in Water at P = 2.69 MPa & T = 274 K.

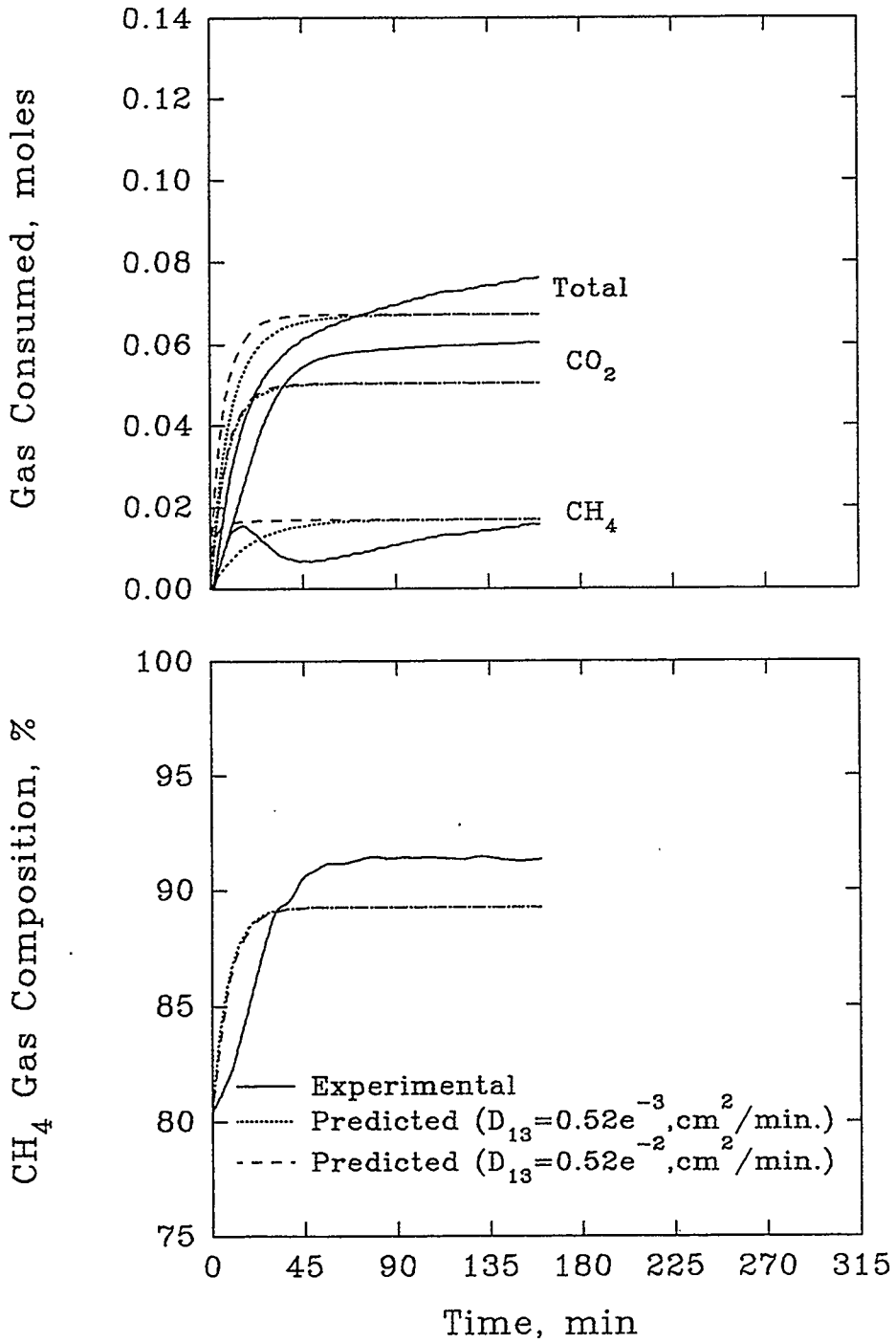

Figure 5.9 Effect of $Đ_{CH4\text{-}H2O}$ on Solubility of CH_4 (80.3%) and CO_2 (19.7%) Gas in Water at P = 2.69 MPa & T = 274 K.

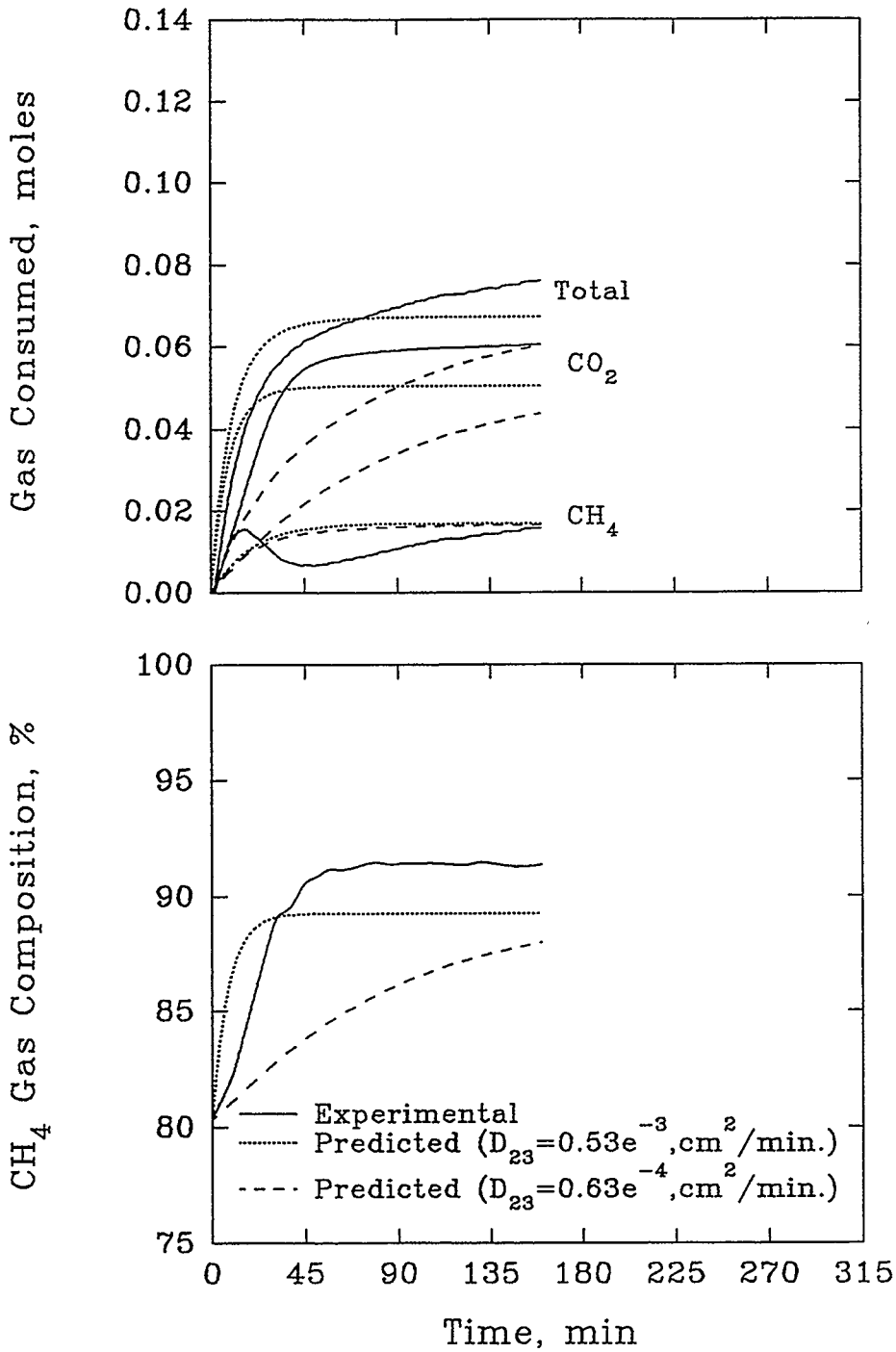

Figure 5.10 Effect of $Đ_{CO2\text{-}H2O}$ on Solubility of CH_4 (80.3%) and CO_2 (19.7%) Gas in Water at P = 2.69 MPa & T = 274 K.

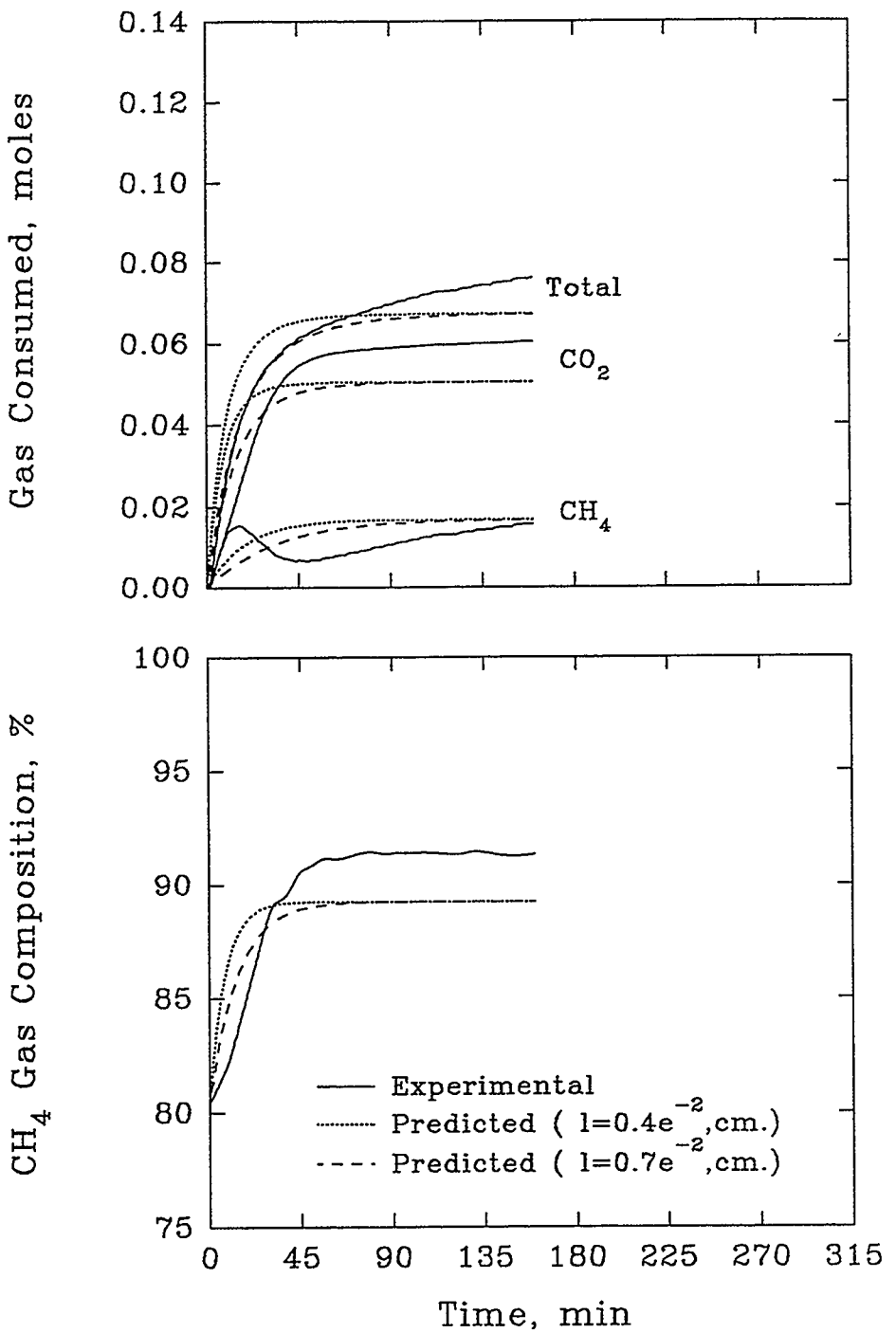

Figure 5.11 Effect of Film Thickness on Solubility of CH_4 (80.3%) and CO_2 (19.7%) Gas in Water at P = 2.69 MPa & T = 274 K.

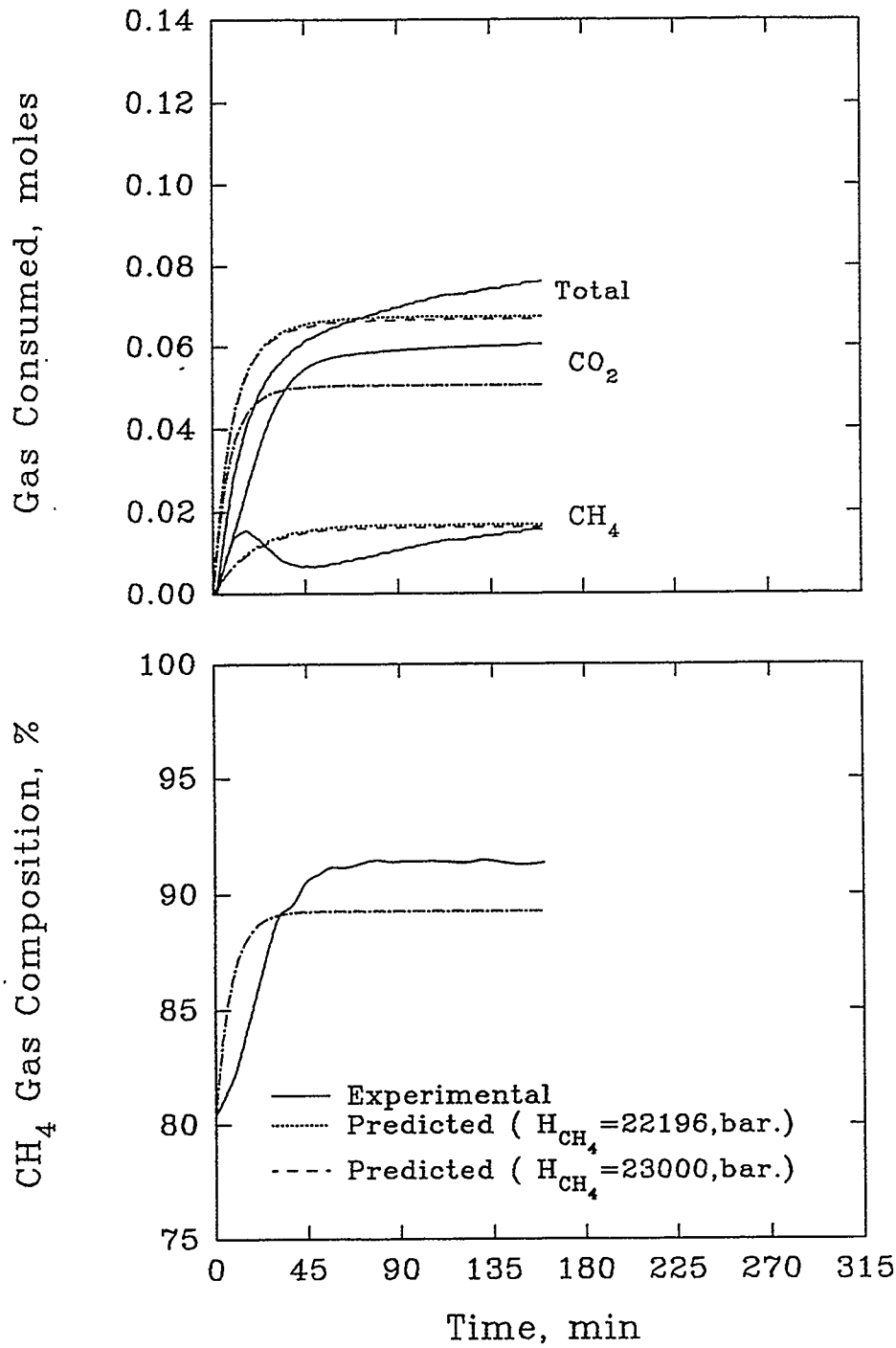

Figure 5.12 Effect of H_{CH4} on Solubility of CH_4 (80.3%) and CO_2 (19.7%) Gas in Water at P = 2.69 MPa & T = 274 K.

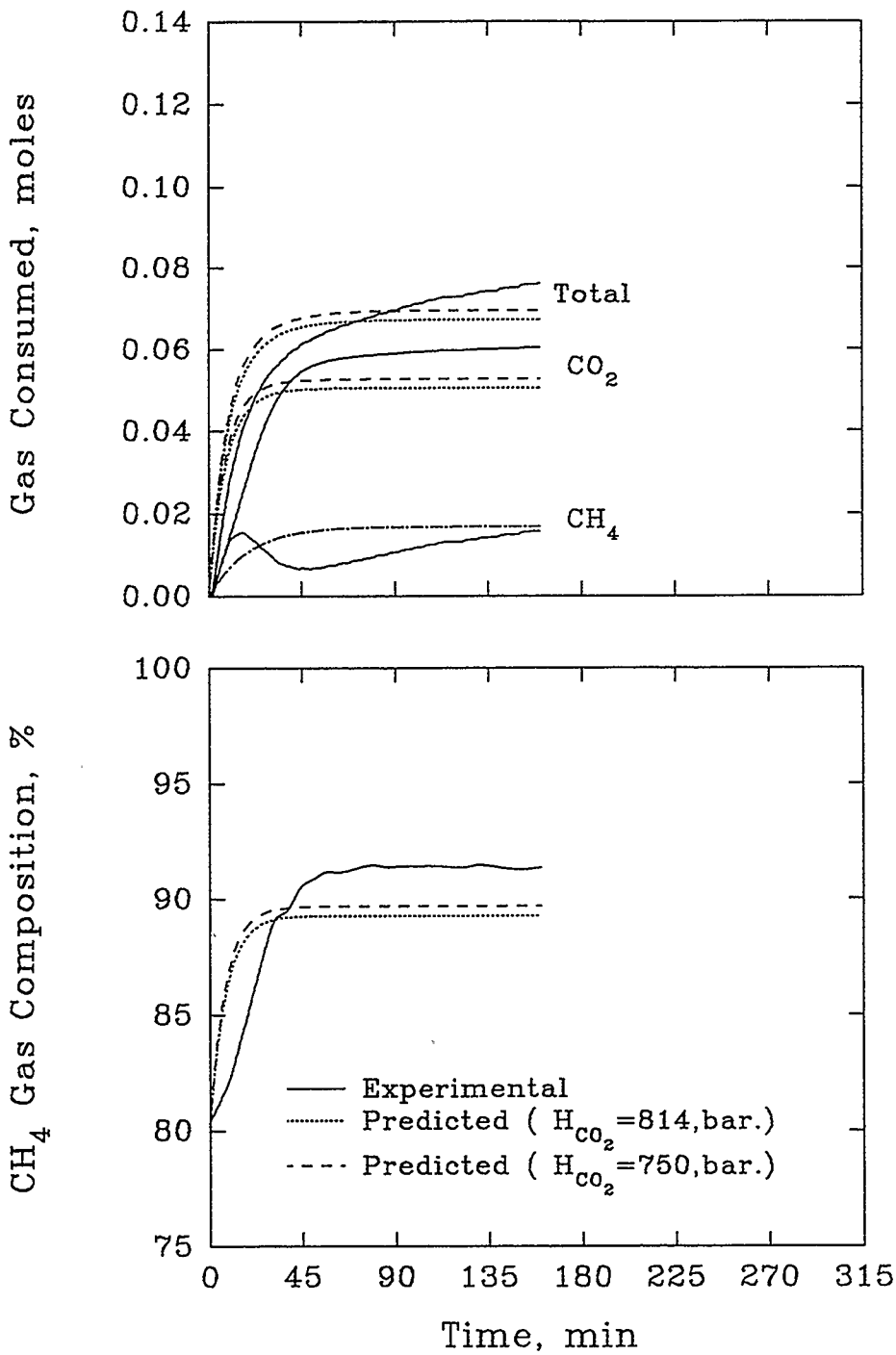

Figure 5.13 Effect of H_{CO2} on Solubility of CH_4 (80.3%) and CO_2 (19.7%) Gas in Water at P = 2.69 MPa & T = 274 K.

6. KINETICS OF GAS MIXTURE HYDRATE FORMATION

An overview of the kinetic model developed by Englezos et al. (1987b) for gas mixture hydrate formation is given here briefly. The model was based on crystallization theory coupled with the two-film theory for gas absorption into a liquid phase. The model does not contain any adjustable parameters. The kinetic rate constants which appear in the model were obtained previously from pure component hydrate formation data. This kinetic model was adapted to predict hydrate formation from CH_4 and CO_2 gas mixtures. Both experimental results and the predictions are presented.

6.1 Kinetic Modeling

Englezos et al. (1987b) considered the growth of a hydrate particle from a mixture of gases as a two-step process. First, the dissolved gases diffuse from the bulk of the solution to the hydrate crystal-liquid water interface and then by an adsorption process, the gas molecules are incorporated into the structured water framework. For modeling this two step process for mixtures, it was assumed that the rate of diffusion and adsorption of a gas are not affected by the presence of the other gas. Thus the total rate of consumption is equal to the sum of the consumption rates of each component gas and was given by

$$\left(\frac{dn}{dt}\right)_p = \sum_{j=1}^{2}\left(\frac{dn_j}{dt}\right)_p = \sum_{j=1}^{2} K_j^* A_p \left(f - f_{eq}\right)_j \qquad 6.1$$

where $(f - f_{eq})_j$ is the driving force of component j, K_j^* is the individual rate constant and A_p is the surface area of each particle. The rate constant, K_j^*, are determined from the modeling of the pure component kinetic data. f_j is the fugacity of the component j in the liquid solution and $f_{eq,j}$ is the fugacity of the component j in the gaseous mixture at the three phase equilibrium pressure for the mixture during hydrate formation. The gas phase

composition was thus incorporated indirectly into the above rate expression through the calculation of the fugacities.

The global reaction rate for all the particles is given by

$$R_y(t) = \int_0^\infty \left(\frac{dn}{dt}\right)_p \phi(s,t)ds \qquad 6.2$$

$$= \int_0^\infty \sum_{j=1}^{2} K_j^* A_p \left(f - f_{eq}\right)_j \phi(s,t)ds \qquad 6.3$$

$$= \pi \mu_2 \sum_{j=1}^{2} K_j^* \left(f - f_{eq}\right)_j \qquad 6.4$$

$$= \sum_{j=1}^{2} K_j \left(f - f_{eq}\right)_j \qquad 6.5$$

where $\phi(s,t)$ is the particle size distribution and μ_2 is the second moment of the particle given by

$$\mu_2 = \int_0^\infty s^2 \phi(s,t)ds \qquad 6.6$$

The two-film theory was used to describe the absorption of the gas at the gas-liquid interface. Assuming quasi-steady-state conditions, equimolar counter diffusion and an ideal liquid solution, the diffusion and reaction in the liquid film are described by the following Equations

$$D_j \frac{d^2 c_j}{dy^2} = K_j \left(f - f_{eq}\right)_j, \qquad j = 1.2. \qquad 6.7$$

Assuming that the number of moles of water remains practically constant, the concentration of the gas 'j' in the aqueous phase at three phase equilibrium can be estimated from :

$$c_{eq,j} = \frac{c_{wo} f_{eq,j}}{\left(H - f_{eq}\right)_j} \qquad 6.8$$

The change in the concentration of the gas in the aqueous phase can be computed as, (refer to Appendix B for the derivation)

$$\delta c_j = \left(\frac{c_{eq,j} + c_{wo}}{H_j - f_{eq,j}}\right) \delta f_j \qquad 6.9$$

where $\delta c_j = c_j - c_{eq,j}$ and $\delta f_j = f_j - f_{eq,j}$. Thus Equation 6.7 can be written as

$$D_j^* \frac{d^2 Y_j}{d y^2} = K_j Y_j, \qquad j = 1,2. \qquad 6.10$$

where,

$$Y_j = \left(f - f_{eq}\right)_j, \qquad D_j^* = D_j \left(\frac{c_{eq,j} + c_{wo}}{H_j - f_{eq,j}}\right) \qquad 6.11$$

Equation 6.10 satisfies the following boundary conditions:

$$\begin{aligned} at \quad y = 0, \qquad & Y_j = \left(f_g - f_{eq}\right)_j \\ at \quad y = y_L, \qquad & Y_j = \left(f_b - f_{eq}\right)_j \end{aligned} \qquad 6.12$$

Here it was assumed that the gas-phase resistance was negligible since the vapor pressure of water is very small and both hydrate forming gases are consumed.

Analytical solution of Equation 6.10 with the above boundary conditions yields the fugacity profile for the gas in the liquid film:

$$f_j = f_{eq,j} + \left(\frac{1}{\sinh \gamma_j}\right)\left\{\left(f_g - f_{eq}\right)_j \sinh\left(\gamma_j\left(1-\frac{y}{y_L}\right)\right) + \left(f_b - f_{eq}\right)_j \sinh\left(\gamma_j \frac{y}{y_L}\right)\right\} \quad 6.13$$

where γ_j is the Hatta number given by :

$$\gamma_j = y_L \sqrt{\frac{\pi K_j^* \mu_2}{D_j^*}} \quad 6.14$$

The flux at the interface can then be obtained from

$$\left(J_j\right)_{y=0} = -D_j\left(\frac{dc_j}{dy}\right)_{y=0} = -D_j^*\left(\frac{df_j}{dy}\right)_{y=0} \quad 6.15$$

The rate of transportation of a gas j to the liquid phase, where it either goes into solution or is converted to hydrates, is related to the flux at the gas-liquid interface by the following Equation:

$$\frac{dn_j}{dt} = \left(J_j\right)_{y=0} A_{(g-l)} \quad 6.16$$

Substitution of Equation 6.13 into Equation 6.15 and subsequent expression into 6.16 yields

$$\frac{dn_j}{dt} = \left(\frac{D_j^* \gamma_j A_{(g-l)}}{y_L}\right)\frac{\left(\left(f_g - f_{eq}\right)_j \cosh\gamma_j - \left(f_b - f_{eq}\right)_j\right)}{\sinh\gamma_j}, \qquad j=1,2. \qquad 6.17$$

The initial condition for this equation is the number of moles of a gas j that have been transported into the aqueous phase up to the "turbidity point". This is available from the experimental data. The variation in the fugacity of a gas in the bulk aqueous phase with respect to time is obtained by a mass balance in the bulk:

$$\frac{df_{b,j}}{dt} = \left(\frac{D_j^* \gamma_j a \left(H - f_{eq}\right)_j^2}{H_j c_{wo} y_L \sinh\gamma_j}\right)\left\{\left(f_g - f_{eq}\right)_j - \left(f_b - f_{eq}\right)_j \cosh\gamma_j\right\} - \frac{\pi K_j^* \mu_2 \left(H - f_{eq}\right)_j^2 \left(f_b - f_{eq}\right)_j}{H_j c_{wo}} \qquad 6.18$$

It was assumed in the model that at the turbidity point the fugacity of gas in the bulk aqueous phase drops to the three-phase equilibrium value instantaneously. Thus $f_{b,j} = f_{eq,j}$.

In addition to the mass balance equations a population balance is required to estimate μ_2 versus time. The equations describing the population balance are the same as those for a pure component hydrate formation i.e. Equations 4.21 to 4.23.

An average growth rate required for the computation of the first and second moments can be defined by Equation 4.24 but the linear growth rate is given by

$$\frac{ds}{dt} = \frac{2M}{\rho}\sum_{j=1}^{2} K_j^*\left(f-f_{eq}\right)_j \qquad 6.19$$

Upon substitution into Equation 4.24 we obtain

$$G_{av} = \left(\frac{2M}{\rho L}\right)\left(y_L \sum_{j=1}^{2} K_j^*\left\{\frac{\left(f_g+f_b-2f_{eq}\right)_j\left(\cosh\gamma_j-1\right)}{\gamma_j \sinh\gamma_j}+\left(L-y_L\right)\left(f_b-f_{eq}\right)_j\right\}\right) \qquad 6.20$$

The number of particles per unit volume of the aqueous phase at turbidity, μ_0^0, is computed from the moles of each gas that have dissolved just prior to the appearance of the hydrates and the critical radius of the nucleus:

$$\mu_0^0 = \frac{3M\left(n_{tb}-n_{eq,1}-n_{eq,2}\right)}{4\pi V_L \rho r_{cr}^3} \qquad 6.21$$

If n_{tb} moles of gas have dissolved into the aqueous phase at the turbidity point then the moles of the gas used up for the formation of the nuclei are equal to n_{tb} - $n_{eq,1}$ - $n_{eq,2}$, where $n_{eq,j}$ is the amount of the gas j dissolved at the three phase equilibrium conditions. The value of n_{eq} is obtained from f_{eq} and Henry's constant. The critical radius of the nucleus (Englezos et al., 1987b) is given by $r_{cr} = -(2\sigma / \Delta g)$. The free energy per unit volume of the product formed, Δg, is obtained from:

$$-\Delta g = \left(\frac{RT_{\exp}}{v_m}\right)\left(\sum_{j=1}^{2}\theta_j \ln\frac{f_{tb,j}}{f_{eq,j}}+\frac{n_w v_w\left(P_{\exp}-P_{eq}\right)}{RT_{\exp}}\right) \qquad 6.22$$

The parameters θ_j are the mole fractions of the gaseous components in the hydrate on a water free basis (Parrish and Prausnitz, 1972) and are calculated at the three-phase equilibrium condition using the method of Ng and Robinson (1976). $f_{tb,j}$ is the bulk fugacity of the gas j in the liquid given by

$$f_{tb,j} = H_j \left(\frac{n_{tb,j}}{n_{wo} + \sum_{j=1}^{2} n_{tb,j}} \right) \qquad 6.23$$

The initial conditions for the other two moments of the particle size distribution are

$$\mu_1^0 = 2 r_{cr} \mu_0^0 \quad \& \quad \mu_2^0 = 4 r_{cr}^2 \mu_0^0 \qquad 6.24$$

In the model developed by Englezos et al. (1987b), the particle size was represented as the particle radius. This term was overlooked as particle diameter while deriving the equation for the initial conditions for the first and second moments of the particle size distribution. Thus in Equations (29) and (30) of Englezos et al. (1987b) the factors of 2 and 4 respectively appeared which for the case of the particle radius do not exist. Hence in this work, the inaccuracy of the above equation was corrected and the equations of the model were re-derived considering the particle size as the particle diameter (Nyvlt et al., 1985).

6.2 Determination of Model Parameters

All the model parameters could be determined *a priori*. The rate constants K_j^* are those estimated from pure methane and pure carbon dioxide formation experiments and are shown in Tables 4.2 and 4.3. The diffusivities of methane and carbon dioxide in pure water were obtained using the Wilke and Chang correlation with improved parameters given by

Hayduk and Laudie (1974). Henry's constant and the liquid mass transfer coefficient, $k_L a$, were calculated from solubility data obtained in our laboratory. Gas phase fugacities were computed with the TB equation of state (Trebble and Bishnoi, 1987 & 1988) using the gas composition at the turbidity point. The gas phase fugacities were assumed to be constant during hydrate formation since the change in the mole fraction of a component in the gas phase from the turbidity point till the end of a run was less than 0.5 mole %, as stated earlier. Three phase equilibrium pressures for methane and carbon dioxide gas mixture were predicted using the correlation given by Adisasmito et al. (1991) and the gas composition at the turbidity point. The gas-liquid interfacial area $A_{(g-l)}$ was determined experimentally by Englezos et al. (1987a) to be 127.7 cm^2. The surface tension , σ, was taken to be equal to that of ice in water.

The film thickness was obtained from

$$y_L = \frac{D_j a}{k_{L,j} a} \qquad 6.25$$

The above equation for CH_4 and CO_2 gas is resulted in two different size of film thickness. But as per film model theory for multicomponent mass transfer, all of the resistance to mass transfer was concentrated in a thin film of the same thickness, 'y_l'. Thus the average of the two was taken as the film thickness.

6.3 Experimental Results and Model Predictions.

The seven ordinary differential Equations 6.17, 6.18, 4.21, 4.22 and 4.23 with their initial conditions constitute the governing equations which describe the dynamic behavior of the physical system. The only experimental information required is the number of moles of each gas that have been dissolved at the turbidity point. There are no adjustable

parameters which need to be estimated in the model. The ODE's were solved simultaneously using IMSL's DGEAR differential equation solver. A total of 12 experiments were performed. The predictions were made for only 6 experiments having lower driving force (No. 1, 2, 5, 6, 9 & 10 of Table 3.1). For the other 6 experiments with higher pressures, the model has failed to compute the critical size of the nucleus because the bulk fugacity of methane gas, based on Henry's law and the gas composition at the turbidity point, were estimated to be less than its equilibrium fugacity.

In Figures 6.1 - 6.6, the experimental data (shown in solid line) along with the model predictions (shown in dotted line) for the binary mixture of methane (80.3 %) and carbon dioxide are shown at three different temperatures. In the above figures the data are shown only after the turbidity point has occurred which is defined as the zero time in plots and the plots are of the methane, carbon dioxide and total gas consumption's versus time. The experimental data indicate that the nature of the total gas consumption curve, which was contributed by methane and carbon dioxide gas, is similar to that of pure gases. However during the hydrate formation, the rate of methane gas consumption is higher than that of carbon dioxide gas consumption. This is because the mole fraction of methane gas in the hydrate phase on a water free basis is higher than carbon dioxide (see Table 3.2). As can be seen from the figures, at higher driving forces the rate of gas hydrate formation is larger.

The model predictions had a large deviation from the experimental data. For the carbon dioxide gas consumption, the prediction was on the higher side while for methane gas consumption the prediction was on the lower side. The maximum prediction error was about 51.2 % for methane, 43.6 % for carbon dioxide and 16.2 % total. It is also seen that for the same temperature and higher pressure the deviation was larger. The deviation between the experimental value and predicted value can be attributed to a limitation of the kinetic model which was based on the assumption that the liquid mixtures are ideal, which

was also the case for the solubility model. Thus a new kinetic model is proposed considering the non-idealities of the liquid mixtures by using the multicomponent mass transfer model which includes the activity coefficients and the reaction term.

6.4 Kinetic Model for Non-Ideal Liquid Mixtures.

The rate of consumption of each component gas is given by Equation 6.1 and a global reaction rate is obtained from Equation 6.5. The film model for multicomponent mass transfer, as described in section 5.1.3, has been used along with the reaction term to describe the complete phenomenon of simultaneous absorption of gas and hydrate formation. By incorporating the reaction term into an equation of continuity, Equation 5.11 reduces to :

$$\frac{dN_i}{dz} = -K_j\left(f - f_{eq}\right)_j, \qquad j = 1,2. \qquad \textbf{6.26}$$

which shows that the molar fluxes for steady diffusion through a liquid film are position variant. The steady state unidirectional diffusion in the liquid film is described by Equations 5.13-5.20 and the boundary conditions are given by Equation 5.21. It is important to note that $[\Phi]$, the matrix of mass transfer rate factors, is a function of η whereas K_j, f_{eq}, c_t, Γ_{ij} and $Đ_{ij}$ are constant along the diffusion path. The diffusion fluxes can be obtained from Equation 5.25 and the molar fluxes from Equation 5.37 and 5.38. The fugacity of gas in the liquid can be related to the liquid mole fraction by the following equation

$$f_j = \gamma_j H_j x_j, \qquad j = 1,2. \qquad \textbf{6.27}$$

Knowing the interface and bulk composition, the above coupled first order differential equations can be solved to obtain the composition profile in the film and the molar fluxes at the interface and in the bulk at any given time 't'. The thermodynamic factor and activity coefficient can be estimated using suitable thermodynamic model.

The rate with which the gas is being transported to the liquid phase and either is dissolved or forms hydrates is related to the flux at the interface by the equation

$$\frac{dn_j}{dt} = \left(N_j\right)_{y=0} A_{(g-l)} \qquad \textbf{6.28}$$

The initial condition for this equation is the number of moles of each gas that have been transported into the aqueous phase up to the "turbidity point". This is available from the experimental data. The variation in the composition of gas in the bulk aqueous phase with respect to time is obtained by a mass balance in the bulk:

$$\frac{dx_{jb}}{dt} = \left(N_j\right)_b A_{(g-l)} - \frac{K_j\left(f_b - f_{eq}\right)_j}{V_L} \qquad \textbf{6.29}$$

At the turbidity point $x_{b,j} = x_{eq,j}$.

In addition to the mass balance equations a population balance is required to estimate μ_2 versus time. The equations describing the population balance are the same as those for the pure component hydrate formation, Equations 4.21 to 4.23 and initial condition are given by Equations 6.21 and 6.24.

An average growth rate required for the computation of the first and second moments can be defined by

$$G_{av} = \left(\frac{2M}{\rho L}\right)\left[\int_0^{y_L}\sum_1^2 K_j^*\left(f-f_{eq}\right)_j dy + \left(L-y_L\right)\sum_1^2 K_j^*\left(f_b-f_{eq}\right)_j\right] \quad \textbf{6.30}$$

The critical radius of the nucleus can be obtained using $r_{cr} = -(2\sigma / \Delta g)$, where the free energy per unit volume of the product formed, Δg, is given by Equation 6.22.

Thus solving the above seven differential Equations 6.28, 6.29, 4.21, 4.22 and 4.23 simultaneously along with the multicomponent mass transfer model will yield the gas consumption curve for methane and carbon dioxide during hydrate formation. This new kinetic model needs evaluation using the experimental data. To solve this model a suitable thermodynamic model is required to predict the thermodynamic factors and activity coefficients for the ternary mixture of methane, carbon dioxide and water. Identifying such a model is beyond the scope of the present work.

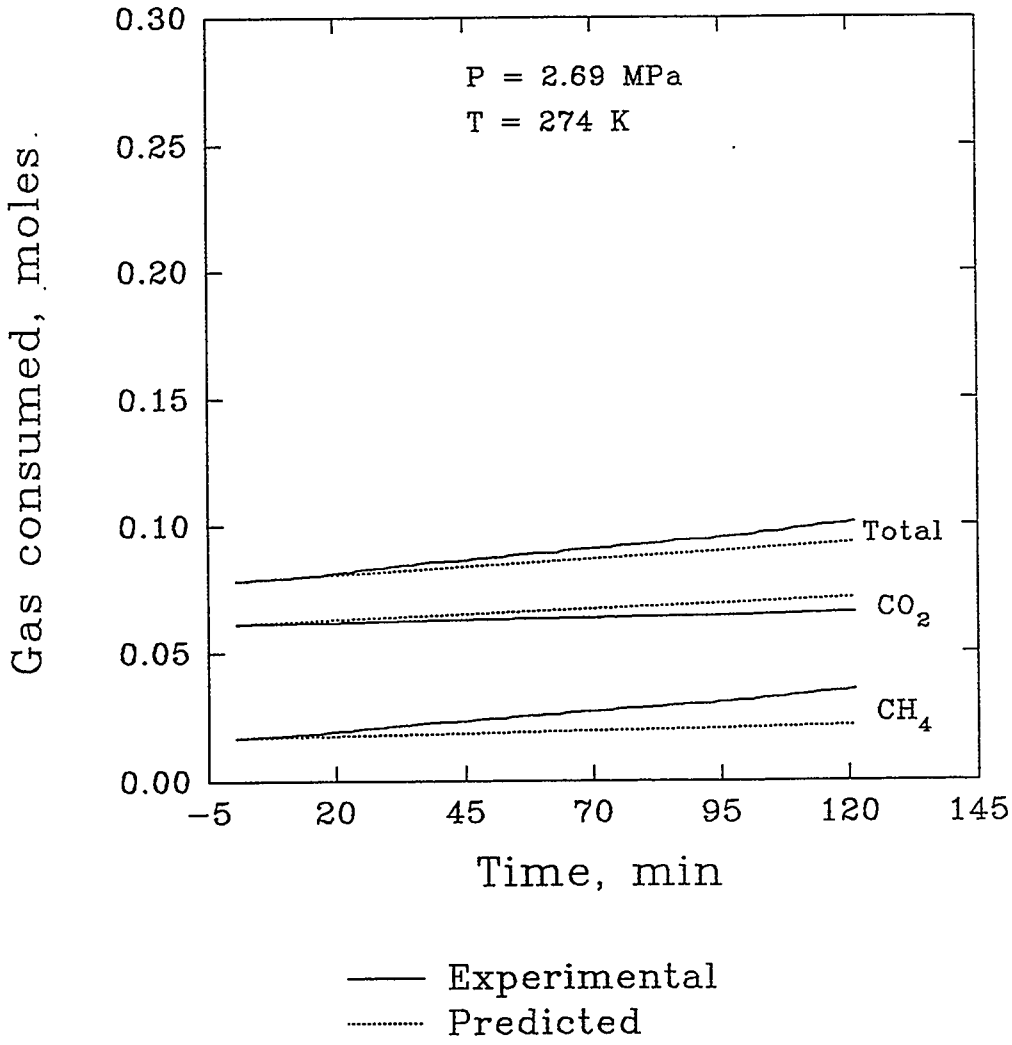

Figure 6.1 **CH_4 (80.3%) and CO_2 (19.7%) Hydrate Formation at a Nominal Temperature of 274 K and P = 2.69 MPa.**

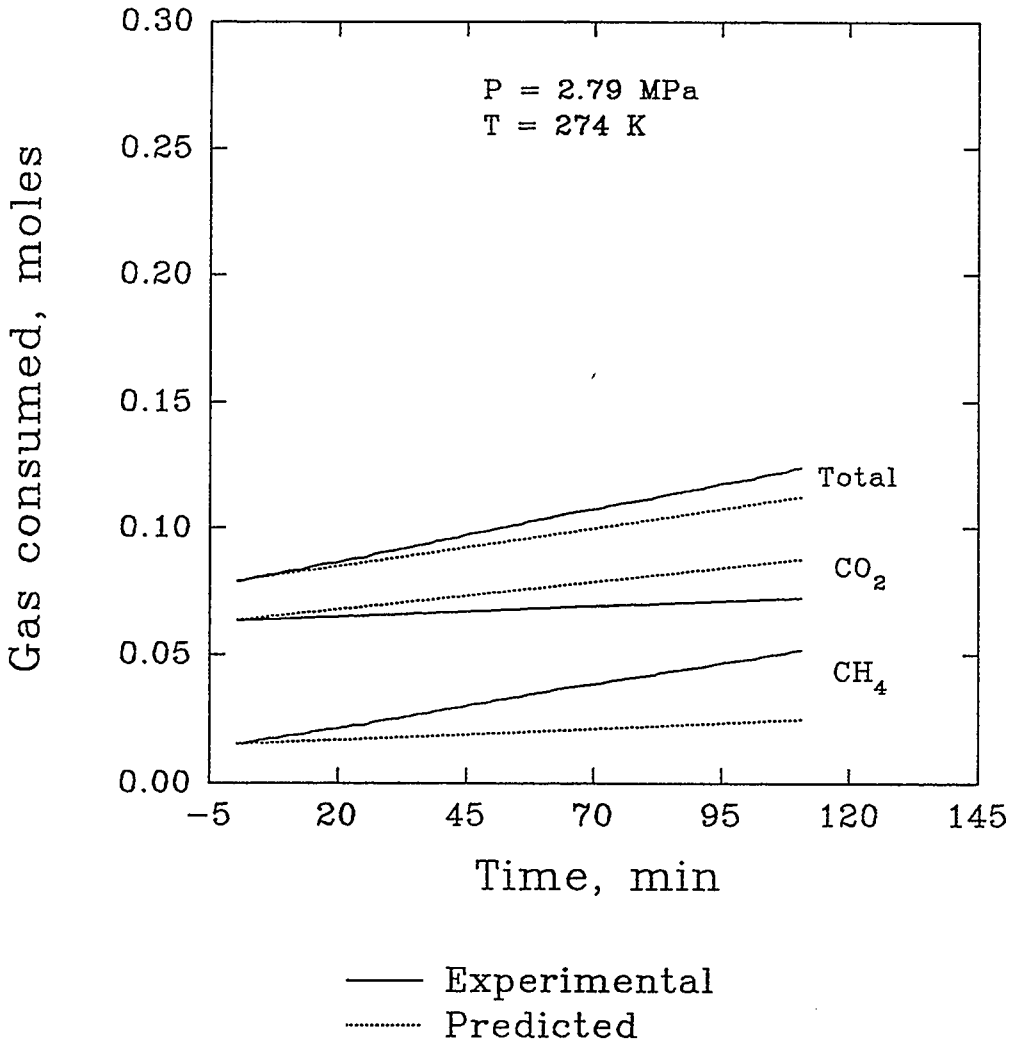

Figure 6.2 **CH_4 (80.3%) and CO_2 (19.7%) Hydrate Formation at a Nominal Temperature of 274 K and P = 2.79 MPa.**

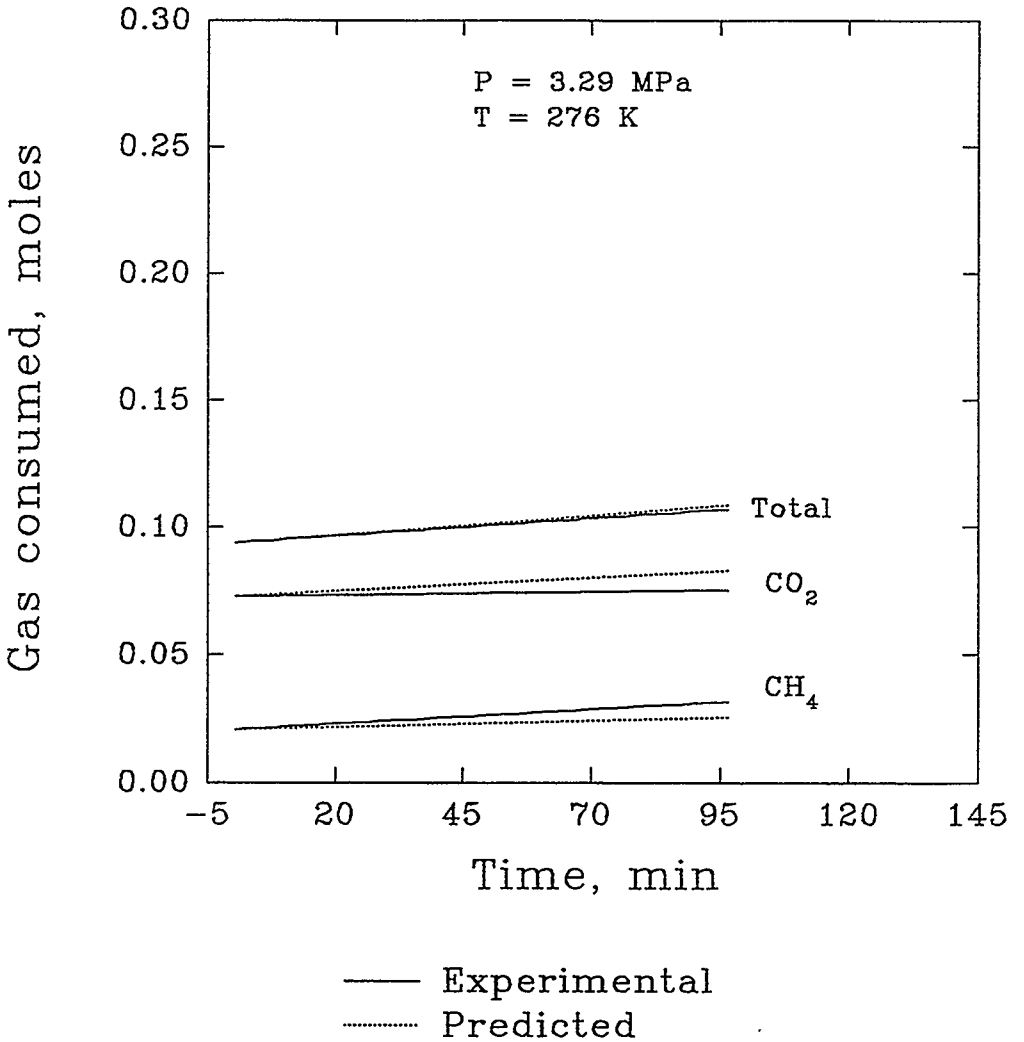

Figure 6.3 CH_4 (80.3%) and CO_2 (19.7%) Hydrate Formation at a Nominal Temperature of 276 K and P = 3.29 MPa.

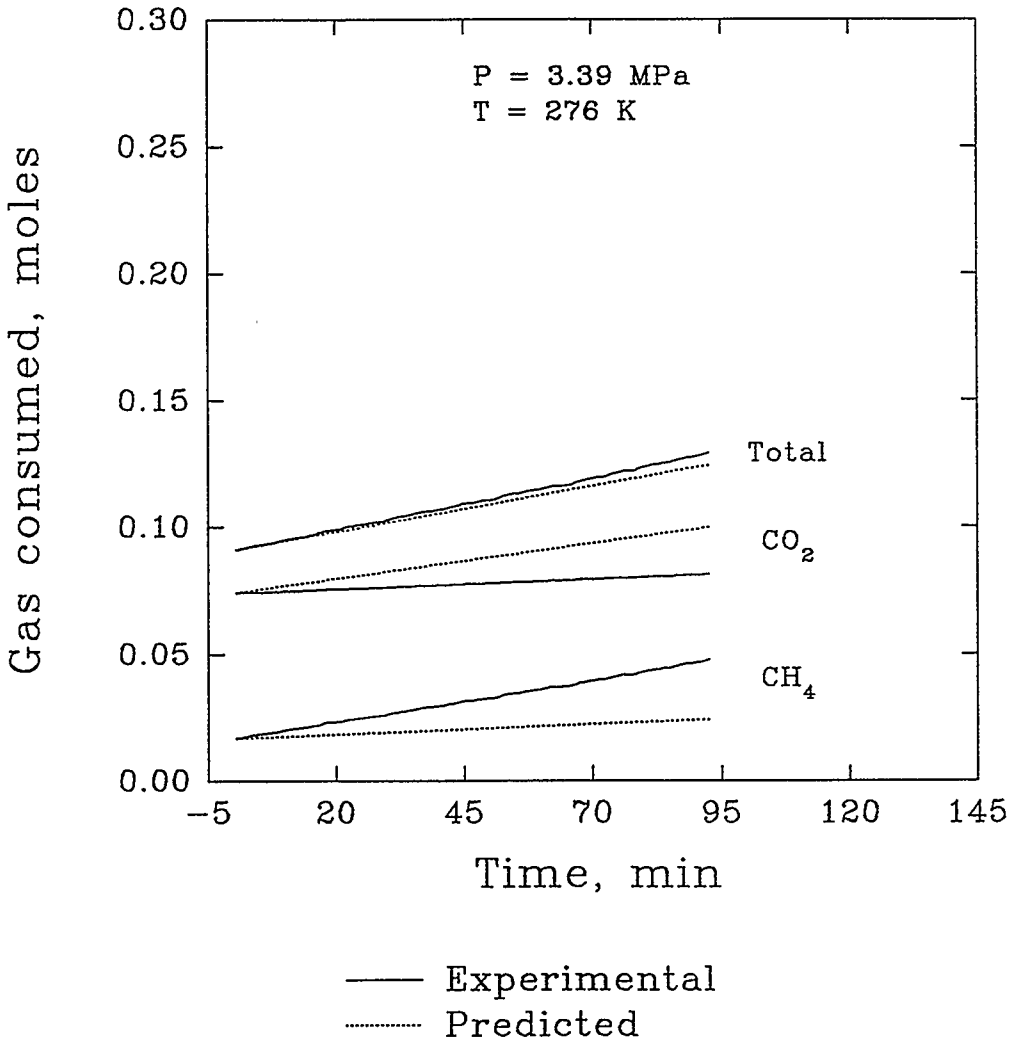

Figure 6.4 **CH_4 (80.3%) and CO_2 (19.7%) Hydrate Formation at a Nominal Temperature of 276 K and P = 3.39 MPa.**

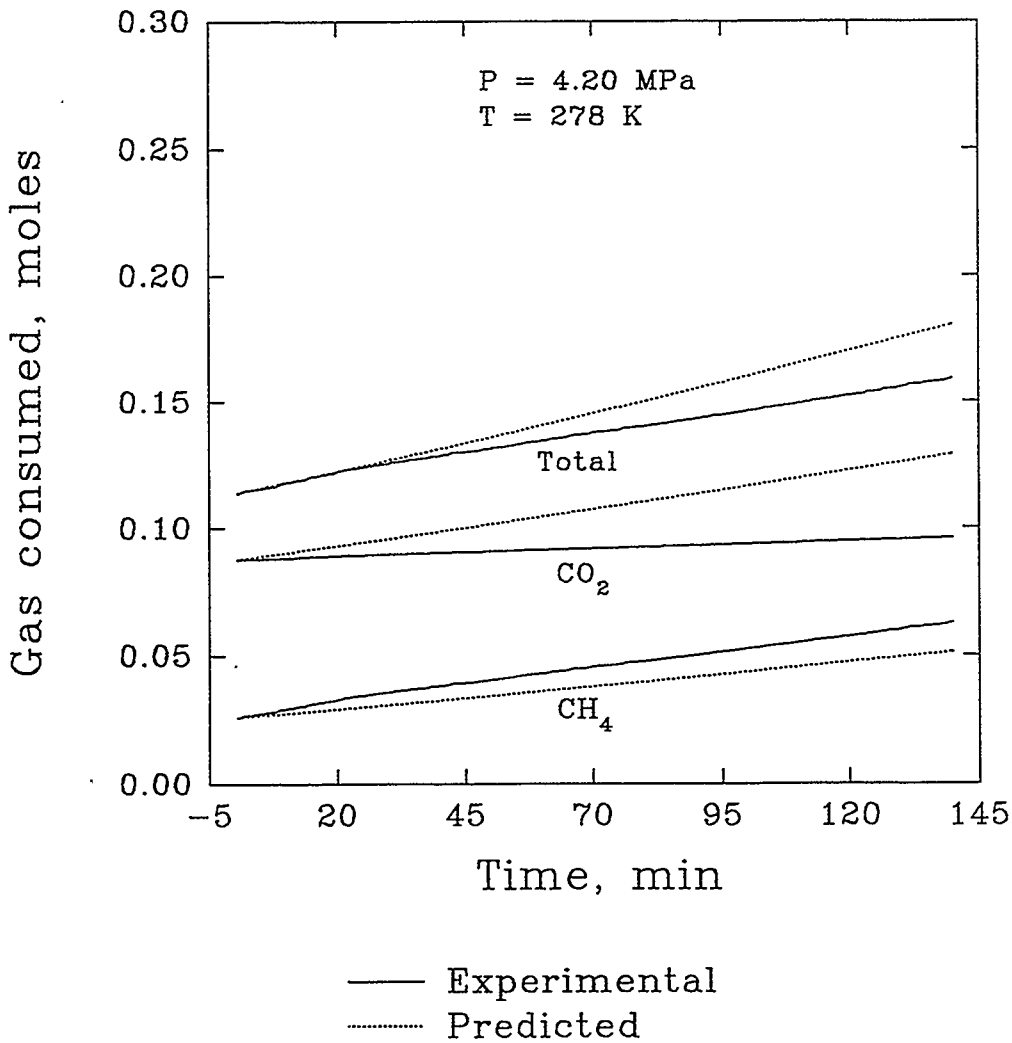

Figure 6.5 **CH_4 (80.3%) and CO_2 (19.7%) Hydrate Formation at a Nominal Temperature of 278 K and P = 4.20 MPa.**

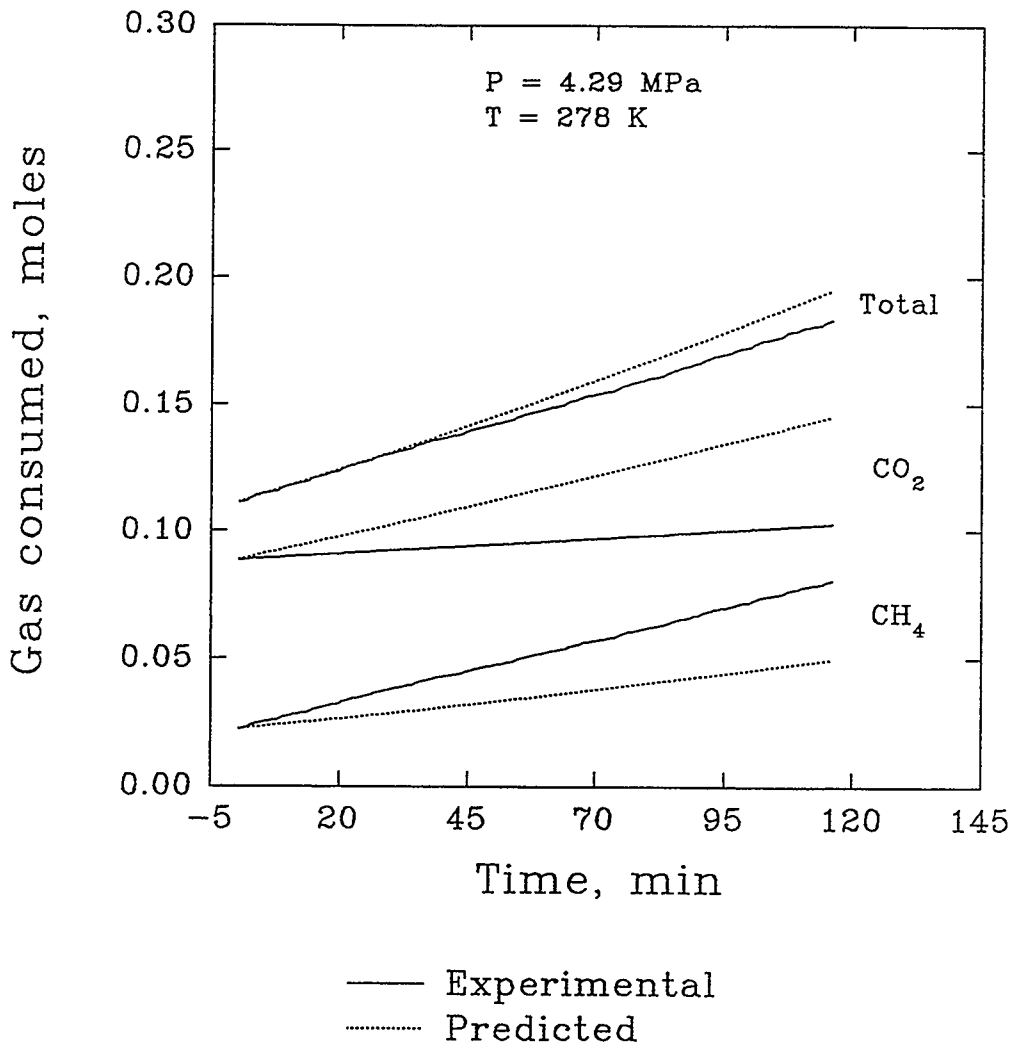

Figure 6.6 **CH_4 (80.3%) and CO_2 (19.7%) Hydrate Formation at a Nominal Temperature of 278 K and P = 4.29 MPa.**

7. CONCLUSIONS AND RECOMMENDATIONS

7.1 Conclusions

Experimental data on the kinetics of methane and carbon dioxide gas mixture hydrate formation were obtained. It was observed experimentally that the methane gas composition in the reactor gas phase increases till the saturation of carbon dioxide in the liquid phase occurs. It then attains a constant value. During the absorption of the two gases (before the turbidity point), there was a reverse diffusion of methane gas indicating a strong interaction between the two gases. During the hydrate formation, the gas composition in the reactor gas phase was almost constant and the rate of methane gas consumption was higher than that of carbon dioxide gas.

The experimental data on the simultaneous absorption of methane and carbon dioxide gases in water were modeled. A solubility model was developed combining the two-film model for multicomponent mass transfer using the exact solution of the Maxwell-Stefan equation. The solubility of gases in water and the methane gas composition in the reactor gas phase was computed. The model could not predict the reverse diffusion behavior obtained for the methane in the mixture. A modification to the solubility model incorporating non-ideal liquid mixtures behavior is proposed. The model needs evaluation and comparison with experimental data.

Kinetic rate constants for methane and carbon dioxide gas hydrate formation were determined using the experimental data obtained from the previous work. The kinetic model developed by Englezos et al. (1987a) was modified slightly for this determinations. It was observed that kinetic rate constant for carbon dioxide gas was higher than methane. The model predictions matched the experimental data very well.

Experimental data on the kinetics of methane and carbon dioxide gas mixture hydrate formation obtained in this work were modeled using a kinetic model developed by Englezos et al. (1987b) for gas mixture hydrate formation. The methane and carbon dioxide gas consumption's during the hydrate formation were predicted. There was a large deviation between the model predictions and the experimental data, which is likely due to the assumption made for the model that the liquid solution was ideal. A new kinetic model for non-ideal liquid mixtures is proposed combining the two-film model for multicomponent mass transfer using the exact solution of the Maxwell-Stefan equation and incorporating the thermodynamic factors and activity coefficients in the model. The proposed model needs evaluation and comparison with experimental data.

7.2 Recommendations

More experiments should be performed for gas mixture hydrate formation with at least two other gas compositions of methane and carbon dioxide mixtures.

A suitable thermodynamic model for the ternary system of methane, carbon dioxide and water should be used to compute the thermodynamic factors and activity coefficients.

The proposed solubility model for non-ideal liquid mixtures should be solved to estimate the solubility of gases in water.

The proposed kinetic model for non-ideal liquid mixtures should be solved to predict the growth rate of gas hydrates.

REFERENCES

Adamson, A. W., 1976, *Physical Chemistry of Surfaces*, 3rd edition, Wiley, New York.

Adisasmito, S., Frank, R. J. and Sloan, E. D., 1991, "Hydrates of Carbon Dioxide and Methane Mixtures." *J. Chem. Eng. Data*, **36**, 68-71.

Bishnoi, P. R., Jeje, A. A., Kalogerakis, N. E. and Saeger, R., 1985, "The Kinetics of Formation and Decomposition from Mixtures of Natural Gas Components - Experimental Data and Development of Generalized Predictive Rate Expressions", Annual Report. *Energy Mines and Resources*, Ottawa, Canada.

Bishnoi, P. R., Jeje, A. A., Kalogerakis, N. E., Dholabhai, P. D. and Englezos, P., 1986, "The Kinetics of Formation and Decomposition of Hydrates from Mixtures of Natural Gas Components", Final Report. *Energy Mines and Resources*, Ottawa, Canada.

Claussen, W. F., 1951, "A Second Water Structure for Inert Gas Hydrates." *Journal of Chemical Physics*, **19**, 259, 662, 1425.

Danckwerts, P. V., 1970, *Gas Liquid Reactions*, pp. 31-70, McGraw-Hill, New York.

Deitz, W. A., 1967, "Response Factors for Gas Chromatographic Analyses." *J. of G. C.*, 68-71.

Dholabhai, P. D., Englezos, P., Kalogerakis, N. and Bishnoi, P. R., 1991, "Equilibrium Conditions for Methane Formation in Aqueous Mixed Electrolyte Solutions." *Can. J. Chem. Eng.*, **69**, 800-805.

Dholabhai, P. D., Kalogerakis, N. and Bishnoi, P. R., 1993, "Kinetics of Methane Hydrate Formation in Aqueous Mixed Electrolyte Solutions." *Can. J. Chem. Eng.*, **71**, 68-74.

Englezos, P. and Bishnoi, P. R., 1988, "Prediction of Gas Hydrate Formation from Aqueous Electrolyte Solutions." *AIChE J.*, **34(10)**, 1718-1721.

Englezos, P. and Bishnoi, P. R., 1991, "Experimental Study on the Equilibrium Ethane Hydrate Formation Conditions in Aqueous Electrolyte Solutions." *Ind. Eng. Chem. Res.*, **30**, 1655-1659.

Englezos, P., Huang, Z. and Bishnoi, P. R., 1991, "Prediction of Natural Gas Hydrate Formation Conditions in the Presence of Methanol Using Trebble-Bishnoi Equation of State." *Journal of Canadian Petroleum Technology*, **30(2)**, 148-155.

Englezos, P., Dholabhai, P. D., Kalogerakis, N. and Bishnoi, P. R., 1987(a), "Kinetics of Formation of Methane and Ethane Gas Hydrates." *Chem. Eng. Sci.*, **42**, 2647-2658.

Englezos, P., Dholabhai, P. D., Kalogerakis, N. and Bishnoi, P. R., 1987(b), "Kinetics of Gas Hydrate Formation from Mixtures of Methane and Ethane." *Chem. Eng. Sci.*, **42**, 2659-2666.

Hayduk, W. and Laudie, H., 1974, "Prediction of Diffusion Coefficients for Non Electrolytes in Dilute Aqueous Solutions." *AIChE J.*, **20**, 611-615.

Holder, G. D., Korbin, G. and Papadopoulus, K. D., 1980, "Thermodynamic and Molecular Properties of Gas Hydrates from Mixtures Containing Methane, Argon and Krypton." *Ind. Eng. Chem. Fundam.*, **19**, 282.

Jeffrey, G. A., and McMullan, R. K., 1967, "The Clathrate Hydrates." *Prog. Inorg. Chem.*, **8**, 43.

John, V. T., Papadopoulus, K. D., and Holder, G. D., 1985, "A Generalized Model for Predicting Equilibrium Conditions for Gas Hydrates." *AIChE J.*, **31**, 252-259.

Kalogerakis, N. E. and Luus, R., 1983, "Improvement of Gauss-Newton Method For Parameter Estimation Through the Use of Information Index." *Ind. Eng. Chem. Fundam.*, **22**, 436-445.

Kane, S. G., Evans, T. W., Brian, P. L. T. and Sarofim, A. F., 1974, "Determination of the kinetics of secondary nucleation in batch crystallizers." *AIChE J.*, **20**, 855-862.

Kim, H. C., Bishnoi, P. R., Heidemann, R. A. and Rizvi, S. S. H., 1987, "Kinetics of Methane Hydrate Decomposition." *Chem. Eng. Sci.*, **42(7)**, 1645-1653.

Krishna, R. and Standart, G. L., 1976, " A Multicomponent Film Model Incorporating an Exact Matrix Method of solution to the Maxwell-Stefan Equations." *AIChE J.*, **22**, 383-389.

Krishna, R. and Standart, G. L., 1979, " Mass and Energy Transfer in Multicomponent Systems." *Chem. Eng. Commun.*, **3**, 201-275.

Krishna, R. and Taylor, R., 1993, *Multicomponent Mass Transfer*, John Wiley & Sons, Inc., New York.

Krishnamurthy, R. and Taylor, R., 1982, "Calculation of Multicomponent Mass Transfer at High Transfer Rates." *Chem. Eng. J.*, **25**, 47-54.

Lekvam, K and Bishnoi, P. R., 1995, "Dissolution of Methane in Water at Low Temperatures and Intermediate Pressures." submitted for publication.

Makogon, Y. F., 1981, *Hydrates of Natural Gas*, (Translated by Cieslewicz, W. J.), PennWell Books, Tulsa, OK.

Marshall, D. R., Saito, S. and Kobayashi, R., 1964, "Hydrates at High Pressures. 1: Methane-Water, Argon-Water and Nitrogen-Water Systems." *AIChE J.*, **10(2)**, 202.

"MATLAB", A computer software package supported by The MathWorks Inc., Cochituate Place, 24 Prime Park Way, Natick, Mass. 01760, USA.

"MEGHA", A computer software package supported by Megha Technologies Inc., Calgary, Alberta, Canada.

Munjal, P. and Stewart, P. B., 1971, "Correlation Equation for Solubility of Carbon Dioxide in Water, Seawater and Seawater Concentrates." *J. Chem. Eng. Data*, **16(2)**, 70.

Ng, H. J. and Robinson, D. B., 1976, "The Measurement and Prediction of Hydrate Formation in Liquid Hydrocarbon - Water System." *Ind. Eng. Chem. Fundam.*, **15**, 59-64.

Nyvlt, J., Sohnel, O., Matuchova, M. and Broul, M., 1985, *The Kinetics of Industrial Crystallization*, Chemical Engineering Monographs, No. 19, Elsevier, Amsterdam.

Parrish, W. R. and Prausnitz, J. M., 1972, "Dissociation Pressures of Gas Hydrates Formed by Gas Mixtures." *Ind. Eng. Chem. Proc. Des. Dev.*, **11(1)**, 26-34.

Reinhardt, D. and Dialer, K., 1981, "Geometrical Relationships for Ternary Gas Diffusion Balances and Criteria for Multicomponent Phenomena." *Chem. Eng. Sci.*, **36**, 1557.

Sloan, E. D., 1990, *Clathrate Hydrates of Natural Gases*; Mercel Dekker Inc., New York.

Smith, L. W. and Taylor, R., 1983, "Film Models for Multicomponent Mass Transfer: A Statistical Comparison." *Ind. Eng. Chem. Fundam.*, **22**, 97-104.

Taylor, R. and Smith, L. W., 1982, "On Some Explicit Approximate Solutions of the Maxwell-Stefan Equations for the Multicomponent Film Model." *Chem. Eng. Commun.*, **14**, 361-370.

Taylor, R. and Webb, D. R., 1980, "Stability of the Film Model for Multicomponent Mass Transfer." *Chem. Eng. Commun.*, **6**, 175-189.

Toor, H. L., 1957, " Diffusion in Three Component Gas Mixtures." *AIChE J.*, **3**, 197-207.

Trebble, M. A., 1990, "An evaluation of Multiple Binary Interaction Parameters in Cubic Equations of State." *Can. J. Chem. Eng.*, **68(3)**, 487.

Trebble, M. A. and Bishnoi, P. R., 1987, "Development of a New Four-Parameter Cubic Equation of State." *Fluid Phase Equilibria*, **35**, 1-18.

Trebble, M. A. and Bishnoi, P. R., 1988, "Thermodynamic Property Predictions with the Trebble-Bishnoi Equation of State." *Fluid Phase Equilibria*, **39**, 111-128.

Trebble, M. A. and Bishnoi, P. R., 1988, "Extension of the Trebble-Bishnoi Equation of State." *Fluid Phase Equilibria*, **40**, 1-21.

van der Waals, J. H. and Platteuw, J. C., 1959, "Clathrate Solutions." *Adv. Chem. Phys.*, **2(1)**, 1.

von Stackelberg, M. and Muller, H.R., 1954, "Feste Gas Hydrate II." *Z. Electrochem.*, **58**, 215.

Vysniauskas, A. and Bishnoi, P.R., 1983, "A Kinetic Study of Methane Hydrate Formation." *Chem. Eng. Sci.*, **38**, 1061-1072.

Vysniauskas, A. and Bishnoi, P.R., 1985 " Kinetics of Ethane Hydrate Formation." *Chem. Eng. Sci.*, **40,** 1061-1072.

APPENDIX A

Physical Absorption of Gas into Quiescent Liquids (Danckwerts, 1970).

During initial dissolution, the gas in the reactor is in contact with the quiescent liquid. The surface is plane and the liquid is infinitely deep. The surface of the liquid first comes into contact with the gas at time t=0 having initial concentration c^0, and it is assumed that from then on the concentration in the plane of the surface is uniformly equal to c^*. This concentration corresponds to the solubility of the gas at the partial pressure prevailing above the surface of the liquid, and it is assumed to be constant.

The variation in time and space of the concentration 'c' of dissolved gas in the liquid is governed by the diffusion Equation

$$D\frac{\partial^2 c}{\partial z^2} = \frac{\partial c}{\partial t} \qquad \text{A-1}$$

where z is the distance measured from the surface z=0, and D is the diffusivity of the dissolved gas. Thus the rate of transfer of dissolved gas across unit surface area of the liquid is

$$R_z = -D\left(\frac{\partial c}{\partial z}\right)_{z=0} \qquad \text{A-2}$$

The solution of Equation A-1 with

$$\begin{aligned} c &= c^*, & z &= 0, & t &> 0 \\ c &= c^0, & z &> 0, & t &= 0 \\ c &= c^0, & z &= \infty, & t &> 0 \end{aligned} \qquad \text{A-3}$$

is

$$c - c^0 = \left(c^* - c^0\right)\left(1 - erf\frac{z}{2\sqrt{Dt}}\right) \qquad \text{A-4}$$

It follows from Equations A-2 and A-4 that

$$R_z = \left(c^* - c^0\right)\sqrt{\frac{D}{\pi t}} \qquad \text{A-5}$$

The amount of the gas absorbed by unit surface area of the liquid in time t is

$$Q = \int_0^t R_z\,dt = 2\left(c^* - c^0\right)\sqrt{\frac{Dt}{\pi}} \qquad \text{A-6}$$

The concentration of the gas can be written in terms of its fugacity, assuming that the number of moles of the water remains practically constant, as

$$c^* = \frac{f c_{w0}}{H} \qquad \text{A-7}$$

Assuming the water is free of the gas initially and using Equations A-6 and A-7, the amount of the gas dissolved in water is given by

$$n = \frac{2A f c_{w0}}{H}\sqrt{\frac{Dt}{\pi}} \qquad \text{A-8}$$

APPENDIX B

The Change in the Concentration of Gas in the Aqueous Phase.

Let us represent δc as the change in the concentration and δf as the change in the fugacity of the gas in an aqueous phase given by

$$\delta c = c - c_{eq} \qquad \text{B-1}$$

$$\delta f = f - f_{eq} \qquad \text{B-2}$$

where subscript 'eq' stands for the three phase equilibrium.

The fugacity of the gas in aqueous phase can be written in terms of its composition as

$$f = Hx \qquad \text{B-3}$$

where H is the Henry's constant.

The concentration of the gas in the aqueous phase is given by

$$c = c_{wo}\left(\frac{x}{1-x}\right) \qquad \text{B-4}$$

where c_{w0} is the initial concentration of water.

Using Equation B-3 in B-4 gives

$$c = c_{wo}\left(\frac{f}{H-f}\right) \qquad \textbf{B-5}$$

Similarly, the concentration of the gas in the aqueous phase at three phase equilibrium is given by

$$c_{eq} = c_{wo}\left(\frac{f_{eq}}{H-f_{eq}}\right) \qquad \textbf{B-6}$$

Combining Equations B-1, B-5 and B-6 gives

$$\delta c = c_{wo}\left(\frac{f}{H-f}\right) - c_{wo}\left(\frac{f_{eq}}{H-f_{eq}}\right) \qquad \textbf{B-7}$$

Using Equation B-2 in B-7 gives

$$\delta c = c_{wo}\left(\frac{f_{eq}+\delta f}{H-f_{eq}-\delta f}\right) - c_{wo}\left(\frac{f_{eq}}{H-f_{eq}}\right) \qquad \textbf{B-8}$$

which simplifies to

$$\delta c = \frac{c_{wo} H \delta f}{\left(H-f_{eq}\right)^2 - \left(H-f_{eq}\right)\delta f} \qquad \textbf{B-9}$$

Neglecting the product $\delta c * \delta f$ after the cross multiplication of Equation B-9 results

$$\delta c = \frac{c_{wo} H \delta f}{\left(H-f_{eq}\right)^2} \qquad \textbf{B-10}$$

which using Equation B-6 can also be written as

$$\delta c = \left(\frac{c_{eq} + c_{wo}}{H - f_{eq}}\right) \delta f \qquad \textbf{B-11}$$

APPENDIX C

Derivation of Equation 5.15 in Chapter 5.

For steady state unidirectional diffusion under isobaric, isothermal conditions the Maxwell-Stefan Equations can be written as

$$\sum_{j=1}^{n-1}\Gamma_{ij}\frac{dx_j}{dz} = \sum_{j=1}^{n}\frac{\left(x_i N_j - x_j N_i\right)}{c_t Đ_{ij}}; \qquad i = 1,2,\ldots,n. \qquad \text{C-1}$$

where $Đ_{ij}$ is the Fick's binary diffusion coefficient of the i-j pairs. The $Đ_{ij}$ and c_t are assumed to be constant in the film. Γ_{ij}, the thermodynamic factor, is defined by

$$\Gamma_{ij} = \delta_{ij} + x_i \left.\frac{\partial \ln \gamma_i}{\partial x_j}\right|_{T,P,x_k,k\neq j=1\ldots n-1} \qquad \text{C-2}$$

Only n-1 of Equation C-1 are independent because the mole fractions add to unity, and the mole fraction gradient ($dx_i/d\eta$) and the molar diffusion fluxes (J_i) sum over n species to zero. Separating the nth term from the right hand side of Equation C-1 gives

$$\sum_{j=1}^{n-1}\Gamma_{ij}\frac{dx_j}{dz} = \sum_{j=1}^{n-1}\frac{\left(x_i N_j - x_j N_i\right)}{c_t Đ_{ij}} + \left(\frac{x_i N_n - x_n N_i}{c_t Đ_{in}}\right); \quad i = 1,2,\ldots,n. \qquad \text{C-3}$$

The x_n is given by

$$x_n = 1 - \sum_{j=1}^{n-1} x_j \qquad \text{C-4}$$

Thus eliminating x_n from Equation C-3 yields

$$\sum_{j=1}^{n-1}\Gamma_{ij}\frac{dx_j}{dz} = \sum_{j=1}^{n-1}\frac{x_i N_j}{c_t \mathcal{D}_{ij}} + \frac{x_i N_n}{c_t \mathcal{D}_{in}} - \sum_{j=1}^{n-1}\frac{x_j N_i}{c_t \mathcal{D}_{ij}} + \sum_{j=1}^{n-1}\frac{x_j N_i}{c_t \mathcal{D}_{in}} - \frac{N_i}{c_t \mathcal{D}_{in}}; \qquad i = 1..n-1 \qquad \text{C-5}$$

Separating the ith term from the right hand side of Equation C-5 gives

$$\sum_{j=1}^{n-1}\Gamma_{ij}\frac{dx_j}{dz} = \sum_{\substack{j=1\\ j\neq i}}^{n-1}\frac{x_i N_j}{c_t \mathcal{D}_{ij}} + \frac{x_i N_n}{c_t \mathcal{D}_{in}} - \sum_{\substack{j=1\\ j\neq i}}^{n-1}\frac{x_j N_i}{c_t \mathcal{D}_{ij}} + \sum_{\substack{j=1\\ j\neq i}}^{n-1}\frac{x_j N_i}{c_t \mathcal{D}_{in}} + \frac{x_i N_i}{c_t \mathcal{D}_{in}} - \frac{N_i}{c_t \mathcal{D}_{in}}; \qquad i = 1..n-1 \qquad \text{C-6}$$

which after simplification yields :

$$\sum_{j=1}^{n-1}\Gamma_{ij}\frac{dx_j}{dz} = \frac{x_i N_i}{c_t \mathcal{D}_{in}} + \sum_{\substack{j=1\\ j\neq i}}^{n}\frac{x_i N_j}{c_t \mathcal{D}_{ij}} + \sum_{\substack{j=1\\ j\neq i}}^{n-1} x_j N_i\left[\frac{1}{c_t \mathcal{D}_{in}} - \frac{1}{c_t \mathcal{D}_{ij}}\right] - \frac{N_i}{c_t \mathcal{D}_{in}}; \qquad i = 1..n-1 \qquad \text{C-7}$$

Let us define η a dimensionless distance by

$$\eta = \frac{z}{l} \qquad \text{C-8}$$

in which l is the film thickness.

Combining Equation C-7 and C-8 gives

$$\sum_{j=1}^{n-1}\Gamma_{ij}\frac{dx_j}{d\eta} = \frac{x_i N_i}{c_t Đ_{in}/l} + \sum_{\substack{j=1\\ j\neq i}}^{n}\frac{x_i N_j}{c_t Đ_{ij}/l} + \sum_{\substack{j=1\\ j\neq i}}^{n-1} x_j N_i\left[\frac{1}{c_t Đ_{in}/l} - \frac{1}{c_t Đ_{ij}/l}\right] - \frac{N_i}{c_t Đ_{in}/l}\,; \qquad i=1..n-1 \qquad \text{C-9}$$

Let us represent the coefficients Φ_{ii}, Φ_{ij} and φ_i by

$$\Phi_{ii} = \frac{N_i}{c_t Đ_{in}/l} + \sum_{\substack{j=1\\ i\neq j}}^{n}\frac{N_j}{c_t Đ_{ij}/l} \qquad \text{C-10}$$

$$\Phi_{ij} = -N_i\left(\frac{1}{c_t Đ_{ij}/l} - \frac{1}{c_t Đ_{in}/l}\right) \qquad \text{C-11}$$

$$\varphi_i = -\frac{N_i}{c_t Đ_{in}/l} \qquad \text{C-12}$$

Finally combining Equations C-9 to C-12 gives

$$\sum_{j=1}^{n-1}\Gamma_{ij}\frac{dx_j}{d\eta} = \Phi_{ii}x_i + \sum_{\substack{j=1\\ j\neq i}}^{n-1}\Phi_{ij}x_j + \varphi_i\,; \qquad i=1,2,\ldots,n-1 \qquad \text{C-13}$$